BUBBLE PROPAGATION THROUGH VISCOPLASTIC FLUIDS

by

NEVILLE DUBASH

BMath (Applied Mathematics) Hons. Co-op, University of Waterloo, 2001

A THESIS SUBMITTED IN PARTIAL FULFILLMENT OF

THE REQUIREMENTS FOR THE DEGREE OF

MASTER OF APPLIED SCIENCE

in

THE FACULTY OF GRADUATE STUDIES

Department of Mechanical Engineering

We accept this thesis as conforming
to the required standard

.....

.....

.....

.....

THE UNIVERSITY OF BRITISH COLUMBIA

August 2003

In presenting this thesis in partial fulfillment of the requirements for an advanced degree at the University of British Columbia, I agree that the Library shall make it freely available for reference and study. I further agree that permission for extensive copying of this thesis for scholarly purposes may be granted by the head of my department or by his or her representatives. It is understood that copying or publication of this thesis for financial gain shall not be allowed without my written permission.

(Signature) _____

Department of Mechanical Engineering
The University of British Columbia
Vancouver, Canada

Date _____

Abstract

In this thesis we consider the propagation of an air bubble in a cylindrical column filled with a viscoplastic fluid. Because of the yield stress of the fluid, it is possible that a bubble will remain trapped in the fluid indefinitely. We restrict our focus to the case of slow moving or near-stopped bubbles.

Using the Herschel-Bulkley constitutive equation to model our viscoplastic fluid, we develop a general variational inequality for our problem. This inequality leads to a stress minimization principle for the solution velocity field. We are also able to prove a stress maximization principle for the solution stress field. Using these two principles we develop three stopping conditions. For a given bubble we can calculate, from our stopping conditions, a critical Bingham number above which the bubble will not move. The first stopping condition is applicable to arbitrary axisymmetric bubbles. It is strongly dependent on the bubble length as well as the general shape of the bubble. The second stopping condition allows us to use existing solutions of simpler problems to calculate additional stopping conditions. We illustrate this second stopping condition using the example of a spherical bubble. The third stopping condition applies to long cylindrical bubbles and is dependent on the radius of the bubble. In addition to our stopping conditions, we determine how the physical parameters of the problem affect the rise velocity of the bubble.

We also conduct a set of experiments using a series of six different Carbopol solutions. From the experiments we examine the dependence of the bubble propagation velocity on the fluid parameters and compare this to our analytic results. We find that there is an interesting discrepancy for low modified Reynolds number flows wherein the bubble velocity increases with a decrease in the modified Reynolds numbers. We also compare our three stopping conditions with the data. It appears that all the stopping conditions seem to be valid for the range of bubbles examined despite the fact that when applying the second and third stopping conditions most bubble shapes are not well approximated by a sphere or a cylinder.

Table of Contents

List of Tables

List of Figures

Acknowledgement

This research was conducted under the supervision of Dr. Ian Frigaard and Dr. Sheldon Green. I would like to thank them both for for their guidance, advice, and encouragement throughout.

I would also like to thank the Natural Sciences and Engineering Research Council of Canada, and the British Columbia Advanced Systems Institute for their generous financial support; and the Canada Foundation for Innivation, the British Columbia Knowledge Development, and the University of British Columbia Blusson Fund for their infrastructure funding that enabled the experimental apparatus to be constructed.

Chapter 1
Introduction

In this thesis we examine the propagation of air bubbles through a viscoplastic fluid. Because of the yield stress of the fluid we have the interesting phenomema that bubbles can become trapped in the fluid indefinitely. We are primarily interested in the of case slow moving and stopped bubbles, and conditions that determine whether a given bubble will rise or remain trapped.

1.1 Viscoplastic Fluids

Viscoplastic fluids are fluids that can behave as both a viscous liquid and as a rigid solid. Which of these two states the material takes is determined by the stress applied to the material. That is, at low stress the material behaves as a solid, capable of rigid motion and rotation. However, when stresses exceed a certain threshold, called the yield stress, the material behaves as a viscous liquid. The solid and liquid regions, called the unyielded and yielded regions respectively, are separated by a distinct yield surface at which the stress equals the yield stress. Some examples of viscoplastic fluids are mud, cement, lava, and paint.

The constitutive models most often used to describe a viscoplastic fluid are the Bingham constitutive model [1] or the slightly more general Herschel-Bulkley constitutive model (2.8)–(2.9). The Bingham constitutive model is a special case ($n = 1$) of the Herschel-Bulkley constitutive model.

In general, foams, slurries, suspensions, and many other industrial fluids behave as viscoplastic fluids. In addition, there are many industrial processes where the generation and behaviour

of bubbles play a significant role in the process. In some situations bubbles are undesirable, and while it would be ideal if they could be eliminated, in practice this is not possible. Hence an understanding of how bubbles behave is beneficial in these areas. Some examples of such processes are

1. When drilling for oil or natural gas a situation known as a kick can occur. A kick occurs when the hydrostatic pressure of the drilling mud becomes less than the pressure of the gas in the rock formation. In this case gas from the formation flows into the wellbore and can cause a blowout (where the gas rises up pushing the drilling mud back out the top of the wellbore) [2]. Blowouts should be avoided as they are dangerous to workers, present environmental hazards, and result in a loss of revenue. The drilling mud is generally a viscoplastic liquid. Thus, knowledge of how bubbles propagate could be used to help control kicks and prevent blowouts.

2. A lot of processed foods (e.g., ketchup, mayonnaise, peanut butter) behave as a viscoplastic liquid. In food processing bubbles are unwanted in the processing and especially the packaging steps. Here knowledge of how bubbles are generated and how they propagate could be used to develop methods to prevent or remove bubbles before processing and packaging.

Moreover, in other situations bubbles are desired or beneficial to the process. An example of such a process is in plastic moulding. One method of manufacturing bottles is to inject a gas into a mould filled with a molten plastic. This gas forces the molten plastic to take the shape of the mould, and once cooled this becomes the bottle. Again, the molten plastic can be considered to be a viscoplastic fluid. An understanding of bubbles could help to improve and streamline this process.

While in this thesis we do not consider any of these problems specifically, the results and analysis, with a little further work, could be applied to these areas.

1.2 Previous and Related Work

Separately bubbles and viscoplastic fluids have been studied quite extensively and for many years, however, the problem of the propagation of a bubble in a viscoplastic fluid has yet to receive much attention. To the best of our knowledge the problem has only been examined in several specific application and situations.

The problems has been examined from the perspective of well drilling, where the gas rise velocity is an important characteristic to know or predict [2] [3] [4]. Santos and Azar [2] measure the gas rise velocities of bubbles rising through an annulus filled with a viscoplastic fluid. They correlate their experimental results with a simple analytic model based on a force balance between viscous drag and buoyancy. To account for variations due to geometry, Reynolds number, and inclination of the annulus they have included some empirical parameters in their formulation. Johnson et al. [3] consider the rise velocity and the void fraction (volume of gas trapped inside the fluid) of bubbles released in a column filled with a viscoplastic fluid. Finally, Johnson and White [4] consider the gas rise velocity of bubbles in a column in which there is already established a pressure driven viscoplastic fluid flow. In particular they compare their results with a similar air-water system and show that despite an increased viscosity the bubbles rise faster in the air-viscoplastic system. These works are primarily experimental in which they examine the variables of interest to petroleum engineers.

In addition, the special case of spherical bubbles has been examined in two papers [5] [6]. In Bhavaraju et al. [5], the authors examine the flow of a single spherical bubble in a Bingham fluid. They consider the case of small Bingham numbers and apply perturbation methods. Using the Bingham number as the perturbation parameter, they obtain a first order correction to the Newtonian solution for flow around a spherical bubble. Their solution, however, is only valid away from the equator of the bubble (great circle in the plane perpendicular to the bubble motion). In addition their solution requires that as the Bingham number goes to zero we recover the Newtonian solution. Whether this is actually the case is unclear. (For example, Beris, et al. [7] claim that this is not the case for a sphere in an unbounded Bingham fluid.) From their

solution they calculate the drag coefficient and the shape of the yield surface. In [6] the authors show that spherical bubbles that are initially trapped in a Bingham fluid can be made to rise by applying an oscillating external pressure to the liquid. They use perturbation methods to derive an analytic solution that consists of a flow due to the pulsation and a flow due to the bubble rising under gravity. They have also conducted experiments that illustrate the phenomenon and that support their analytic results.

A related problem that has received more attention is the problem of slow flow past a solid sphere in viscoplastic fluids. A key paper is that by Beris, et al. [7]. They examine the fall of a sphere due to gravity in an infinite Bingham fluid. Using a finite element numerical simulation they obtain the flow field and the yield surfaces in the flow. In addition, using asymptotic analysis they obtain analytic values for the drag coefficient in the limiting cases of low and high (near the critical value where the sphere ceases to move) Bingham numbers. Adding to the work of Beris, et al., Atapattu, et al., [8], conducted experiments with spheres in viscoplastics to determine the drag coefficient, the terminal velocity, and the shape of the yielded region. Their results, when compared to those of Beris, et al., are qualitatively the same though some discrepancies did exist. One point of note is that Carbopol, the viscoplastic fluid used by Atapattu, et al., (and the same fluid used in this study) is not a perfect Bingham fluid. It is much more accurately modelled using the Herschel-Bulkley constitutive model.

Spheres falling in tubes filled with a Bingham fluid are examined by Blackery and Mitsoulis [9]. They conduct numerical simulations to obtain the flow field for different values of the ratio of sphere radius to column radius. While the shape of the yielded region is qualitatively the same, it does not agree entirely with either that of Beris, et al. or of Atapattu, et al. (In the case of the largest diameter cylinder the walls are sufficiently far away that the result should be identical to the flow in an infinite liquid.)

In addition, some work has been done to generalize the equation for the Newtonian drag coefficient for a sphere to one for a sphere in viscoplastic fluids [10] [11]. The results from these papers correspond well with the results of Beris et al. Some work has even been done with

mixed slip-stick boundary conditions on the sphere [12] and also to experimentally determine the drag coefficient for other shapes (such as discs, cylinders, cubes, and cones) in viscoplastic fluids [13]. And finally, Li and Renardy have numerically examined deformations of a viscous fluid frop in a Bingham fluid [14].

The experimental work on creeping flow around a sphere in viscoplastic fluids has concentrated more on corroborating theoretical results. Unfortunately insufficient attention has be given to ensuring that the experiments are repeatable and that the results obtained are reliable. Gheissary and van den Brule [15] have shown that in practice viscoplastic fluids have a relaxation time. In general, the terminal velocity of a sphere increases with subsequent releases of spheres. Only if a sufficiently long amount of time between spheres is given (or if the liquid is stirred) does the subsequent sphere fall at the same velocity as the first. In Carbopol, a viscoplastic commonly used in experiments, the result of releasing subsequent spheres is even more surprising. Subsequent spheres dropped in relatively quick succession have an increasing terminal velocity. If a sufficient amount of time elapses (on the order of tens of hours) then a sphere will again fall with a velocity the same as the first sphere, however, if an insufficient amount of time elapses, say only a few hours, the velocity of the next sphere will jump to a value higher than that of all the previous spheres. Thus in any experiment it is extremely important to ensure that before each test the fluid is "reset" to some initial state, thus avoiding the complication of the time dependency.

Another closely related problem is that of the propagation of a bubble in non-viscoplastic fluids. Bubbles in Newtonian fluids have been studied for quite some time and there are several books that cover the collection of related work [16] [17]. Also of note, Bretherton [18] has also examined the flow, including effects of surface tension, of long thin bubbles moving in tubes filled with a Newtonian fluid. Moving to the realm of non-Newtonian fluids, Bhavaraju, et al. [5] using their perturbation methods determined the flow around a spherical bubble in a power law fluid. Again their result is only valid away from the equator of the sphere. Vasil'chenko [19] experimentally compares the rise velocities of bubbles in a tube filled with a viscoplastic-elastic fluid against the rise velocities of bubbles in tubes filled with pure viscoplastic and viscoelastic

fluids. The former case exhibits an unusual behaviour not seen in the pure fluids. In the viscoplatic-elastic fluid, for large bubbles that fill the tube, the rise velocity is an increasing function of the bubble length, whereas for the pure liquids the rise velocity is constant.

Finally, some of the methods used in this study, in particular the variational methods, have already been used to examine viscoplastic flows; however, as yet flows with bubbles have not been considered in this way. The first instance of a variational minimum and maximum principle for Bingham fluids is attributed to Prager [20]. In a series of papers, [21], [22], and [23], Mosolov and Miasnikov used Prager's minimum and maximum principles to study two-dimensional flow in pipes of arbitrary cross section and two-dimensional flow around an arbitrary solid body in a channel. They determined some of the characteristics of the flows and developed ways to compare flows. More recently Glowinski has used the variational methods with numerical calculations [24] [25]. Huilgol has used the variational principles in cases where there is slip present at walls [26], and when inertial effects are included [27] [28]. Frigaard, et al. have used variational methods to study exchange flows and displacements flows of two viscoplastic fluids [29] [30]. We mention these papers here since, in addition to the general methodology, some specific techniques are taken from these.

1.3 Outline of Thesis

In this thesis we consider the propagation of a single air bubble in a cylindrical column filled with a viscoplastic fluid. We focus our attention on slow moving and stopped bubbles, and the conditions required for a bubble to become trapped. In chapter 2 we describe the physical problem and write out the full equations that govern the flow. We also nondimensionalize the problem and introduce the important dimensionless parameters. In chapter 3 we simplify the full problem and develop two variational results: a variational inequality that leads to a rate of strain minimization, and a stress maximization result. In chapter 4 we use our variational results to obtain stopping conditions, under which a bubble will not move. The first condition is a general result that applies to axisymmetric bubbles of arbitrary shape. The second condition allows us to use existing solutions of simpler problems to obtain extra stopping conditions.

Finally the third stopping condition applies to the special case of long cylindrical bubbles. In chapter 5 we derive several results relating the bubble propagation velocity to the physical parameters of the problem. Finally, in chapter 6 we describe an experimental setup which we use to observe the the propagation of bubbles in a cylindrical column. We present our experimental results and analyze the data. In addition, we compare the experimental results to our previous analytic results.

Chapter 2
Problem Description

2.1 Physical Setup

The problem we are considering is that of the flow (or lack thereof) of a single gas bubble in a cylindrical column filled with a viscoplastic fluid. The basic physical setup is shown in figure 2.1. Our entire domain is divided into two connected regions, Ω, comprising the liquid

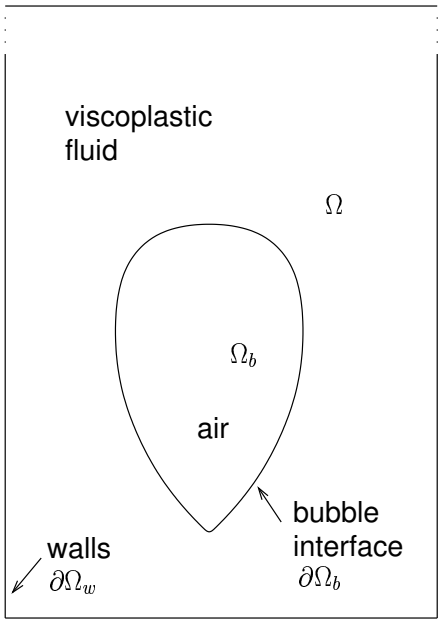

Figure 2.1: Physical setup of the problem.

region, and Ω_b, comprising the gas domain (i.e., the bubble). The boundary of Ω, consisting of the cylinder walls and the bubble surface, will be referred to as $\partial\Omega$. The bubble surface on its own will be referred to as $\partial\Omega_b$, and the walls of the cylinder on their own will be referred to as

$\partial\Omega_w$ or simply as the "cylinder walls". Quantities denoted with a hat " $\hat{}$ " are dimensional while quantities without a hat are dimensionless. We also adopt the Einstien summation convention for the indices.

The equations of motion in the liquid region, Ω, are

$$\hat{\rho}_\ell \frac{D\hat{u}_i}{D\hat{t}} = -\frac{\partial \hat{p}}{\partial \hat{x}_i} + \hat{\rho}_\ell \hat{g}_i + \frac{\partial \hat{\tau}_{\ell,ij}(\hat{\boldsymbol{u}})}{\partial \hat{x}_j}, \tag{2.1}$$

$$\frac{\partial \hat{u}_i}{\partial \hat{x}_i} = 0, \tag{2.2}$$

where $\frac{D}{D\hat{t}} = \frac{\partial}{\partial \hat{t}} + \hat{u}_i \frac{\partial}{\partial \hat{x}_i}$ is the material derivative, $\hat{\boldsymbol{u}} = (\hat{u}_1, \hat{u}_2, \hat{u}_3)$ is the velocity, $\hat{p}$ is the pressure, $\hat{\rho}_\ell$ is the liquid density, $\hat{\tau}_{\ell,ij}(\hat{\boldsymbol{u}})$ is the deviatoric stress tensor for the liquid, and $\hat{g}_i = (0, 0, -\hat{g})$ is the gravitational acceleration.

In the gas region, Ω_b, the equations of motion are

$$\hat{\rho}_g \frac{D\hat{u}_i}{D\hat{t}} = -\frac{\partial \hat{p}}{\partial \hat{x}_i} + \hat{\rho}_g \hat{g}_i + \frac{\partial \hat{\tau}_{g,ij}(\hat{\boldsymbol{u}})}{\partial \hat{x}_j}, \tag{2.3}$$

$$\frac{\partial \hat{\rho}_g}{\partial \hat{t}} + \frac{\partial}{\partial \hat{x}_i}(\hat{\rho}_g \hat{u}_i) = 0, \tag{2.4}$$

where $\hat{\rho}_g$ is the gas density, and $\hat{\tau}_{g,ij}$ is the deviatoric stress tensor for the gas.

The second invariants of the rate of strain tensor and the deviatoric stress tensor are defined as

$$\hat{\dot{\gamma}}(\hat{\boldsymbol{u}}) = \sqrt{\frac{1}{2}\hat{\dot{\gamma}}_{ij}(\hat{\boldsymbol{u}})\hat{\dot{\gamma}}_{ij}(\hat{\boldsymbol{u}})}, \tag{2.5}$$

$$\hat{\boldsymbol{\tau}}_k(\hat{\boldsymbol{u}}) = \sqrt{\frac{1}{2}\hat{\tau}_{k,ij}(\hat{\boldsymbol{u}})\hat{\tau}_{k,ij}(\hat{\boldsymbol{u}})}, \qquad k = \ell, g \tag{2.6}$$

where

$$\hat{\dot{\gamma}}_{ij}(\hat{\boldsymbol{u}}) = \frac{\partial \hat{u}_i}{\partial \hat{x}_j} + \frac{\partial \hat{u}_j}{\partial \hat{x}_i}, \tag{2.7}$$

is the rate of strain tensor.

The liquid, being viscoplastic, is modelled as a Herschel-Bulkley fluid. The constitutive equations for a Herschel-Bulkley fluid are

$$\hat{\dot{\gamma}}_{ij}(\hat{\boldsymbol{u}}) = 0 \qquad \text{if } \hat{\boldsymbol{\tau}}_\ell(\hat{\boldsymbol{u}}) \le \hat{\tau}_Y \tag{2.8}$$

$$\hat{\tau}_{\ell,ij}(\hat{\boldsymbol{u}}) = \left(\hat{\mu}_\ell \hat{\dot{\boldsymbol{\gamma}}}(\hat{\boldsymbol{u}})^{n-1} + \frac{\hat{\tau}_Y}{\hat{\dot{\boldsymbol{\gamma}}}(\hat{\boldsymbol{u}})}\right) \hat{\dot{\gamma}}_{ij}(\hat{\boldsymbol{u}}) \quad \text{if } \hat{\boldsymbol{\tau}}_\ell(\hat{\boldsymbol{u}}) > \hat{\tau}_Y \tag{2.9}$$

where $\hat{\mu}_\ell$ is the consistency, n is the power law index, and $\hat{\tau}_Y$ is the yield stress. All three of these parameters are positive constants. The gas, considered to be Newtonian, has the constitutive equations

$$\hat{\tau}_{g,ij}(\hat{\boldsymbol{u}}) = \hat{\mu}_g \hat{\dot{\gamma}}_{ij}(\hat{\boldsymbol{u}}), \tag{2.10}$$

where $\hat{\mu}_g$ is the viscosity of the gas.

Note that for a Herschel-Bulkley fluid the domain Ω will be divided into two (not necessarily connected) regions, determined by equations (2.8)–(2.9). One region is where the stress in the fluid does not exceed the yield stress and equation (2.8) is valid. This is referred to as the unyielded region. The other region is where the stress in the fluid exceeds the yield stress, and equation (2.9) is valid. This region is called the yielded region. The yielded and unyielded regions are separated by a yield surface at which the stress is equal to the yield stress.

In addition, we have boundary conditions that must be satisfied on the cylinder walls and on the bubble surface. On the walls of the cylinder we have a no-slip condition:

$$\hat{u}_i = 0, \qquad \text{on } \partial\Omega_w. \tag{2.11}$$

Physically we actually have a free surface at the top of the cylinder; the free surface can rise to account for any expansion of the bubble due to the change in hydrostatic pressure as it rises. However, later on, in section 3.2, we show that in the case of slow flow the bubble can effectively be considered to be incompressible. With incompressibility we no longer need the free surface to be able to rise, i.e., the average height of the liquid in the column will be constant. Moreover, for any finite yield stress and a sufficiently long column, there will be a finite length below the free surface for which the fluid is not yielded. As we will show in Appendix A it is possible to introduce a wall at any point in an unyielded region without affecting the flow. Thus considering a column with a rigid top that is completely filled with a Herschel-Bulkley fluid is a mathematically equivalent problem.

On the bubble surface we have a set of jump conditions involving the velocity and the traction.

The traction vector is defined as

$$\hat{\sigma}_{k,n_b i}(\hat{\boldsymbol{u}}) = \hat{\sigma}_{k,ij}(\hat{\boldsymbol{u}}) n_{b,j}, \qquad k = \ell, g \tag{2.12}$$

where

$$\hat{\sigma}_{k,ij}(\hat{\boldsymbol{u}}) = -\hat{p}\delta_{ij} + \hat{\tau}_{k,ij}(\hat{\boldsymbol{u}}), \qquad k = \ell, g \tag{2.13}$$

and $n_{b,j}$ is the outward unit normal of the bubble (i.e., pointing into the liquid). The velocity and the tangential components of the traction must be continuous across the bubble surface:

$$\hat{u}_{\ell,i} - \hat{u}_{g,i} = 0, \tag{2.14}$$

$$\left[\hat{\sigma}_{\ell,n_b i}(\hat{\boldsymbol{u}}) - \hat{\sigma}_{g,n_b i}(\hat{\boldsymbol{u}})\right] t_{1,i} = 0, \tag{2.15}$$

$$\left[\hat{\sigma}_{\ell,n_b i}(\hat{\boldsymbol{u}}) - \hat{\sigma}_{g,n_b i}(\hat{\boldsymbol{u}})\right] t_{2,i} = 0, \tag{2.16}$$

on $\partial\Omega_b$, where $t_{1,i}$ and $t_{2,i}$ are any two linearly independent unit tangent vectors of the bubble surface. For the normal component of traction

$$\left[\hat{\sigma}_{\ell,n_b i}(\hat{\boldsymbol{u}}) - \hat{\sigma}_{g,n_b i}(\hat{\boldsymbol{u}})\right] n_{b,i} = \hat{\xi}\left(\frac{1}{\hat{R}_1} + \frac{1}{\hat{R}_2}\right), \tag{2.17}$$

on $\partial\Omega_b$, where $n_{b,i}$ is again the outward unit normal of the bubble surface, $\hat{\xi}$ is the surface tension, and $\left(\frac{1}{\hat{R}_1} + \frac{1}{\hat{R}_2}\right)$ is twice the mean curvature of the bubble surface ($\hat{R}_1$ and $\hat{R}_2$ are the radii of curvature in the principle directions).

Finally, having determined the velocity, $\hat{\boldsymbol{u}}$, the bubble interface, $\partial\Omega_b$, whose location is denoted by $F(\boldsymbol{x}, t) = 0$, evolves according to the kinematic condition

$$\frac{\partial F}{\partial \hat{t}} + \hat{u}_i \frac{\partial F}{\partial \hat{x}_i} = 0. \tag{2.18}$$

Thus for a given bubble, the solution velocity field must satisfy equations (2.1)–(2.18).

2.2 Non-dimensionalized Equations

To non-dimensionalize (2.1)–(2.18) we take relevant dimensional scales from the physical problem. For the length scale there are two natural choices, either the column radius or the effective

bubble radius. Here we choose the effective bubble radius as the desired length scale. The effective bubble radius plays a more significant role in influencing the flow. This will become evident in the other dimensional scales that we use. Thus we take our length scale to be

$$\hat{x}_i \sim \hat{R}, \tag{2.19}$$

where $\hat{R} = \sqrt[3]{\frac{3}{4\pi}\hat{V}_b}$ and $\hat{V}_b$ is the bubble volume at the injection pressure. Another advantage of this scaling for length is that in the experiments we control the volume (and thereby the effective radius) of the injected bubble. The velocity scale is chosen through an approximate force balance. As we are primarily interested in slow flows and cases where bubbles are static or "stopped", there should be an approximate balance between the buoyancy force on the bubble and the viscous force on the bubble. The buoyancy force $\sim (\hat{\rho}_\ell - \hat{\rho}_g^*)\hat{g}\hat{R}^3$ and the viscous force $\sim \frac{\hat{\mu}_\ell \hat{U}^n}{\hat{R}^{n-2}}$. Since the gas density is not constant, we have written

$$\hat{\rho}_g = \hat{\rho}_g^* \rho_g, \tag{2.20}$$

where $\hat{\rho}_g^*$ is the gas density at the injection pressure and ρ_g is the non-dimensional gas density. Since the gas density is very small compared to the liquid density (i.e., $\hat{\rho}_\ell - \hat{\rho}_g^* \approx \hat{\rho}_\ell$) we take the velocity scale as

$$\hat{u}_i \sim \hat{U} \equiv \left(\frac{\hat{\rho}_\ell \hat{g} \hat{R}^{n+1}}{\hat{\mu}_\ell} \right)^{\frac{1}{n}}. \tag{2.21}$$

It turns out that using $\hat{\rho}_\ell$ instead of $\hat{\rho}_\ell - \hat{\rho}_g^*$ is a better choice for $\hat{U}$. Finally we scale the pressure hydrostatically as

$$\hat{p} \sim \hat{\rho}_\ell \hat{g} \hat{R}. \tag{2.22}$$

We define the dimensionless length, velocity, time, and pressure (x_i, u_i, t, and p respectively) by

$$\hat{x}_i = \hat{R} x_i, \tag{2.23}$$

$$\hat{u}_i = \hat{U} u_i = \left(\frac{\hat{\rho}_\ell \hat{g} \hat{R}^{n+1}}{\hat{\mu}_\ell} \right)^{\frac{1}{n}} u_i, \tag{2.24}$$

$$\hat{t} = \frac{\hat{R}}{\hat{U}} t, \qquad \text{and} \tag{2.25}$$

$$\hat{p} = \hat{\rho}_\ell \hat{g} \hat{R} p. \tag{2.26}$$

The rate of strain tensor becomes

$$\dot{\gamma}_{ij}(\boldsymbol{u}) = \frac{\partial u_i}{\partial x_j} + \frac{\partial u_j}{\partial x_i} \qquad \text{where} \qquad \hat{\dot{\gamma}}_{ij}(\hat{\boldsymbol{u}}) = \frac{\hat{U}}{\hat{R}}\dot{\gamma}_{ij}(\boldsymbol{u}). \tag{2.27}$$

The dimensionless constitutive equations for a Herschel-Bulkley fluid are

$$\dot{\gamma}_{ij}(\boldsymbol{u}) = 0 \qquad \text{if } \boldsymbol{\tau}_\ell(\boldsymbol{u}) \le B, \tag{2.28}$$

$$\tau_{\ell,ij}(\boldsymbol{u}) = \left(\dot{\boldsymbol{\gamma}}(\boldsymbol{u})^{n-1} + \frac{B}{\dot{\boldsymbol{\gamma}}(\boldsymbol{u})}\right)\dot{\gamma}_{ij}(\boldsymbol{u}) \quad \text{if } \boldsymbol{\tau}_\ell(\boldsymbol{u}) > B, \tag{2.29}$$

where

$$\hat{\tau}_{\ell,ij}(\hat{\boldsymbol{u}}) = \frac{\hat{\mu}_\ell \hat{U}^n}{\hat{R}^n}\tau_{\ell,ij}(\boldsymbol{u}), \qquad \text{and} \tag{2.30}$$

$$B = \frac{\hat{\tau}_Y \hat{R}^n}{\hat{\mu}_\ell \hat{U}^n} = \frac{\hat{\tau}_Y}{\hat{\rho}_\ell \hat{g}\hat{R}} \tag{2.31}$$

is the (dimensionless) Bingham number. The second invariants of the dimensionless rate of strain and stress tensors are

$$\dot{\boldsymbol{\gamma}}(\boldsymbol{u}) = \sqrt{\frac{1}{2}\dot{\gamma}_{ij}(\boldsymbol{u})\dot{\gamma}_{ij}(\boldsymbol{u})}, \qquad \text{and} \tag{2.32}$$

$$\boldsymbol{\tau}_\ell(\boldsymbol{u}) = \sqrt{\frac{1}{2}\tau_{\ell,ij}(\boldsymbol{u})\tau_{\ell,ij}(\boldsymbol{u})}. \tag{2.33}$$

The constitutive equations for the gas simply become

$$\tau_{g,ij}(\boldsymbol{u}) = \delta\dot{\gamma}_{ij}(\boldsymbol{u}) \tag{2.34}$$

where

$$\hat{\tau}_{g,ij}(\hat{\boldsymbol{u}}) = \frac{\hat{\mu}_\ell \hat{U}^n}{\hat{R}^n}\tau_{g,ij}(\boldsymbol{u}), \tag{2.35}$$

and

$$\delta = \frac{\hat{\mu}_g \hat{R}^{n-1}}{\hat{\mu}_\ell \hat{U}^{n-1}}. \tag{2.36}$$

The non-dimensional versions of (2.1) and (2.2), valid in the liquid region, are

$$Fr^2\frac{Du_i}{Dt} = -\frac{\partial p}{\partial x_i} - \delta_{i3} + \frac{\partial \tau_{\ell,ij}(\boldsymbol{u})}{\partial x_j}, \tag{2.37}$$

$$\frac{\partial u_i}{\partial x_i} = 0, \tag{2.38}$$

and the non-dimensional versions of (2.3) and (2.4) are

$$\epsilon\rho_g Fr^2 \frac{Du_i}{Dt} = -\frac{\partial p}{\partial x_i} - \epsilon\rho_g \delta_{i3} + \delta \frac{\partial \dot{\gamma}_{ij}(\boldsymbol{u})}{\partial x_j}, \tag{2.39}$$

$$\frac{\partial \rho_g}{\partial t} + \frac{\partial}{\partial x_i}(\rho_g u_i) = 0, \tag{2.40}$$

where the dimensionless parameters are

$$Fr = \frac{\hat{U}}{\sqrt{\hat{g}\hat{R}}}, \tag{2.41}$$

$$\epsilon = \frac{\hat{\rho}_g^*}{\hat{\rho}_\ell}, \tag{2.42}$$

$$\delta = \frac{\hat{\mu}_g \hat{R}^{n-1}}{\hat{\mu}_\ell \hat{U}^{n-1}} \tag{2.43}$$

and δ_{ij} is the Kronecker delta.

The boundary conditions (2.11) and (2.14) remain the same:

$$u_i = 0 \qquad \text{on } \partial\Omega_w, \tag{2.44}$$

$$u_{\ell,i} - u_{g,i} = 0 \qquad \text{across } \partial\Omega_b. \tag{2.45}$$

The dimensionless traction conditions are

$$\tau_{\ell,n_b t_1} - \tau_{g,n_b t_1} = 0, \tag{2.46}$$

$$\tau_{\ell,n_b t_2} - \tau_{g,n_b t_2} = 0, \tag{2.47}$$

$$-p_\ell + p_g + \tau_{\ell,n_b n_b} - \tau_{g,n_b n_b} = \beta \left(\frac{1}{R_1} + \frac{1}{R_2} \right), \tag{2.48}$$

across $\partial\Omega_b$, where

$$\beta = \frac{\hat{\xi}}{\hat{\rho}_\ell \hat{g} \hat{R}^2} \tag{2.49}$$

is the dimensionless surface tension, and $R_1 = \frac{\hat{R}_1}{\hat{R}}$ and $R_2 = \frac{\hat{R}_2}{\hat{R}}$ are the dimensionless radii of curvature. Note that $\tau_{g,ij}$ is in general $O(\delta)$ smaller than $\tau_{\ell,ij}$; see (2.28)–(2.30), (2.34), and (2.35).

Finally, the kinematic condition for the bubble surface, (2.18), remains the same

$$\frac{\partial F}{\partial t} + u_i \frac{\partial F}{\partial x_i} = 0. \tag{2.50}$$

Chapter 3
Variational Formulation

3.1 Introduction

The existence of the yield stress, and hence the possibility of a yield surface, makes the classical approach of directly solving the Naiver-Stokes equations impractical. The location of a yield surface is determined by the stress field and the yield surface in turn determines the boundary conditions for the system. Furthermore, the yield surface need not be static, nor is it a material surface. In essence we have a complex free boundary problem, for which an analytic solution can be obtained only in special cases.

Another approach which can be used is to formulate the problem as a variational problem, where the actual flow field distinguishes itself from all other possible flows in that the actual flow minimizes or maximizes some functional. While the variational formulation does not result in an explicit solution for the flow field, we can nevertheless learn a lot about the behaviour of the solution. The main motivation for using a variational formulation is that it eliminates the need to know the location of the yield surface beforehand.

3.2 Simplification of the Full Problem

For convenience we rewrite the full non-dimensional problem. In the liquid region, the non-dimensionalized equations of motion are

$$Fr^2 \frac{Du_i}{Dt} = -\frac{\partial p}{\partial x_i} - \delta_{i3} + \frac{\partial \tau_{\ell,ij}(\boldsymbol{u})}{\partial x_j}, \tag{3.1}$$

$$\frac{\partial u_i}{\partial x_i} = 0, \tag{3.2}$$

and in the gas region the equations of motion are

$$\epsilon \rho_g Fr^2 \frac{Du_i}{Dt} = -\frac{\partial p}{\partial x_i} - \epsilon \rho_g \delta_{i3} + \delta \frac{\partial \dot{\gamma}_{ij}(\boldsymbol{u})}{\partial x_j}, \tag{3.3}$$

$$\frac{\partial \rho_g}{\partial t} + \frac{\partial}{\partial x_i}(\rho_g u_i) = 0, \tag{3.4}$$

where $Fr = \frac{\hat{U}}{\sqrt{\hat{g}\hat{R}}}$ is the Froude number, δ_{ij} is the Kronecker delta, $\epsilon = \frac{\hat{\rho}_g^*}{\hat{\rho}_\ell}$, $\delta = \frac{\hat{\mu}_g \hat{R}^{n-1}}{\hat{\mu}_\ell \hat{U}^{n-1}}$, and $B = \frac{\hat{\tau}_Y \hat{R}^n}{\hat{\mu}_\ell \hat{U}^n} = \frac{\hat{\tau}_Y}{\hat{\rho}_\ell \hat{g} \hat{R}}$ is the Bingham number.

For a Herschel-Bulkley fluid the (dimensionless) constitutive equations are

$$\dot{\gamma}_{ij}(\boldsymbol{u}) = 0 \qquad \text{if } \boldsymbol{\tau}_\ell(\boldsymbol{u}) \leq B, \tag{3.5}$$

$$\tau_{\ell,ij}(\boldsymbol{u}) = \left(\dot{\boldsymbol{\gamma}}(\boldsymbol{u})^{n-1} + \frac{B}{\dot{\boldsymbol{\gamma}}(\boldsymbol{u})} \right) \dot{\gamma}_{ij}(\boldsymbol{u}) \quad \text{if } \boldsymbol{\tau}_\ell(\boldsymbol{u}) > B, \tag{3.6}$$

and for the gas the (dimensionless) constitutive equations are

$$\tau_{g,ij}(\boldsymbol{u}) = \delta \dot{\gamma}_{ij}(\boldsymbol{u}), \tag{3.7}$$

where

$$\dot{\boldsymbol{\gamma}}(\boldsymbol{u}) = \sqrt{\frac{1}{2}\dot{\gamma}_{ij}(\boldsymbol{u})\dot{\gamma}_{ij}(\boldsymbol{u})}, \qquad \text{and} \tag{3.8}$$

$$\boldsymbol{\tau}_\ell(\boldsymbol{u}) = \sqrt{\frac{1}{2}\tau_{\ell,ij}(\boldsymbol{u})\tau_{\ell,ij}(\boldsymbol{u})}. \tag{3.9}$$

As for boundary conditions, we still have zero flow at the cylinder walls:

$$u_i = 0 \qquad \text{on } \partial\Omega_w. \tag{3.10}$$

Across the bubble interface, $\partial\Omega_b$, the dimensionless velocity and traction conditions are

$$u_{\ell,i} - u_{g,i} = 0, \tag{3.11}$$

$$\tau_{\ell,n_b t_1} - \tau_{g,n_b t_1} = 0, \tag{3.12}$$

$$\tau_{\ell,n_b t_2} - \tau_{g,n_b t_2} = 0, \tag{3.13}$$

$$-p_\ell + p_g + \tau_{\ell,n_b n_b} - \tau_{g,n_b n_b} = \beta \left(\frac{1}{R_1} + \frac{1}{R_2} \right), \tag{3.14}$$

where $\boldsymbol{n_b}$ is the outward normal to the bubble surface, t_1 and t_2 are two linearly independent tangent vectors of the bubble surface, and R_1 and R_2 are the dimensionless radii of curvature in the principle directions. And finally, the kinematic condition for the bubble surface is

$$\frac{\partial F}{\partial t} + u_i \frac{\partial F}{\partial x_i} = 0, \tag{3.15}$$

where $F(\boldsymbol{x}, t) = 0$ is the location of the bubble surface.

For slow flows we can ignore the inertial terms. The inertial terms scale as $\sim u_i^2$, while the remaining terms scale as $\sim u_i$. Since we are interested in the phenomena of stopped bubbles and "nearly" stopped bubbles, the inertial terms can be considered to be an order of magnitude smaller that the other terms. Also for our system of polymer solution and air $\delta \sim 10^{-6}$ and $\epsilon \sim 10^{-3}$. Thus, as a first approximation, we ignore the inertial terms and the terms containing δ and ϵ. Equations (3.1) and (3.3) become

$$\text{liquid:} \qquad 0 = -\frac{\partial p}{\partial x_i} - \delta_{i3} + \frac{\partial \tau_{\ell,ij}(\boldsymbol{u})}{\partial x_j}, \tag{3.16}$$

$$\text{gas:} \qquad 0 = -\frac{\partial p}{\partial x_i} \tag{3.17}$$

respectively. Equation (3.17) implies that the pressure in the bubble is constant (really $p = p(t)$). The dimensional version of equation (3.4) can be written as

$$\begin{aligned}
\frac{\partial \hat{\rho}_g}{\partial \hat{t}} + \hat{u}_i \frac{\partial \hat{\rho}_g}{\partial \hat{x}_i} + \hat{\rho}_g \frac{\partial \hat{u}_i}{\partial \hat{x}_i} &= 0 \\
\frac{1}{\hat{\rho}_g} \frac{\partial \hat{\rho}_g}{\partial \hat{p}} \left(\frac{\partial \hat{p}}{\partial \hat{t}} + \hat{u}_i \frac{\partial \hat{p}}{\partial \hat{x}_i} \right) + \frac{\partial \hat{u}_i}{\partial \hat{x}_i} &= 0 \\
\frac{1}{\hat{\rho}_g} \frac{\partial \hat{\rho}_g}{\partial \hat{p}} \frac{\partial \hat{p}}{\partial \hat{t}} + \frac{\partial \hat{u}_i}{\partial \hat{x}_i} &= 0 \\
\frac{1}{\hat{\rho}_g \hat{c}_g^2} \frac{\partial \hat{p}}{\partial \hat{t}} + \frac{\partial \hat{u}_i}{\partial \hat{x}_i} &= 0,
\end{aligned} \tag{3.18}$$

where $\hat{c}_g = \sqrt{\frac{\partial \hat{p}}{\partial \hat{\rho}_g}}$ is the speed of sound in the gas. The main change in the pressure is due to the static pressure of the liquid, as the bubble rises; this changes like $\hat{\rho}_\ell \hat{g} \hat{U}$. Examining the relative sizes of the two terms in (3.18) we have $\frac{\partial \hat{u}_i}{\partial \hat{x}_i} \sim \frac{\hat{U}}{\hat{R}}$ and $\frac{1}{\hat{\rho}_g \hat{c}_g^2} \frac{\partial \hat{p}}{\partial \hat{t}} \sim \frac{\hat{g}\hat{U}}{\epsilon \hat{c}_g^2}$. So

$$\frac{\frac{1}{\hat{\rho}_g \hat{c}_g^2} \frac{\partial \hat{p}}{\partial \hat{t}}}{\frac{\partial \hat{u}_i}{\partial \hat{x}_i}} \sim \frac{\frac{\hat{U}}{\hat{R}}}{\frac{\hat{g}\hat{U}}{\epsilon \hat{c}_g^2}} = \frac{\hat{g}\hat{R}}{\epsilon \hat{c}_g^2} \approx \frac{(10)(10^{-2})}{(10^{-3})(10^5)} = 10^{-3}.$$

Thus we can make the approximation of incompressibility,

$$\frac{\partial \hat{u}_i}{\partial \hat{x}_i} = 0 \qquad \text{or} \qquad \frac{\partial u_i}{\partial x_i} = 0, \tag{3.19}$$

in the bubble.

Lastly the traction conditions at the bubble interface, $\partial\Omega_b$ simplify to

$$\tau_{\ell,n_b t_1} = 0, \tag{3.20}$$

$$\tau_{\ell,n_b t_2} = 0, \qquad \text{and} \tag{3.21}$$

$$-p_\ell + p_g + \tau_{\ell,n_b n_b} = \beta \left(\frac{1}{R_1} + \frac{1}{R_2} \right) \tag{3.22}$$

since $\tau_{g,ij}$ is $O(\delta)$ smaller than $\tau_{\ell,ij}$.

Equations (3.16), (3.17), (3.2), and (3.19), with the constitutive equations (3.5)–(3.7), and boundary conditions (3.10), (3.11), and (3.20)–(3.22) comprise the simplified system for which we will develop a variational formulation.

3.3 Variational Inequality (Rate of Strain Minimization)

For the variational inequality we obtain a result where the solution function (in this case a velocity field), chosen from a given function space, satisfies certain criteria with respect to the other functions in the function space. The space of functions we consider, denoted V, is the space of all vector-valued functions $\boldsymbol{v} = (v_1, v_2, v_3)$ such that

$$v_i \in C^\infty(\Omega), \tag{3.23}$$

$$\frac{\partial v_i}{\partial x_i} = 0 \qquad \text{in } \Omega, \text{ and} \tag{3.24}$$

$$v_i = 0 \qquad \text{on } \partial\Omega_w. \tag{3.25}$$

It is clear that the actual solution $\boldsymbol{u} \in V$.

3.3.1 A Preliminary Inequality

First we will derive an inequality which will be employed in our variational derivation. Let u_i be a velocity field that satisfies equations (3.2), (3.5)–(3.11), (3.16), (3.17), and (3.19)–(3.22),

and let v_i be any admissible velocity field from our functional space, V.

In the unyielded regions, equation (3.5) holds and the quantity $\frac{1}{2}\tau_{\ell,ij}(\boldsymbol{u})\dot{\gamma}_{ij}(\boldsymbol{u})$ satisfies

$$\frac{1}{2}\tau_{\ell,ij}(\boldsymbol{u})\dot{\gamma}_{ij}(\boldsymbol{u}) = 0 = \frac{1}{2}\dot{\boldsymbol{\gamma}}(\boldsymbol{u})^{n-1}\dot{\gamma}_{ij}(\boldsymbol{u})\dot{\gamma}_{ij}(\boldsymbol{u}) + B\dot{\boldsymbol{\gamma}}(\boldsymbol{u}), \tag{3.26}$$

since both $\dot{\gamma}_{ij}(\boldsymbol{u}) = 0$ and $\dot{\boldsymbol{\gamma}}(\boldsymbol{u}) = 0$. Also the quantity $\frac{1}{2}\tau_{\ell,ij}(\boldsymbol{u})\dot{\gamma}_{ij}(\boldsymbol{v})$ satisfies

$$\begin{aligned}\frac{1}{2}\tau_{\ell,ij}(\boldsymbol{u})\dot{\gamma}_{ij}(\boldsymbol{v}) &\leq \boldsymbol{\tau}_\ell(\boldsymbol{u})\dot{\boldsymbol{\gamma}}(\boldsymbol{v}) \\ &\leq B\dot{\boldsymbol{\gamma}}(\boldsymbol{v}) \\ &= \frac{1}{2}\dot{\boldsymbol{\gamma}}(\boldsymbol{u})^{n-1}\dot{\gamma}_{ij}(\boldsymbol{u})\dot{\gamma}_{ij}(\boldsymbol{v}) + B\dot{\boldsymbol{\gamma}}(\boldsymbol{v}).\end{aligned} \tag{3.27}$$

Here we have used the Cauchy-Schwarz inequality $\alpha_{ij}\beta_{ij} \leq \sqrt{\alpha_{ij}\alpha_{ij}}\sqrt{\beta_{ij}\beta_{ij}}$, and that while we do not know the exact value of $\boldsymbol{\tau}_\ell(\boldsymbol{u})$ in the unyielded region we know that it is less than the yield stress, B. Again $\dot{\gamma}_{ij}(\boldsymbol{u})$ is simply zero.

In the yielded regions, equation (3.6) holds, and the quantity $\frac{1}{2}\tau_{\ell,ij}(\boldsymbol{u})\dot{\gamma}_{ij}(\boldsymbol{u})$ satisfies

$$\begin{aligned}\frac{1}{2}\tau_{\ell,ij}(\boldsymbol{u})\dot{\gamma}_{ij}(\boldsymbol{u}) &= \frac{1}{2}\left(\dot{\boldsymbol{\gamma}}(\boldsymbol{u})^{n-1} + \frac{B}{\dot{\boldsymbol{\gamma}}(\boldsymbol{u})}\right)\dot{\gamma}_{ij}(\boldsymbol{u})\dot{\gamma}_{ij}(\boldsymbol{u}) \\ &= \frac{1}{2}\dot{\boldsymbol{\gamma}}(\boldsymbol{u})^{n-1}\dot{\gamma}_{ij}(\boldsymbol{u})\dot{\gamma}_{ij}(\boldsymbol{u}) + \frac{1}{2}\frac{B}{\dot{\boldsymbol{\gamma}}(\boldsymbol{u})}\dot{\gamma}_{ij}(\boldsymbol{u})\dot{\gamma}_{ij}(\boldsymbol{u}) \\ &= \frac{1}{2}\dot{\boldsymbol{\gamma}}(\boldsymbol{u})^{n-1}\dot{\gamma}_{ij}(\boldsymbol{u})\dot{\gamma}_{ij}(\boldsymbol{u}) + B\dot{\boldsymbol{\gamma}}(\boldsymbol{u}).\end{aligned} \tag{3.28}$$

And the quantity $\frac{1}{2}\tau_{\ell,ij}(\boldsymbol{u})\dot{\gamma}_{ij}(\boldsymbol{v})$ satisfies

$$\begin{aligned}\frac{1}{2}\tau_{\ell,ij}(\boldsymbol{u})\dot{\gamma}_{ij}(\boldsymbol{v}) &= \frac{1}{2}\left(\dot{\boldsymbol{\gamma}}(\boldsymbol{u})^{n-1} + \frac{B}{\dot{\boldsymbol{\gamma}}(\boldsymbol{u})}\right)\dot{\gamma}_{ij}(\boldsymbol{u})\dot{\gamma}_{ij}(\boldsymbol{v}) \\ &= \frac{1}{2}\dot{\boldsymbol{\gamma}}(\boldsymbol{u})^{n-1}\dot{\gamma}_{ij}(\boldsymbol{u})\dot{\gamma}_{ij}(\boldsymbol{v}) + \frac{1}{2}\frac{B}{\dot{\boldsymbol{\gamma}}(\boldsymbol{u})}\dot{\gamma}_{ij}(\boldsymbol{u})\dot{\gamma}_{ij}(\boldsymbol{v}) \\ &\leq \frac{1}{2}\dot{\boldsymbol{\gamma}}(\boldsymbol{u})^{n-1}\dot{\gamma}_{ij}(\boldsymbol{u})\dot{\gamma}_{ij}(\boldsymbol{v}) + B\dot{\boldsymbol{\gamma}}(\boldsymbol{v}),\end{aligned} \tag{3.29}$$

where we have again use the Cauchy-Schwarz inequality in the last line.

Comparing equations (3.26) and (3.28), we can see that the equality

$$\frac{1}{2}\tau_{\ell,ij}(\boldsymbol{u})\dot{\gamma}_{ij}(\boldsymbol{u}) = \frac{1}{2}\dot{\boldsymbol{\gamma}}(\boldsymbol{u})^{n-1}\dot{\gamma}_{ij}(\boldsymbol{u})\dot{\gamma}_{ij}(\boldsymbol{u}) + B\dot{\boldsymbol{\gamma}}(\boldsymbol{u}) \tag{3.30}$$

holds in both the unyielded and yielded regions. Similarly, from the inequalities (3.27) and (3.29), we have that the inequality

$$\frac{1}{2}\tau_{\ell,ij}(\boldsymbol{u})\dot{\gamma}_{ij}(\boldsymbol{v}) \leq \frac{1}{2}\dot{\boldsymbol{\gamma}}(\boldsymbol{u})^{n-1}\dot{\gamma}_{ij}(\boldsymbol{u})\dot{\gamma}_{ij}(\boldsymbol{v}) + B\dot{\boldsymbol{\gamma}}(\boldsymbol{v}) \tag{3.31}$$

also holds in both the unyielded and yielded regions.

Subtracting (3.30) from (3.31) we have that

$$\begin{aligned}
&\frac{1}{2}\tau_{\ell,ij}(\boldsymbol{u})\left(\dot{\gamma}_{ij}(\boldsymbol{v}) - \dot{\gamma}_{ij}(\boldsymbol{u})\right) \leq \frac{1}{2}\dot{\boldsymbol{\gamma}}(\boldsymbol{u})^{n-1}\dot{\gamma}_{ij}(\boldsymbol{u})\left(\dot{\gamma}_{ij}(\boldsymbol{v}) - \dot{\gamma}_{ij}(\boldsymbol{u})\right) + B\dot{\boldsymbol{\gamma}}(\boldsymbol{v}) - B\dot{\boldsymbol{\gamma}}(\boldsymbol{u}) \\
&\quad \Rightarrow \frac{1}{2}\tau_{\ell,ij}(\boldsymbol{u})\dot{\gamma}_{ij}(\boldsymbol{v}-\boldsymbol{u}) \leq \frac{1}{2}\dot{\boldsymbol{\gamma}}(\boldsymbol{u})^{n-1}\dot{\gamma}_{ij}(\boldsymbol{u})\dot{\gamma}_{ij}(\boldsymbol{v}-\boldsymbol{u}) + B\dot{\boldsymbol{\gamma}}(\boldsymbol{v}) - B\dot{\boldsymbol{\gamma}}(\boldsymbol{u}),
\end{aligned} \tag{3.32}$$

since $\dot{\gamma}_{ij}(\cdot)$ is linear in its argument.

Inequality (3.32) is crucial to the variational formulation. Inequality (3.32) avoids the problem of determining where the yielded and unyielded regions are located – it is valid throughout the liquid domain Ω. Later in our variational formulation we will return to this inequality.

3.3.2 Derivation of the Variational Inequality

Again let u_i be a velocity field that satisfies equations (3.2), (3.5)–(3.11), (3.16), (3.17), and (3.19)–(3.22), and let v_i be any admissible velocity field from our functional space, V. Multiplying equation (3.16) by $(v_i - u_i)$ and summing over the index i we have

$$\begin{aligned}
0 &= -\left(\frac{\partial p}{\partial x_i} + \delta_{i3}\right)(v_i - u_i) + \frac{\partial \tau_{\ell,ij}(\boldsymbol{u})}{\partial x_j}(v_i - u_i) \\
&= -\left(\frac{\partial p}{\partial x_i} + \delta_{i3}\right)(v_i - u_i) + \frac{\partial}{\partial x_j}\left[\tau_{\ell,ij}(\boldsymbol{u})(v_i - u_i)\right] - \tau_{\ell,ij}(\boldsymbol{u})\frac{\partial}{\partial x_j}(v_i - u_i),
\end{aligned} \tag{3.33}$$

where we have used the chain rule to rewrite the last term.

Since $\tau_{\ell,ij}(\boldsymbol{u})$ is a symmetric tensor the last term of equation (3.33) can be written

$$\begin{aligned}
\tau_{\ell,ij}(\boldsymbol{u})\frac{\partial}{\partial x_j}(v_i-u_i) &= \frac{1}{2}\tau_{\ell,ij}(\boldsymbol{u})\frac{\partial}{\partial x_j}(v_i-u_i)+\frac{1}{2}\tau_{\ell,ij}(\boldsymbol{u})\frac{\partial}{\partial x_j}(v_i-u_i)\\
&= \frac{1}{2}\tau_{\ell,ij}(\boldsymbol{u})\frac{\partial}{\partial x_j}(v_i-u_i)+\frac{1}{2}\tau_{\ell,ji}(\boldsymbol{u})\frac{\partial}{\partial x_i}(v_j-u_j)\\
&= \frac{1}{2}\tau_{\ell,ij}(\boldsymbol{u})\frac{\partial}{\partial x_j}(v_i-u_i)+\frac{1}{2}\tau_{\ell,ij}(\boldsymbol{u})\frac{\partial}{\partial x_i}(v_j-u_j)\\
&= \tau_{\ell,ij}(\boldsymbol{u})\left[\frac{1}{2}\left(\frac{\partial}{\partial x_j}(v_i-u_i)+\frac{\partial}{\partial x_i}(v_j-u_j)\right)\right]\\
&= \frac{1}{2}\tau_{\ell,ij}(\boldsymbol{u})\dot{\gamma}_{ij}(\boldsymbol{v}-\boldsymbol{u}). \qquad (3.34)
\end{aligned}$$

Furthermore, due to incompressibility $\frac{\partial(v_i-u_i)}{\partial x_i}=0$, so the first two terms of equation (3.33) can be written

$$\begin{aligned}
&-\left(\frac{\partial p}{\partial x_i}+\delta_{i3}\right)(v_i-u_i)+\frac{\partial}{\partial x_j}\left[\tau_{\ell,ij}(\boldsymbol{u})(v_i-u_i)\right]\\
&\qquad = -\frac{\partial p}{\partial x_i}(v_i-u_i)-(v_3-u_3)+\frac{\partial}{\partial x_j}\left[\tau_{\ell,ij}(\boldsymbol{u})(v_i-u_i)\right]\\
&\qquad = -\frac{\partial}{\partial x_i}\left[p(v_i-u_i)\right]-(v_3-u_3)+\frac{\partial}{\partial x_j}\left[\tau_{\ell,ij}(\boldsymbol{u})(v_i-u_i)\right]\\
&\qquad = -\frac{\partial}{\partial x_j}\left[p\delta_{ij}(v_i-u_i)\right]-(v_3-u_3)+\frac{\partial}{\partial x_j}\left[\tau_{\ell,ij}(\boldsymbol{u})(v_i-u_i)\right]\\
&\qquad = -(v_3-u_3)+\frac{\partial}{\partial x_j}\Big[\left[-p\delta_{ij}+\tau_{\ell,ij}(\boldsymbol{u})\right](v_i-u_i)\Big]\\
&\qquad = -(v_3-u_3)+\frac{\partial}{\partial x_j}\left[\sigma_{\ell,ij}(\boldsymbol{u})(v_i-u_i)\right], \qquad (3.35)
\end{aligned}$$

where $\sigma_{\ell,ij}(\boldsymbol{u})=-p\delta_{ij}+\tau_{\ell,ij}(\boldsymbol{u})$ is the dimensionless traction.

Thus equation (3.33) can be be written

$$\frac{1}{2}\tau_{\ell,ij}(\boldsymbol{u})\dot{\gamma}_{ij}(\boldsymbol{v}-\boldsymbol{u})=-(v_3-u_3)+\frac{\partial}{\partial x_j}\left[\sigma_{\ell,ij}(\boldsymbol{u})(v_i-u_i)\right]. \qquad (3.36)$$

Now we use the inequality (3.32) on the left hand side:

$$\frac{1}{2}\dot{\boldsymbol{\gamma}}(\boldsymbol{u})^{n-1}\dot{\gamma}_{ij}(\boldsymbol{u})\dot{\gamma}_{ij}(\boldsymbol{v}-\boldsymbol{u})+B\dot{\boldsymbol{\gamma}}(\boldsymbol{v})-B\dot{\boldsymbol{\gamma}}(\boldsymbol{u})\geq -(v_3-u_3)+\frac{\partial}{\partial x_j}\left[\sigma_{\ell,ij}(\boldsymbol{u})(v_i-u_i)\right]. \qquad (3.37)$$

Finally we integrate equation (3.37) over the domain Ω to obtain

$$a(\boldsymbol{u},\boldsymbol{v}-\boldsymbol{u})+j(\boldsymbol{v})-j(\boldsymbol{u})\geq -\int_\Omega (v_3-u_3)\,d\Omega+\int_\Omega \frac{\partial}{\partial x_j}\left[\sigma_{\ell,ij}(\boldsymbol{u})(v_i-u_i)\right]\,d\Omega \qquad (3.38)$$

where

$$a(\boldsymbol{u},\boldsymbol{v}) = \frac{1}{2}\int_\Omega \dot{\boldsymbol{\gamma}}(\boldsymbol{u})^{n-1}\dot{\gamma}_{ij}(\boldsymbol{u})\dot{\gamma}_{ij}(\boldsymbol{v})\,d\Omega, \quad \text{and}$$
$$j(\boldsymbol{u}) = B\int_\Omega \dot{\boldsymbol{\gamma}}(\boldsymbol{u})\,d\Omega.$$

Applying the divergence theorem to the last term of the right hand side of equation (3.38) we have

$$a(\boldsymbol{u},\boldsymbol{v}-\boldsymbol{u}) + j(\boldsymbol{v}) - j(\boldsymbol{u}) \geq -\int_\Omega (v_3 - u_3)\,d\Omega + \int_{\partial\Omega} \sigma_{\ell,ij}(\boldsymbol{u})(v_i - u_i)n_j\,ds, \tag{3.39}$$

where n_j is the outward unit normal of $\partial\Omega$. Splitting the boundary into the wall boundary and the bubble surface, and noting that $n_j = -n_{b,j}$ on $\partial\Omega_b$, we can write

$$\begin{aligned} a(\boldsymbol{u},\boldsymbol{v}-\boldsymbol{u}) + j(\boldsymbol{v}) - j(\boldsymbol{u}) \geq &-\int_\Omega (v_3 - u_3)\,d\Omega \\ &+ \int_{\partial\Omega_w} \sigma_{\ell,ij}(\boldsymbol{u})(v_i - u_i)n_j\,ds - \int_{\partial\Omega_b} \sigma_{\ell,ij}(\boldsymbol{u})(v_i - u_i)n_{b,j}\,ds \end{aligned} \tag{3.40}$$

Recall that $n_{b,j}$ is the outward unit normal of the bubble. Now on $\partial\Omega_w$ the veocities, v_i and u_i are defined to be zero. Thus the integral over $\partial\Omega_w$ in equation (3.40) vanishes. Futhermore, on the bubble surface, $\partial\Omega_b$, the traction must satisfy conditions (3.20)–(3.22). We can write

$$\begin{aligned} \int_{\partial\Omega_b} \sigma_{\ell,ij}(\boldsymbol{u})(v_i - u_i)n_{b,j}\,ds = \int_{\partial\Omega_b} \big[&\sigma_{\ell,n_b n_b}(\boldsymbol{u})(v_{n_b} - u_{n_b}) \\ &+ \sigma_{\ell,n_b t_1}(\boldsymbol{u})(v_{t_1} - u_{t_1}) + \sigma_{\ell,n_b t_2}(\boldsymbol{u})(v_{t_2} - u_{t_2})\big]\,ds. \end{aligned} \tag{3.41}$$

From (3.20) and (3.21) the last two terms are zero, and for the remaining term, using (3.22) we can write

$$\int_{\partial\Omega_b} \sigma_{\ell,ij}(\boldsymbol{u})(v_i - u_i)n_{b,j}\,ds = \int_{\partial\Omega_b} \left[-p_g + \beta\left(\frac{1}{R_1} + \frac{1}{R_2}\right)\right](v_{n_b} - u_{n_b})\,ds. \tag{3.42}$$

Now, since the velocity is zero along the cylinder walls,

$$\begin{aligned}\int_{\partial\Omega_b} -p_g(v_{n_b} - u_{n_b})\,ds &= \int_{\partial\Omega_b} p_g(v_i - u_i)(-n_{b,i})\,ds + \int_{\partial\Omega_w} p_g(v_i - u_i)n_i\,ds \\ &= \int_{\partial\Omega} p_g(v_i - u_i)(n_i)\,ds \\ &= \int_{\Omega} \nabla\cdot[p_g(v_i - u_i)]\,d\Omega \\ &= p_g \int_{\Omega} \nabla\cdot(v_i - u_i)\,d\Omega \\ &= 0 \qquad \text{(from incompressibility; see (3.2))}\end{aligned}$$

Thus the integral over the bubble surface, equation (3.42), reduces to

$$\int_{\partial\Omega_b} \sigma_{\ell,ij}(\boldsymbol{u})(v_i - u_i)n_{b,j}\,ds = \int_{\partial\Omega_b} \beta\left(\frac{1}{R_1} + \frac{1}{R_2}\right)(v_i - u_i)n_{b,i}\,ds \tag{3.43}$$

Finally, from equations (3.39) and (3.43), we arrive at the final variational inequality for the problem:

$$a(\boldsymbol{u}, \boldsymbol{v} - \boldsymbol{u}) + j(\boldsymbol{v}) - j(\boldsymbol{u}) \geq L(\boldsymbol{v} - \boldsymbol{u}) \qquad \forall \boldsymbol{v} \in V \tag{3.44}$$

where

$$a(\boldsymbol{u}, \boldsymbol{v}) = \frac{1}{2}\int_{\Omega} \dot{\boldsymbol{\gamma}}(\boldsymbol{u})^{n-1}\dot{\gamma}_{ij}(\boldsymbol{u})\dot{\gamma}_{ij}(\boldsymbol{v})\,d\Omega, \tag{3.45}$$

$$j(\boldsymbol{u}) = B\int_{\Omega} \dot{\boldsymbol{\gamma}}(\boldsymbol{u})\,d\Omega, \quad \text{and} \tag{3.46}$$

$$L(\boldsymbol{u}) = -\int_{\Omega} u_3\,d\Omega - \int_{\partial\Omega_b} \beta\left(\frac{1}{R_1} + \frac{1}{R_2}\right)u_i n_{b,i}\,ds. \tag{3.47}$$

It should be noted that $a(\cdot,\cdot)$ is linear in its second argument and $L(\cdot)$ is linear, while $j(\cdot)$ is non-linear. In some of the literature $a(\cdot,\cdot)$ is referred to as the viscous dissipation rate and $j(\cdot)$ is called the yield stress dissipation rate.

3.3.3 An Alternate Formulation

Equation (3.44) requires us to find a $\boldsymbol{u} \in V$ such that for all other $\boldsymbol{v} \in V$ the inequality (3.44) holds. Alternately we can formulate the problem as a pure minimization problem.

Consider the function

$$H(\boldsymbol{u}) = \frac{1}{n+1}a(\boldsymbol{u}, \boldsymbol{u}) = \frac{1}{2(n+1)}\int_{\Omega} \dot{\boldsymbol{\gamma}}(\boldsymbol{u})^{n-1}\dot{\gamma}_{ij}(\boldsymbol{u})\dot{\gamma}_{ij}(\boldsymbol{u})\,d\Omega. \tag{3.48}$$

The Gâteaux derivative of H in the direction $\boldsymbol{v}$ is

$$\delta H(\boldsymbol{u};\boldsymbol{v}) = \frac{1}{2}\int_\Omega \dot{\boldsymbol{\gamma}}(\boldsymbol{u})^{n-1}\dot{\gamma}_{ij}(\boldsymbol{u})\dot{\gamma}_{ij}(\boldsymbol{v})\,d\Omega \tag{3.49}$$

$$= a(\boldsymbol{u},\boldsymbol{v}). \tag{3.50}$$

Furthermore H is convex. Since H is Gâteaux differentiable and convex we have from [25] that

$$H(\boldsymbol{v}) - H(\boldsymbol{u}) \geq \delta H(\boldsymbol{u};\boldsymbol{v}-\boldsymbol{u})$$

$$\Rightarrow \frac{1}{n+1}a(\boldsymbol{v},\boldsymbol{v}) - \frac{1}{n+1}a(\boldsymbol{u},\boldsymbol{u}) \geq a(\boldsymbol{u},\boldsymbol{v}-\boldsymbol{u}) \tag{3.51}$$

Substituting (3.51) into (3.44) and recalling that $L(\cdot)$ is linear we obtain

$$\frac{1}{n+1}a(\boldsymbol{v},\boldsymbol{v}) - \frac{1}{n+1}a(\boldsymbol{u},\boldsymbol{u}) + j(\boldsymbol{v}) - j(\boldsymbol{u}) \geq L(\boldsymbol{v}) - L(\boldsymbol{u})$$

$$\Rightarrow \frac{1}{n+1}a(\boldsymbol{v},\boldsymbol{v}) + j(\boldsymbol{v}) - L(\boldsymbol{v}) \geq \frac{1}{n+1}a(\boldsymbol{u},\boldsymbol{u}) + j(\boldsymbol{u}) - L(\boldsymbol{u}) \qquad \forall \boldsymbol{v} \in V. \tag{3.52}$$

So the true velocity field, $\boldsymbol{u}$, distinguishes itself from all other velocity fields, $\boldsymbol{v} \in V$, in that $\boldsymbol{u}$ minimizes the functional

$$J(\boldsymbol{v}) \equiv \frac{1}{n+1}a(\boldsymbol{v},\boldsymbol{v}) + j(\boldsymbol{v}) - L(\boldsymbol{v}) \tag{3.53}$$

over the functional space V.

Also in equation (3.44), if we let $\boldsymbol{v} = 2\boldsymbol{u}$ then

$$a(\boldsymbol{u},\boldsymbol{u}) + j(\boldsymbol{u}) \geq L(\boldsymbol{u}), \tag{3.54}$$

where from equations (3.46) and (3.8) we have written $j(2\boldsymbol{u}) = 2j(\boldsymbol{u})$. Taking $\boldsymbol{v} = 0$ in equation (3.44) we obtain

$$-a(\boldsymbol{u},\boldsymbol{u}) - j(\boldsymbol{u}) \geq -L(\boldsymbol{u})$$

$$\Rightarrow a(\boldsymbol{u},\boldsymbol{u}) + j(\boldsymbol{u}) \leq L(\boldsymbol{u}). \tag{3.55}$$

Equation (3.54) and (3.55) imply that the true velocity field, $\boldsymbol{u}$, must satisfy

$$a(\boldsymbol{u},\boldsymbol{u}) + j(\boldsymbol{u}) = L(\boldsymbol{u}). \tag{3.56}$$

Thus, from (3.56), we also know the value of the functional J at the minimum:

$$J(\boldsymbol{u}) = -\frac{n}{n+1}a(\boldsymbol{u},\boldsymbol{u}). \tag{3.57}$$

3.3.4 Existence/Uniqueness

For the special case of $n = 1$ in the Herschel-Bulkley constitutive equations (3.5)–(3.6) (the case of a Bingham fluid), the variational equality (3.44) and the minimization problem (3.53) have a unique solution in the functional space. This is shown by directly applying Theorem 4.1 and Lemma 4.1 from chapter 1 of Glowinski [25]. For the case of $n \neq 1$, to the best of our knowledge, no general existence/uniqueness results exist. However, if existence can be shown, it is then easy to show uniqueness using the method used by Glowinski. Throughout we will assume that there exists a unique solution to (3.44) and (3.53).

3.4 Stress Maximization Principle

The earlier result, (3.53), derived from the variational inequality is also known as a rate of strain minimization. Similarly there is another formulation that leads to a stress maximization principle. Consider a stress field $\tilde{\sigma}_{\ell,ij}$.

We say that the stress field $\tilde{\sigma}_{\ell,ij} = -\tilde{p_\ell}\delta ij + \tilde{\tau}_{\ell,ij}$ or equivalently the pair $(\tilde{p_\ell}, \tilde{\tau}_{\ell,ij})$ is admissible if

$$0 = -\frac{\partial \tilde{p}_\ell}{\partial x_i} + \frac{\partial \tilde{\tau}_{\ell,ij}}{\partial x_j} - \delta_{i3} \qquad \text{in } \Omega, \tag{3.58}$$

$$\tilde{\tau}_{\ell,n_b t_1} = 0 \qquad \text{on } \partial\Omega_b, \tag{3.59}$$

$$\tilde{\tau}_{\ell,n_b t_2} = 0 \qquad \text{on } \partial\Omega_b, \tag{3.60}$$

$$-\tilde{p_\ell} + \tilde{\tau}_{\ell,n_b n_b} = -p_g + \beta\left(\frac{1}{R_1} + \frac{1}{R_2}\right) \qquad \text{on } \partial\Omega_b. \tag{3.61}$$

Let T denote the set of all admissible $(\tilde{p_\ell}, \tilde{\tau}_{\ell,ij})$.

Theorem: If u_i is the actual solution of the classical problem, then the true stress field, $\tau_{\ell,ij}$, maximizes the functional

$$F(\tilde{\tau}_{\ell,ij}) = -\frac{1}{2^{\frac{1}{n}+1}}\frac{n}{n+1}\int_\Omega (|\tilde{\boldsymbol{\tau}}_\ell - B| + \tilde{\boldsymbol{\tau}}_\ell - B)^{\frac{1}{n}+1}\, d\Omega + \int_\Omega \tilde{\tau}_{\ell,ij}\dot{\gamma}_{ij}(\boldsymbol{u})\, d\Omega, \qquad \forall\, (\tilde{p_\ell}, \tilde{\tau}_{\ell,ij}) \in T. \tag{3.62}$$

Proof: The proof is taken from [30], suitably modified.

$$F(\tau_{\ell,ij}) - F(\tilde{\tau}_{\ell,ij}) = \int_\Omega \frac{1}{2^{\frac{1}{n}+1}} \frac{n}{n+1} \left[(|\tilde{\boldsymbol{\tau}}_\ell - B| + \tilde{\boldsymbol{\tau}}_\ell - B)^{\frac{1}{n}+1} - (|\boldsymbol{\tau}_\ell - B| + \boldsymbol{\tau}_\ell - B)^{\frac{1}{n}+1} \right] d\Omega$$
$$- \int_\Omega (\tilde{\tau}_{\ell,ij} - \tau_{\ell,ij}) \dot{\gamma}_{ij}(\boldsymbol{u})\, d\Omega \quad (3.63)$$

Consider the integrand

$$I = \frac{1}{2^{\frac{1}{n}+1}} \frac{n}{n+1} \left[(|\tilde{\boldsymbol{\tau}}_\ell - B| + \tilde{\boldsymbol{\tau}}_\ell - B)^{\frac{1}{n}+1} - (|\boldsymbol{\tau}_\ell - B| + \boldsymbol{\tau}_\ell - B)^{\frac{1}{n}+1} \right] - (\tilde{\tau}_{\ell,ij} - \tau_{\ell,ij}) \dot{\gamma}_{ij}(\boldsymbol{u}).$$

We will show that at any point in Ω, $I \geq 0$, and thus the integral (3.63) is greater than or equal to zero.

The constitutive equations for a Herschel-Bulkley fluid can also be written as

$$\dot{\gamma}_{ij} = 0 \qquad \text{if } \boldsymbol{\tau}_\ell \leq B \quad (3.64)$$

$$\dot{\gamma}_{ij} = (\boldsymbol{\tau}_\ell - B)^{\frac{1}{n}} \frac{\tau_{\ell,ij}}{\boldsymbol{\tau}_\ell} \qquad \text{if } \boldsymbol{\tau}_\ell > B \quad (3.65)$$

Case 1: $\dot{\gamma}_{ij} = 0 \Rightarrow \boldsymbol{\tau}_\ell \leq B$

Then

$$I = \frac{1}{2^{\frac{1}{n}+1}} \frac{n}{n+1} (|\tilde{\boldsymbol{\tau}}_\ell - B| + \tilde{\boldsymbol{\tau}}_\ell - B)^{\frac{1}{n}+1} \geq 0.$$

Case 2: $\dot{\boldsymbol{\gamma}} > 0 \Rightarrow \boldsymbol{\tau}_\ell > B$

Then using (3.65),

$$I = \frac{1}{2^{\frac{1}{n}+1}} \frac{n}{n+1} \left[(|\tilde{\boldsymbol{\tau}}_\ell - B| + \tilde{\boldsymbol{\tau}}_\ell - B)^{\frac{1}{n}+1} - (|\boldsymbol{\tau}_\ell - B| + \boldsymbol{\tau}_\ell - B)^{\frac{1}{n}+1} \right]$$
$$- (\boldsymbol{\tau}_\ell - B)^{\frac{1}{n}} (\tilde{\tau}_{\ell,ij} - \tau_{\ell,ij}) \frac{\tau_{\ell,ij}}{\boldsymbol{\tau}_\ell}. \quad (3.66)$$

Case 2a: $\tilde{\boldsymbol{\tau}}_\ell > B$

Since we also have $\boldsymbol{\tau}_\ell > B$, (3.66) simplifies to

$$I = \frac{n}{n+1} \left[(\tilde{\boldsymbol{\tau}}_\ell - B)^{\frac{1}{n}+1} - (\boldsymbol{\tau}_\ell - B)^{\frac{1}{n}+1} \right] - (\boldsymbol{\tau}_\ell - B)^{\frac{1}{n}} (\tilde{\tau}_{\ell,ij} - \tau_{\ell,ij}) \frac{\tau_{\ell,ij}}{\boldsymbol{\tau}_\ell}. \quad (3.67)$$

For all $\tilde{\tau}_{\ell,ij}$ of a fixed magnitude I is minimized when $\tilde{\tau}_{\ell,ij} \parallel \tau_{\ell,ij}$, i.e., $\tilde{\tau}_{\ell,ij} = \lambda\tau_{\ell,ij}$. We can also write

$$\boldsymbol{\tau}_\ell = \theta B \tag{3.68}$$

for some $\theta > 1$. Similarly,

$$\tilde{\boldsymbol{\tau}}_\ell = \lambda\boldsymbol{\tau}_\ell = \lambda\theta B, \tag{3.69}$$

where $\lambda\theta > 1$.

Substituting (3.68), (3.69), and $\tilde{\tau}_{\ell,ij} = \lambda\tau_{\ell,ij}$ into (3.67) we obtain

$$I \geq I^*(\lambda) = B^{\frac{1}{n}+1}\left[\frac{n}{n+1}\left((\lambda\theta-1)^{\frac{1}{n}+1} - (\theta-1)^{\frac{1}{n}+1}\right) - \theta(\theta-1)^{\frac{1}{n}}(\lambda-1)\right].$$

Looking for the minimum of $I^*(\lambda)$,

$$\frac{dI^*}{d\lambda} = B^{\frac{1}{n}+1}\left[\theta(\lambda\theta-1)^{\frac{1}{n}} - \theta(\theta-1)^{\frac{1}{n}}\right] = 0$$

when $\lambda = 1$. Also

$$\frac{d^2I^*}{d\lambda^2} = \frac{1}{n}B^{\frac{1}{n}+1}\theta^2(\lambda\theta-1)^{\frac{1}{n}-1} > 0$$

since $\lambda\theta > 1$. Thus $I^*(\lambda)$ is minimized at $\lambda = 1$. Therefore

$$I \geq I^*(1) = 0.$$

Case 2b: $\tilde{\boldsymbol{\tau}}_\ell \leq B$

Also $\boldsymbol{\tau}_\ell > B$, so (3.66) simplifies to

$$I = -\frac{n}{n+1}(\boldsymbol{\tau}_\ell - B)^{\frac{1}{n}+1} - (\boldsymbol{\tau}_\ell - B)^{\frac{1}{n}}(\tilde{\tau}_{\ell,ij} - \tau_{\ell,ij})\frac{\tau_{\ell,ij}}{\boldsymbol{\tau}_\ell}. \tag{3.70}$$

Again for all $\tilde{\tau}_{\ell,ij}$ of a fixed magnitude I is minimized when $\tilde{\tau}_{\ell,ij} \parallel \tau_{\ell,ij}$, i.e., $\tilde{\tau}_{\ell,ij} = \lambda\tau_{\ell,ij}$. We can again write

$$\boldsymbol{\tau}_\ell = \theta B \tag{3.71}$$

for some $\theta > 1$. Similarly,

$$\tilde{\boldsymbol{\tau}}_\ell = \lambda\boldsymbol{\tau}_\ell = \lambda\theta B, \tag{3.72}$$

where $\lambda\theta \leq 1$.

Substituting (3.71), (3.72), and $\tilde{\tau}_{\ell,ij} = \lambda\tau_{\ell,ij}$ into (3.70) we obtain

$$I \geq I^*(\lambda) = B^{\frac{1}{n}+1}\left[\frac{n}{n+1}(\theta-1)^{\frac{1}{n}+1} - \theta(\theta-1)^{\frac{1}{n}}(\lambda-1)\right].$$

$I^*(\lambda)$ is linear in λ and decreases as λ increases. The maximum allowable value of λ is restricted by

$$\lambda\theta \leq 1 \Rightarrow \lambda \leq \frac{1}{\theta}$$

Thus $I^*(\lambda)$ is minimized at $\lambda = \frac{1}{\theta}$. Therefore

$$\begin{aligned} I \geq I^*\left(\frac{1}{\theta}\right) &= \frac{1}{n+1}B^{\frac{1}{n}+1}(\theta-1)^{\frac{1}{n}+1} \\ &\geq 0, \end{aligned}$$

since $\theta > 1$. □

The above proof does not make use of any the conditions of an admissible stress field. Using these conditions, we can obtain a useful relation. The derivation of the relation is almost exactly the same as the derivation at the beginning of section 3.3.2. The admissible stress field satisfies (3.58) and the fluid is incompressible (i.e., $\frac{\partial u_i}{\partial x_i} = 0$), so for the true velocity field u_i, we have

$$\begin{aligned} 0 &= -\frac{\partial \tilde{p_\ell}}{\partial x_i}u_i - u_3 + \frac{\partial \tilde{\tau}_{\ell,ij}}{\partial x_j}u_i \\ \Rightarrow 0 &= -\frac{\partial}{\partial x_i}(\tilde{p_\ell}u_i) - u_3 + \frac{\partial}{\partial x_j}(\tilde{\tau}_{\ell,ij}u_i) - \tilde{\tau}_{\ell,ij}\frac{\partial u_i}{\partial x_j}. \end{aligned} \tag{3.73}$$

Since $\tilde{\tau}_{\ell,ij}$ is symmetric (see section 3.3.2, equation (3.34)),

$$\tilde{\tau}_{\ell,ij}\frac{\partial u_i}{\partial x_j} = \frac{1}{2}\tilde{\tau}_{\ell,ij}\dot{\gamma}_{ij}(\boldsymbol{u}). \tag{3.74}$$

Combining (3.73) and (3.74), we have

$$\frac{1}{2}\tilde{\tau}_{\ell,ij}\dot{\gamma}_{ij}(\boldsymbol{u}) = -u_3 + \frac{\partial}{\partial x_j}[(-\tilde{p}_\ell\delta_{ij} + \tilde{\tau}_{\ell,ij})u_i].$$

Integrating this equation over the domain Ω, and applying the divergence theorem to the last term, we obtain

$$\frac{1}{2}\int_\Omega \tilde{\tau}_{\ell,ij}\dot{\gamma}_{ij}(\boldsymbol{u})\,d\Omega = -\int_\Omega u_3\,d\Omega - \int_{\partial\Omega_b}(-\tilde{p}_\ell\delta_{ij} + \tilde{\tau}_{\ell,ij})u_i n_{b,j}\,ds. \tag{3.75}$$

The sign in front of the last term changes since we have changed from the outward normal of Ω on the bubble interface to the outward normal of the bubble; $n_{b,i} = -n_i$ on $\partial\Omega_b$, where n_i is the outward normal of Ω. On the bubble surface, we consider a local coordinate system, $\{\boldsymbol{n_b}, \boldsymbol{t_1}, \boldsymbol{t_2}\}$, with one axis, $(\boldsymbol{n_b})$, perpendicular to the surface of the bubble. Then

$$\begin{aligned}\int_{\partial\Omega_b} (-\tilde{p}_\ell \delta_{ij} + \tilde{\tau}_{\ell,ij}) u_i n_{b,j}\, ds &= \int_{\partial\Omega_b} (-\tilde{p}_\ell \delta_{in_b} + \tilde{\tau}_{\ell,in_b}) u_i ds \\ &= \int_{\partial\Omega_b} [(-\tilde{p}_\ell + \tilde{\tau}_{\ell,n_b n_b}) u_{n_b} + \tilde{\tau}_{\ell,t_1 n_b} u_{t_1} + \tilde{\tau}_{\ell,t_2 n_b} u_{t_2}]\, ds. \end{aligned} \tag{3.76}$$

From the conditions for an admissible stress field (3.59), (3.60), and (3.61) we can write

$$\int_{\partial\Omega_b} (-p_\ell \delta_{ij} + \tilde{\tau}_{\ell,ij}) u_i n_{b,j}\, ds = \int_{\partial\Omega_b} \left[-p_g + \beta \left(\frac{1}{R_1} + \frac{1}{R_2} \right) \right] u_i n_{b,i}\, ds \tag{3.77}$$

Now since the velocity is zero along the cylinder walls and the pressure in the bubble is constant (see (3.17)),

$$\begin{aligned}\int_{\partial\Omega_b} -p_g u_i n_{b,i}\, ds &= \int_{\partial\Omega_b} p_g u_i (-n_{b,i})\, ds + \int_{\partial\Omega_w} p_g u_i n_i\, ds \\ &= \int_{\partial\Omega} p_g u_i n_i\, ds \\ &= \int_\Omega \frac{\partial}{\partial x_i} (p_g u_i) d\Omega \\ &= p_g \int_\Omega \frac{\partial u_i}{\partial x_i}\, d\Omega \\ &= 0. \qquad \text{(from incompressibility; see (3.2)).}\end{aligned}$$

Thus combining this result with (3.77), (3.75) becomes

$$\frac{1}{2} \int_\Omega \tilde{\tau}_{\ell,ij} \dot{\gamma}_{ij}(\boldsymbol{u})\, d\Omega = -\int_\Omega u_3\, d\Omega - \int_{\partial\Omega_b} \beta \left(\frac{1}{R_1} + \frac{1}{R_2} \right) u_i n_{b,i}\, ds. \tag{3.78}$$

Therefore we can we can write the functional (3.62) as

$$\begin{aligned}F(\tilde{\tau}_{\ell,ij}) = -\frac{1}{2^{\frac{1}{n}+1}} \frac{n}{n+1} \int_\Omega (|\tilde{\boldsymbol{\tau}}_\ell - B| + \tilde{\boldsymbol{\tau}}_\ell - B)^{\frac{1}{n}+1}\, d\Omega \\ - 2\int_\Omega u_3\, d\Omega - 2\int_{\partial\Omega_b} \beta \left(\frac{1}{R_1} + \frac{1}{R_2} \right) u_i n_{b,i}\, ds.\end{aligned} \tag{3.79}$$

The last two terms on the right-hand side of (3.79) are constant for a given bubble, only the first term depends on $\tilde{\tau}_{\ell,ij}$. Thus the stress minimization principle can be stated as: For a bubble of given volume and fixed shape, the true stress field maximizes the functional

$$G(\tilde{\tau}_{\ell,ij}) = -\frac{1}{2^{\frac{1}{n}+1}} \frac{n}{n+1} \int_{\Omega} (|\tilde{\boldsymbol{\tau}}_{\ell} - B| + \tilde{\boldsymbol{\tau}}_{\ell} - B)^{\frac{1}{n}+1} \, d\Omega, \qquad \forall \, (\tilde{p_{\ell}}, \tilde{\tau}_{\ell,ij}) \in T. \tag{3.80}$$

Chapter 4
Stopping Condition Results

We are primarily concerned with slow moving and stopped bubbles, and conditions which determine whether a given bubble will propagate in the viscoplatic fluid or will become trapped. In this chapter we use the variational results of the previous chapter to derive conditions under which a bubble will not move.

4.1 First Stopping Condition

4.1.1 Condition On B For No Motion

From our variational formulation we have that the actual velocity field, $\boldsymbol{u}$, satisfies the equality (3.56). The term

$$a(\boldsymbol{u},\boldsymbol{u}) \equiv \frac{1}{2}\int_\Omega \dot{\boldsymbol{\gamma}}(\boldsymbol{u})^{n-1}\dot{\gamma}_{ij}(\boldsymbol{u})\dot{\gamma}_{ij}(\boldsymbol{u})\,d\Omega \geq 0$$

so we have the inequality

$$j(\boldsymbol{u}) \leq L(\boldsymbol{u})$$

Thus, in a situation where the actual solution velocity is non-zero

$$B\int_\Omega \dot{\boldsymbol{\gamma}}(\boldsymbol{u})\,d\Omega \leq -\int_\Omega u_3\,d\Omega - \int_{\partial\Omega_b}\beta\left(\frac{1}{R_1}+\frac{1}{R_2}\right)u_i n_{b,i}\,ds,$$

$$B \leq -\frac{\int_\Omega u_3\,d\Omega}{\int_\Omega \dot{\boldsymbol{\gamma}}(\boldsymbol{u})\,d\Omega} - \frac{\int_{\partial\Omega_b}\beta\left(\frac{1}{R_1}+\frac{1}{R_2}\right)u_i n_{b,i}\,ds}{\int_\Omega \dot{\boldsymbol{\gamma}}(\boldsymbol{u})\,d\Omega}. \tag{4.1}$$

Or equivalently, for

$$B \geq \sup_{all\ \boldsymbol{v}\in V}\left\{-\frac{\int_\Omega v_3\,d\Omega}{\int_\Omega \dot{\boldsymbol{\gamma}}(\boldsymbol{v})\,d\Omega} - \frac{\int_{\partial\Omega_b}\beta\left(\frac{1}{R_1}+\frac{1}{R_2}\right)v_i n_{b,i}\,ds}{\int_\Omega \dot{\boldsymbol{\gamma}}(\boldsymbol{v})\,d\Omega}\right\} \tag{4.2}$$

the only possible solution is one with $\boldsymbol{u} = 0$ identically over Ω. These results hold in general for any arbitrary bubble shape and bubble velocity. Using (4.1) we could, for example, determine, for a given Bingham number (and a given volume), shapes that will not move, if such shapes exist. From (4.2) we could find, for a given bubble (shape and volume), an estimate of the "critical" Bingham number, above which the bubble will not move. From this point on we will restrict our attention to steadily moving axisymmetric bubbles.

4.1.2 Surface Integral Term

Consider an axisymmetric bubble moving along the axis of symmetry in a cylindrical column, as depicted in figure 4.1. The radius of the bubble at a height z is given by the function $r = f(z)$,

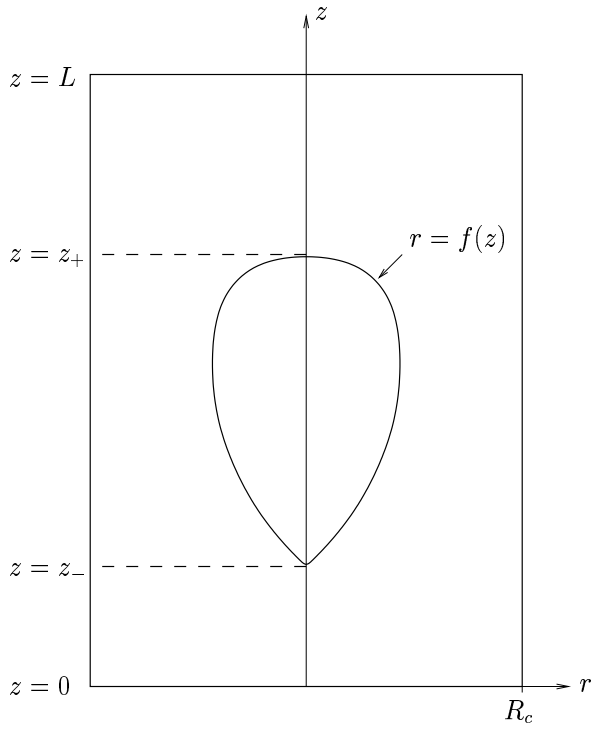

Figure 4.1: Axisymmetric bubble centred in the column.

with $f(z) = 0$ for $z \geq z_+$ and for $z \leq z_-$.

The second term in (4.1),

$$\frac{\int_{\partial\Omega_b} \beta \left(\frac{1}{R_1} + \frac{1}{R_2}\right) u_i n_{b,i}\, ds}{\int_\Omega \dot{\boldsymbol{\gamma}}(\boldsymbol{u})\, d\Omega} \tag{4.3}$$

involves an integral of the mean curvature of the bubble over the surface of the bubble and is, therefore, explicitly dependent on the shape of the bubble. For the analysis of this term we make use of some basic differential geometry results, taken from [31], to obtain an expression for the mean curvature in terms of the functional shape of the bubble. The calculation of these results are contained in Appendix B.

In this derivation we assume that we have an axisymmetric steady bubble travelling along the axis of symmetry of the column. In this case the curvature of the bubble is only a function of z. Let

$$\alpha(z) = \beta\left(\frac{1}{R_1} + \frac{1}{R_2}\right).$$

Then, using incompressibility, we can write

$$\frac{\partial}{\partial x_i}(\alpha(z)u_i) = u_i\frac{\partial \alpha(z)}{\partial x_i} = u_3\frac{\partial \alpha(z)}{\partial z}. \tag{4.4}$$

Integrating (4.4) over a small horizontal slice of fluid, as depicted in figure 4.2, and applying

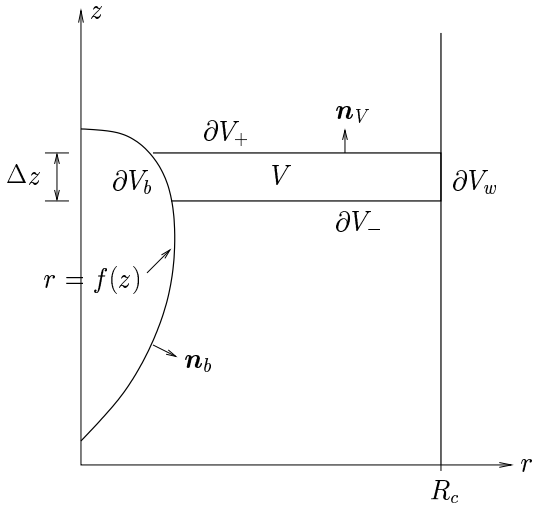

Figure 4.2: Annular slice of volume, V, over which we are integrating.

the divergence theorem to the left hand side we obtain

$$\int_{\partial V} \alpha(z)u_i n_{V,i} ds = \int_V u_3\frac{\partial \alpha(z)}{\partial z} dv, \tag{4.5}$$

where $n_{V,i}$ is the outward unit normal of the fluid element V. It should be noted that for the portion of ∂V that lies on the bubble surface, $n_{V,i}$ has opposite direction to $n_{b,i}$, the outward

unit normal of the bubble. Expanding the left hand side of (4.5) into the separate sections of of ∂V we have

$$\int_{\partial V_b} \alpha(z) u_i n_{V,i} ds + \int_{\partial V_+} \alpha(z) u_i n_{V,i} ds + \int_{\partial V_-} \alpha(z) u_i n_{V,i} ds + \int_{\partial V_w} \alpha(z) u_i n_{V,i} ds = \int_V u_3 \frac{\partial \alpha(z)}{\partial z} dv$$

$$\int_z^{z+\Delta z} 2\pi\alpha(z) f(z) \sqrt{1 + (f'(z))^2}\, u_i n_{V,i} dz + \int_{\partial V_+} \alpha(z) u_3 ds - \int_{\partial V_-} \alpha(z) u_3 ds + 0 = \int_V u_3 \frac{\partial \alpha(z)}{\partial z} dv.$$

Here we have used the result (B.13) from Appendix B. Dividing by Δz and taking the limit as $\Delta z \to 0^+$,

$$2\pi\alpha(z) f(z) \sqrt{1 + (f'(z))^2}\, u_i n_{V,i} + \frac{\partial}{\partial z}\left(\int_S \alpha(z) u_3 ds\right) = \frac{\partial \alpha(z)}{\partial z} \int_S u_3 ds$$

$$\Rightarrow 2\pi\alpha(z) f(z) \sqrt{1 + (f'(z))^2}\, u_i n_{V,i} = -\alpha(z) \frac{\partial}{\partial z}\left(\int_S u_3 ds\right), \tag{4.6}$$

where S is the horizontal surface at height z that passes though the fluid region (see figure 4.3).

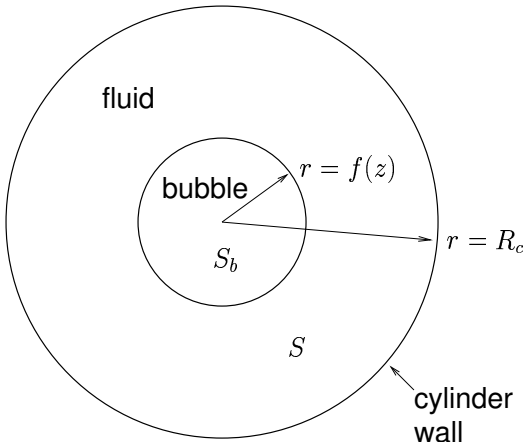

Figure 4.3: Top view of the horizontal cross section S and S_b.

Now for the entire cross section of the column, $S \cup S_b$, shown in figure 4.3, the flux through this surface must be zero. In fact, across any complete cross section of the column the flux must be

zero. Thus

$$\int_S u_3\,ds + \int_{S_b} u_{b,3}\,ds = 0$$

$$\frac{\partial}{\partial z}\left(\int_S u_3\,ds + \int_{S_b} u_{b,3}\,ds\right) = 0$$

$$\Rightarrow \frac{\partial}{\partial z}\left(\int_S u_3\,ds\right) = -\frac{\partial}{\partial z}\left(\int_{S_b} u_{b,3}\,ds\right), \tag{4.7}$$

where $u_{b,3}$ is the vertical component of the velocity of the bubble surface at a given point. For a steady bubble (i.e., for a constant interface shape and constant interface velocity), $u_{b,3}$ is just the constant bubble rise velocity which we denote U_b. Then

$$\int_{S_b} u_{b,3}\,ds = U_b \int_{S_b} (1) ds$$

$$= U_b \times (\text{cross sectional area of bubble}).$$

For an axisymmetric bubble with profile $r = f(z)$, as in figure 4.1, the cross sectional area is $\pi(f(z))^2$. So from (4.7),

$$\begin{aligned}\frac{\partial}{\partial z}\left(\int_S u_3\,ds\right) &= -\frac{\partial}{\partial z}\left(\pi U_b (f(z))^2\right) \\ &= -2\pi U_b f(z) f'(z)\end{aligned} \tag{4.8}$$

Combining (4.8) with (4.6),

$$2\pi\alpha(z) f(z)\sqrt{1+(f'(z))^2}\,u_i n_{V,i} = 2\pi U_b \alpha(z) f(z) f'(z)$$

$$\Rightarrow \alpha(z) u_i n_{b,i} = -\frac{U_b \alpha(z) f'(z)}{\sqrt{1+(f'(z))^2}} \tag{4.9}$$

Using the result (B.12) from Appendix B, for the mean curvature of an axisymmetric surface,

$$\alpha(z) = \beta\left(\frac{1}{R_1} + \frac{1}{R_2}\right) = -\beta\frac{f''f - (f')^2 - 1}{f\left((f')^2+1\right)^{\frac{3}{2}}} \tag{4.10}$$

where $f = f(z)$. Also since there is no net flow out of the cylinder

$$\begin{aligned}\int_\Omega u_3\,d\Omega &= -\int_{\Omega_b} u_{b,3}\,d\Omega \\ &= -U_b \int_{\Omega_b} (1)\,d\Omega \\ &= -U_b V_b \\ \Rightarrow U_b &= -\frac{1}{V_b}\int_\Omega u_3\,d\Omega\end{aligned} \tag{4.11}$$

where V_b is the volume of the bubble.

From (4.9), (4.10), and (4.11),

$$\int_{\partial\Omega_b} \beta\left(\frac{1}{R_1}+\frac{1}{R_2}\right) u_i n_{b,i}\, ds = -\frac{\beta}{V_b}\left(\int_\Omega u_3\, d\Omega\right)\int_{\partial\Omega_b} \frac{f'(f''f-(f')^2-1)}{f\left((f')^2+1\right)^2}\, ds \tag{4.12}$$

From Appendix B the surface integral over the bubble is given by (B.13),

$$\int_{\partial\Omega_b} ds = \int_0^{2\pi}\int_{z_-}^{z_+} f\sqrt{(f')^2+1}\, dz\, d\theta. \tag{4.13}$$

Therefore (4.12) simplifies to

$$\int_{\partial\Omega_b} \beta\left(\frac{1}{R_1}+\frac{1}{R_2}\right) u_i n_{b,i}\, ds = -\frac{2\pi\beta}{V_b}\left(\int_\Omega u_3\, d\Omega\right)\int_{z_-}^{z_+} \frac{f'(f''f-(f')^2-1)}{\left((f')^2+1\right)^{\frac{3}{2}}}\, dz \tag{4.14}$$

4.1.3 Bubbles Which Never Move

Substituting the expression (4.14) into (4.1) we obtain the result that for a non-zero solution to exist

$$\begin{aligned} B &\le -\frac{\int_\Omega u_3\, d\Omega}{\int_\Omega \dot{\boldsymbol{\gamma}}(\boldsymbol{u})\, d\Omega} + \frac{2\pi\beta}{V_b}\left(\frac{\int_\Omega u_3\, d\Omega}{\int_\Omega \dot{\boldsymbol{\gamma}}(\boldsymbol{u})\, d\Omega}\right)\int_{z_-}^{z_+} \frac{f'(f''f-(f')^2-1)}{\left((f')^2+1\right)^{\frac{3}{2}}}\, dz \\ B &\le -\frac{\int_\Omega u_3\, d\Omega}{\int_\Omega \dot{\boldsymbol{\gamma}}(\boldsymbol{u})\, d\Omega}\left(1-\frac{2\pi\beta}{V_b}\int_{z_-}^{z_+} \frac{f'(f''f-(f')^2-1)}{\left((f')^2+1\right)^{\frac{3}{2}}}\, dz\right) \end{aligned} \tag{4.15}$$

For a stationary or upward moving bubble, the net flux of fluid through any horizontal surface must be less than or equal to zero. So if the bubble is actually moving upwards the integral of the vertical velocity will be strictly negative (and equal to $-U_b V_b$). Also $\dot{\boldsymbol{\gamma}}(\boldsymbol{u})$ is always greater than or equal to zero. And for a bubble that is moving (i.e., that has yielded the fluid in some region) the integral of $\dot{\boldsymbol{\gamma}}(\boldsymbol{u})$ over Ω will be strictly positive. Therefore the term $-\frac{\int_\Omega u_3\, d\Omega}{\int_\Omega \dot{\boldsymbol{\gamma}}(\boldsymbol{u})\, d\Omega}$ in (4.15) is strictly positive. So if

$$1-\frac{2\pi\beta}{V_b}\int_{z_-}^{z_+} \frac{f'(f''f-(f')^2-1)}{\left((f')^2+1\right)^{\frac{3}{2}}}\, dz \le 0 \tag{4.16}$$

then it is impossible for (4.15), and hence (4.1) to be true, and thus the only possible solution is one which is identically zero.

The expression in (4.16) can, in theory, be made to be less than or equal to zero if the shape of the bubble is such that the integral

$$S = \int_{z-}^{z+} \frac{f'(f''f - (f')^2 - 1)}{\left((f')^2 + 1\right)^{\frac{3}{2}}}\, dz \tag{4.17}$$

is sufficiently large. It should be noted that mathematically it is always possible to construct a shape for which this term is positive. For a given shape, if S is not positive, then reflecting the shape in a horizontal plane would change the sign of the integral, resulting in a positive value. (Essentially we are applying the transformation $z \to -z \Rightarrow f \to f$, $f' \to -f'$, and $f'' \to f''$, which we can see changes the sign of S.)

To show that in practice it is also possible to have both negative and positive values of the surface integral term, S, in figure 4.4 we show two actual bubble profiles (bubble velocity is upwards) for which S has opposite sign.

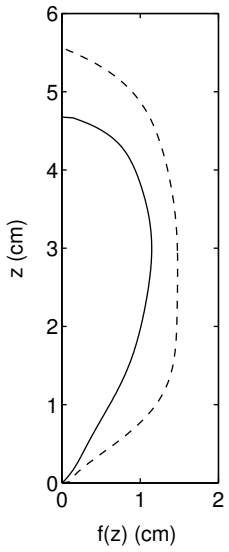

Figure 4.4: Two bubble profiles. For the solid line $S = -0.010$, and for the dashed line $S = 0.012$ (S is nondimensional).

4.1.4 Bounding $-\frac{\int_\Omega u_3\, d\Omega}{\int_\Omega \dot{\gamma}(u)\, d\Omega}$

We can use the result of the previous section to determine which shapes of bubbles will not propagate for a given yield stress. Another problem of interest is the opposite problem: for

what yield stress will a given bubble no longer propagate. For this problem we use the stopping condition (4.2). Including the result (4.14), condition (4.2) becomes

$$B \geq \sup_{all\, \boldsymbol{v}} \left\{ -\frac{\int_\Omega u_3 \, d\Omega}{\int_\Omega \dot{\boldsymbol{\gamma}}(\boldsymbol{u}) \, d\Omega} \left(1 - \frac{2\pi\beta}{V_b} \int_{z_-}^{z_+} \frac{f'(f''f - (f')^2 - 1)}{\left((f')^2 + 1\right)^{\frac{3}{2}}} \, dz \right) \right\} \tag{4.18}$$

In order to use (4.18) we need to find an upper bound for the term

$$\frac{-\int_\Omega u_3 \, d\Omega}{\int_\Omega \dot{\boldsymbol{\gamma}}(\boldsymbol{u}) \, d\Omega}. \tag{4.19}$$

While we could use our previous result that $-\int_\Omega u_3 \, d\Omega = U_b V_b$, we instead relate $\int_\Omega u_3 \, d\Omega$ to $\int_\Omega \dot{\boldsymbol{\gamma}}(\boldsymbol{u}) \, d\Omega$ so that we can obtain a uniform upper bound that does not change as we move to the limit of a stopped bubble. To do this we consider the fluid domain Ω divided into three regions: the fluid above z_+, the fluid below z_- and the fluid between z_- and z_+.

For the fluid above z_+

$$u_3 = \int_L^z \frac{\partial u_3}{\partial \tilde{z}}(x, y, \tilde{z}) \, d\tilde{z}.$$

This follows from the fundamental theorem of calculus and the fact that $\boldsymbol{u} = 0$ (in particular $u_3 = 0$) at the top wall of the cylinder (i.e., at $z = L$). So for a horizontal cross section at height $z > z_+$

$$\begin{aligned} \int_{x,y} u_3 \, dx \, dy &= \int_{x,y} \left(\int_L^z \frac{\partial u_3}{\partial \tilde{z}}(x, y, \tilde{z}) \, d\tilde{z} \right) dx \, dy \\ &= \int_L^z \left(\int_{x,y} \frac{\partial u_3}{\partial \tilde{z}}(x, y, \tilde{z}) \, dx \, dy \right) d\tilde{z} \\ &= \int_L^z \frac{\partial}{\partial \tilde{z}} \left(\int_{x,y} u_3(x, y, \tilde{z}) \, dx \, dy \right) d\tilde{z}. \end{aligned} \tag{4.20}$$

The integral over x, y is simply the net flux through a horizontal cross section. Since the fluid is incompressible, we must have conservation of volume in the region above this plane. Thus the net flux across this plane must be zero:

$$\int_{x,y} u_3 \, dx \, dy = 0. \tag{4.21}$$

Similarly for the fluid below z_-

$$u_3 = \int_0^z \frac{\partial u_3}{\partial \tilde{z}}(x, y, \tilde{z}) \, d\tilde{z}.$$

For a cross section at a height $z < z_-$, using conservation of mass of the fluid below the surface,

$$\begin{aligned}\int_{x,y} u_3\,dx\,dy &= \int_{x,y}\left(\int_0^z \frac{\partial u_3}{\partial \tilde{z}}(x,y,\tilde{z})\,d\tilde{z}\right)\,dx\,dy \\ &= \int_0^z \left(\int_{x,y} \frac{\partial u_3}{\partial \tilde{z}}(x,y,\tilde{z})\,dx\,dy\right)\,d\tilde{z} \\ &= \int_0^z \frac{\partial}{\partial \tilde{z}}\left(\int_{x,y} u_3(x,y,\tilde{z})\,dx\,dy\right)\,d\tilde{z} \\ \Rightarrow \int_{x,y} u_3\,dx\,dy &= 0. \end{aligned} \tag{4.22}$$

Thus the only contribution to the numerator (4.19) is from the fluid between z_+ and z_-. So

$$\int_\Omega u_3\,d\Omega = \int_{z_-}^{z_+}\left(\int_{f(z)^2\le x^2+y^2\le R_c^2} u_3(x,y,z)\,dx\,dy\right)\,dz. \tag{4.23}$$

To relate this to the rate of strain we again use the fundamental theorem of calculus to write the velocity in terms of its derivative, and then relate the derivative to the (second invariant of the) rate of strain. Let $z_{\frac{1}{2}} = \frac{z_+ + z_-}{2}$ be the midpoint of the bubble length and let Ω_+ be the region of Ω above $z_{\frac{1}{2}}$ and Ω_- be the region of Ω below $z_{\frac{1}{2}}$, then for $z \ge z_{\frac{1}{2}}$ we have

$$\begin{aligned}\int_{f(z)^2\le x^2+y^2\le R_c^2} u_3\,dx\,dy &= \int_{x,y}\left(\int_{z_{\frac{1}{2}}}^z \frac{\partial u_3}{\partial \tilde{z}}(x,y,\tilde{z})\,d\tilde{z}\right)\,dx\,dy \\ &\le \int_{z_{\frac{1}{2}}}^z \left(\int_{f(\tilde{z})^2\le x^2+y^2\le R_c^2}\left|\frac{\partial u_3}{\partial \tilde{z}}(x,y,\tilde{z})\right|\,dx\,dy\right)\,d\tilde{z} \\ &\le \int_{z_{\frac{1}{2}}}^z \left(\int_{f(\tilde{z})^2\le x^2+y^2\le R_c^2} \frac{1}{\sqrt{2}}\dot{\boldsymbol{\gamma}}(\boldsymbol{u}(x,y,\tilde{z}))\,dx\,dy\right)\,d\tilde{z} \\ &\le \frac{1}{\sqrt{2}}\int_{z_{\frac{1}{2}}}^L \left(\int_{f(\tilde{z})^2\le x^2+y^2\le R_c^2} \dot{\boldsymbol{\gamma}}(\boldsymbol{u}(x,y,\tilde{z}))\,dx\,dy\right)\,d\tilde{z} \\ &= \frac{1}{\sqrt{2}}\int_{\Omega_+}\dot{\boldsymbol{\gamma}}(\boldsymbol{u})\,d\Omega. \end{aligned}$$

Similarly for $z < z_{\frac{1}{2}}$ we have

$$\int_{f(z)^2\le x^2+y^2\le R_c^2} u_3\,dx\,dy \le \frac{1}{\sqrt{2}}\int_{\Omega_-}\dot{\boldsymbol{\gamma}}(\boldsymbol{u})\,d\Omega.$$

Hence from (4.23) we obtain

$$\begin{aligned}\int_\Omega u_3\,d\Omega &\le \int_{z_-}^{z_{\frac{1}{2}}}\left(\frac{1}{\sqrt{2}}\int_{\Omega_-}\dot{\boldsymbol{\gamma}}(\boldsymbol{u})\,d\Omega\right)dz+\int_{z_{\frac{1}{2}}}^{z_+}\left(\frac{1}{\sqrt{2}}\int_{\Omega_+}\dot{\boldsymbol{\gamma}}(\boldsymbol{u})\,d\Omega\right)dz\\ &=\frac{1}{\sqrt{2}}\frac{z_+-z_-}{2}\int_{\Omega_-}\dot{\boldsymbol{\gamma}}(\boldsymbol{u})\,d\Omega+\frac{1}{\sqrt{2}}\frac{z_+-z_-}{2}\int_{\Omega_+}\dot{\boldsymbol{\gamma}}(\boldsymbol{u})\,d\Omega\\ &=\frac{1}{2\sqrt{2}}(z_+-z_-)\int_\Omega\dot{\boldsymbol{\gamma}}(\boldsymbol{u})\,d\Omega. \end{aligned}\tag{4.24}$$

Using (4.24) we get a bound for (4.19),

$$\frac{-\int_\Omega u_3\,d\Omega}{\int_\Omega\dot{\boldsymbol{\gamma}}(\boldsymbol{u})\,d\Omega}\le\frac{1}{2\sqrt{2}}(z_+-z_-).\tag{4.25}$$

Thus from (4.18) we can write

$$B\ge\frac{1}{2\sqrt{2}}(z_+-z_-)\left(1-\frac{2\pi\beta}{V_b}\int_{z_-}^{z_+}\frac{f'(f''f-(f')^2-1)}{\left((f')^2+1\right)^{\frac{3}{2}}}\,dz\right).\tag{4.26}$$

Note that this no longer depends on the velocity field. So if (4.26) is true, then the only possible solution is the zero solution.

4.2 Second Stopping Condition

In the previous section we used the rate of strain minimization result to obtain the stopping condition. For our second stopping condition we use result (3.80) from section 3.4: The actual stress field, $\tau_{\ell,ij}$, maximizes the functional

$$G(\tilde{\tau}_{\ell,ij})=-\frac{1}{2^{\frac{1}{n}+1}}\frac{n}{n+1}\int_\Omega(|\tilde{\boldsymbol{\tau}}_\ell-B|+\tilde{\boldsymbol{\tau}}_\ell-B)^{\frac{1}{n}+1}\,d\Omega,\tag{4.27}$$

over all admissible stress fields $(\tilde{p}_\ell,\tilde{\tau}_{\ell,ij})\in T$. Clearly the integrand in (4.27) is always non-negative. Thus

$$G(\tilde{\tau}_{\ell,ij})\le 0\qquad\forall\,(\tilde{p}_\ell,\tilde{\tau}_{\ell,ij})\in T.\tag{4.28}$$

The integrand in (4.27) will have a non-zero contribution to $G(\tilde{\tau}_{\ell,ij})$ if and only if $\tilde{\boldsymbol{\tau}}>B$ at some point $\boldsymbol{x}\in\Omega$. Thus if we can find an admissible stress field with

$$G(\tilde{\tau}_{\ell,ij})=0,\tag{4.29}$$

then for the actual solution, $\tau_{\ell,ij}$,

$$0 = G(\tilde{\tau}_{\ell,ij}) \leq G(\tau_{\ell,ij}) \leq 0, \tag{4.30}$$

and therefore $G(\tau_{\ell,ij}) = 0$ and $\boldsymbol{\tau} \leq B$ everywhere in Ω. Thus, if for a given problem we can find an admissible stress field then we can obtain a stopping criterion. Possible admissible stress fields can be obtained from the solutions of simpler problems. The solution of a problem with the same geometry but with a Newtonian fluid (or a Power Law fluid) would provide an admissible stress field. We could also extend the fluid domain to be infinite. The stress field solution to this new problem, suitably truncated, will also be an admissible stress field. Moreover we could combine these two simplification and consider a problem with the same bubble geometry but in an infinite Newtonian fluid. As an example we consider the case of a spherical bubble and obtain a new stopping condition based on this method.

4.2.1 Second Stopping Condition for a Spherical Bubble

For the case of a spherical bubble, the admissible stress field that we will consider is the stress field for a Stokes flow solution for a spherical bubble rising under the influence of gravity in an infinite Newtonian fluid. We truncate the stress field appropriately to fit inside our finite domain Ω. We denote this truncated stress field for the Newtonian case as $\tau^N_{\ell,ij}$.

Since the Newtonian stress field is obtained directly from solving the Stokes equations in an infinite domain, $\tau^N_{\ell,ij}$ will satisfy the momentum equations in Ω. Also the conditions (3.59)–(3.61) are imposed boundary conditions in Newtonian problem. Hence $\tau^N_{\ell,ij}$ is an admissible stress field.

Stokes Flow Solution for a Spherical Bubble in a Newtonian Fluid

The derivation of this result was first done by Rybczynski, and independently by Hadamard in 1911, and can be found in several standard textbooks [32] [33].

Using a spherical coordinate system (r, θ, ϕ) with the variables defined as in figure 4.5, the

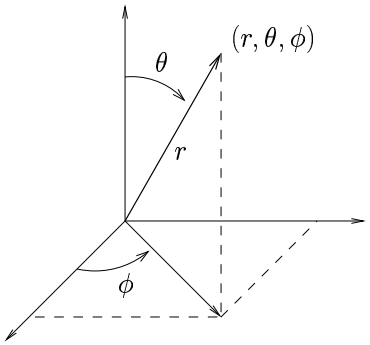

Figure 4.5: Spherical coordinates.

solution of the non-dimensional problem (using the scalings from section 2.2 with $n = 1$) is

$$\boldsymbol{u}^N = (u^N, v^N, w^N) = \left(\frac{\cos\theta}{3r}, -\frac{\sin\theta}{6r}, 0 \right). \tag{4.31}$$

For the Newtonian fluid

$$\tau^N_{\ell,ij} = \dot{\gamma}_{ij}, \tag{4.32}$$

so

$$\begin{aligned} &\tau^N_{\ell,rr} = -\frac{2\cos\theta}{3r^2}, \qquad \tau^N_{\ell,\theta\theta} = \frac{\cos\theta}{3r^2}, \qquad \tau^N_{\ell,\phi\phi} = \frac{\cos\theta}{3r^2}, \\ &\tau^N_{\ell,r\theta} = 0, \qquad \tau^N_{\ell,r\phi} = 0, \qquad \tau^N_{\ell,\theta\phi} = 0, \\ \Rightarrow\ &\boldsymbol{\tau}^N = \frac{|\cos\theta|}{\sqrt{3}r^2}. \end{aligned} \tag{4.33}$$

With our scalings the surface of the bubble is given by $r = 1$, so

$$\boldsymbol{\tau}^N \leq \frac{1}{\sqrt{3}}, \qquad \forall\, \boldsymbol{x} \in \Omega. \tag{4.34}$$

Thus with $B = \frac{1}{\sqrt{3}}$ we have $\boldsymbol{\tau}^N \leq B$ and thus (4.29) and (4.30) are true. The only way $G(\tau_{\ell,ij}) = 0$ is if $\boldsymbol{\tau} \leq B$ everywhere in Ω. Thus for

$$B \geq \frac{1}{\sqrt{3}} \tag{4.35}$$

the whole region Ω is unyielded and the bubble does not move.

Comparison with the First Stopping Condition

Using our first stopping condition,

$$B \geq \frac{1}{2\sqrt{2}}(z_+ - z_-)\left(1 - \frac{2\pi\beta}{V_b}\int_{z_-}^{z_+} \frac{f'(f''f - (f')^2 - 1)}{\left((f')^2+1\right)^{\frac{3}{2}}}\,dz\right), \tag{4.36}$$

we can also get an estimate for the critical Bingham number, above which the bubble will not move.

For a spherical bubble (or any bubble that is symmetric through a horizontal plane) the surface integral in (4.36) is zero. This is most easily seen by recalling that the integral is antisymmetric in z. Thus for any bubble shape which is the same under the transformation $z \to -z$, the integral must be zero. This leaves us with

$$B \geq \frac{1}{2\sqrt{2}}(z_+ - z_-). \tag{4.37}$$

$(z_+ - z_-)$ is just the diameter of the sphere which is 2. Thus from the first stopping condition we get an estimate for the critical Bingham number of

$$B \geq \frac{1}{\sqrt{2}}. \tag{4.38}$$

Our new estimate of $B \geq \frac{1}{\sqrt{3}}$ is better and is possibly quite sharp. The estimate we get from the first stopping condition is less accurate since we have made many more approximations to obtain the more general result.

4.3 Third Stopping Condition: for Long Cylindrical Bubbles

Here we consider the case of long cylindrical bubbles. For our analysis we assume that the bubble is formed of a long cylindrical body with spherical cap ends (see figure 4.6). Furthermore we divide the fluid domain Ω into three regions, Ω_1, Ω_2, and Ω_3; Ω_3 being the horizontal section of fluid where the bubble has a cylindrical body, and Ω_1 and Ω_2 are respectively the remaining regions of fluid above and below Ω_3.

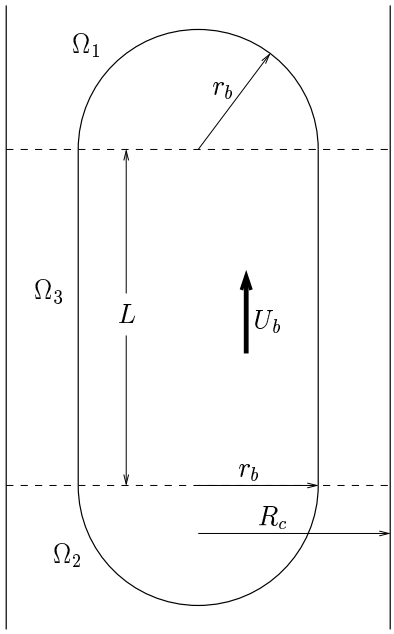

Figure 4.6: A long ($r_b \ll L$) cylindrical bubble.

We begin with the stopping condition (4.2): For

$$B \geq \sup_{all\ \boldsymbol{v} \in V} \left\{ -\frac{\int_\Omega v_3 \, d\Omega}{\int_\Omega \dot{\boldsymbol{\gamma}}(\boldsymbol{v}) \, d\Omega} - \frac{\int_{\partial\Omega_b} \beta \left(\frac{1}{R_1} + \frac{1}{R_2} \right) v_i n_{b,i} \, ds}{\int_\Omega \dot{\boldsymbol{\gamma}}(\boldsymbol{v}) \, d\Omega} \right\}, \tag{4.39}$$

the only possible solution is one with $\boldsymbol{u} = 0$ over Ω. We first note that since our bubble is symmetric through a horizontal plane, the surface integral term in (4.39) is zero. Thus (4.39) becomes

$$B \geq -\frac{\int_\Omega u_3 \, d\Omega}{\int_\Omega \dot{\boldsymbol{\gamma}}(\boldsymbol{u}) \, d\Omega}. \tag{4.40}$$

We can make the further simplification that

$$-\frac{\int_\Omega u_3 \, d\Omega}{\int_\Omega \dot{\boldsymbol{\gamma}}(\boldsymbol{u}) \, d\Omega} \leq -\frac{\int_\Omega u_3 \, d\Omega}{\int_{\Omega_3} \dot{\boldsymbol{\gamma}}(\boldsymbol{u}) \, d\Omega}.$$

So for

$$B \geq -\frac{\int_\Omega u_3 \, d\Omega}{\int_{\Omega_3} \dot{\boldsymbol{\gamma}}(\boldsymbol{u}) \, d\Omega} \tag{4.41}$$

we will also have no flow.

We first consider the numerator of expression (4.41): $-\int_\Omega u_3\, d\Omega$. We note that

$$-\int_\Omega u_3\, d\Omega = V_b U_b$$
$$= \left(\frac{4}{3}\pi {r_b}^3 + \pi {r_b}^2 L\right) U_b, \tag{4.42}$$

where V_b is the bubble volume, U_b is the bubble velocity, r_b is the radius of the cylindrical portion of the bubble, and L is the length of the cylindrical portion of the bubble (see figure 4.6). Also, from our non-dimensional scaling $V_b = \frac{4\pi}{3}$ (since $V_b = \frac{\hat{V}_b}{\hat{R}^3}$ and $\hat{R} = \sqrt[3]{\frac{3}{4\pi}\hat{V}_b}$) so

$$\frac{4\pi}{3}{r_b}^3 + \pi {r_b}^2 L = \frac{4\pi}{3}, \tag{4.43}$$

and for $L \gg r_b$ we get

$$L \sim \frac{4}{3{r_b}^2}, \qquad \text{or} \qquad \frac{3{r_b}^2 L}{4} \sim 1. \tag{4.44}$$

Hence

$$-\int_\Omega u_3\, d\Omega \sim \pi {r_b}^2 L U_b + O\left(\frac{r_b}{L}\right). \tag{4.45}$$

To obtain an estimate of $\int_{\Omega_3} \dot{\boldsymbol{\gamma}}(\boldsymbol{u})\, d\Omega$ we approximate the flow as a one-dimensional axisymmetric flow. For a long bubble, the effects at the ends of the cylindrical section where this assumption breaks down should not significantly affect the order analysis. The flow in Ω_3 will have velocity profile similar to that in figure 4.7. In this case the only non-zero component of

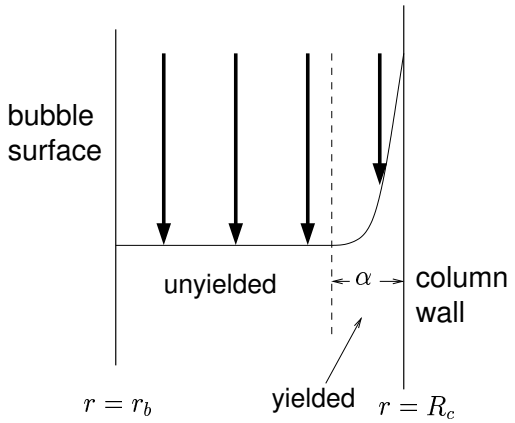

Figure 4.7: Velocity profile of the flow around the cylindrical section of the bubble.

the stress is $\frac{\partial u_3}{\partial r}$. At the bubble wall, where we have zero tangential stress, the fluid will be

unyielded. The fluid will only be yielded in a narrow region of thickness α near the column wall. The mean velocity of the flow is $U_{\text{avg}} = \frac{\pi {r_b}^2 U_b}{\pi({R_c}^2 - {r_b}^2)}$. So

$$\begin{aligned}
\int_{\Omega_3} \dot{\boldsymbol{\gamma}}(\boldsymbol{u})\, d\Omega &\sim \int_0^L \int_0^{2\pi} \int_{R_c-\alpha}^{R_c} \frac{\partial u_3}{\partial r}\, dr\, d\phi\, dz \\
&\sim \left(\frac{\frac{\pi {r_b}^2 U_b}{\pi({R_c}^2 - {r_b}^2)}}{\alpha} \right) (2\pi\alpha R_c L) \\
&\sim \frac{2\pi {r_b}^2 R_c L U_b}{{R_c}^2 - {r_b}^2}. \qquad (4.46)
\end{aligned}$$

Combining (4.45) and (4.46), we see that for $r_b \ll L$, the stopping condition (4.41) becomes: For

$$B \gtrsim \frac{1}{2} \frac{{R_c}^2 - {r_b}^2}{R_c}, \qquad (4.47)$$

the only possible solution is one with $\boldsymbol{u} = 0$ over Ω. We can also write this in terms of L, using (4.44) as

$$B \gtrsim \frac{1}{2} \frac{{R_c}^2 - \frac{4}{3L}}{R_c}. \qquad (4.48)$$

Chapter 5
Parameter Dependence

Using the variational inequality from the rate of strain minimization, (3.44), we can determine the monotonicity of the individual dissipation terms with respect to the physical parameters of the problem. The dimensional version of (3.44), suitably simplified, is

$$\frac{1}{2}\hat{\mu}_\ell \int_\Omega \hat{\dot{\boldsymbol{\gamma}}}^{n-1} \hat{\dot{\gamma}}_{ij}(\hat{\boldsymbol{u}}) \hat{\dot{\gamma}}_{ij}(\hat{\boldsymbol{v}} - \hat{\boldsymbol{u}})\, d\hat{\Omega} + \hat{\tau}_Y \left(\int_\Omega \hat{\dot{\boldsymbol{\gamma}}}(\hat{\boldsymbol{v}})\, d\hat{\Omega} - \int_\Omega \hat{\dot{\boldsymbol{\gamma}}}(\hat{\boldsymbol{u}})\, d\hat{\Omega} \right)$$
$$\geq -\hat{\rho}_\ell \hat{g} \int_\Omega (\hat{v}_3 - \hat{u}_3)\, d\hat{\Omega} - \hat{\xi} \int_{\partial\Omega_b} \left(\frac{1}{\hat{R}_1} + \frac{1}{\hat{R}_2} \right) (\hat{v}_i - \hat{u}_i) n_{b,i}\, d\hat{s}. \quad (5.1)$$

Note that the physical parameters $\hat{\mu}_\ell$, $\hat{\tau}_Y$, $\hat{\rho}_\ell$, and $\hat{\xi}$ (respectively consistency, yield stress, liquid density, and surface tension) all appear individually in front of separate terms. $\hat{\mu}_\ell$ appears in front of the dimensional equivalent of the $a(\cdot,\cdot)$ term, $\hat{\tau}_Y$ appears in front of the dimensional equivalent of the $j(\cdot)$ terms, etc.

To determine the monotonicity of the dissipation terms with respect to the physical parameters, we would like to be able to vary one parameter leaving all other parameters (including bubble shape) fixed, and determine the effect on the dissipation terms. For the yield stress and the surface tension, there are the respective dimensionless parameters, B and β already contained in (3.44). Thus we can vary B and β to determine the influence of varying $\hat{\tau}_Y$ and $\hat{\xi}$. For the consistency and the liquid density, based on (5.1), it suffices to add to a dimensionless parameter, which characterizes a change from a typical value of consistency or of liquid density, in front of the appropriate term in (3.44). For example, to characterize a change in consistency we need only consider a dimensionless parameter $\mu_\ell = \frac{\hat{\mu}_\ell}{\hat{\mu}_\ell^*}$, where $\hat{\mu}_\ell^*$ is a typical consistency,

and the variational inequality

$$\mu_\ell a(\boldsymbol{u}, \boldsymbol{v} - \boldsymbol{u}) + j(\boldsymbol{v}) - j(\boldsymbol{u}) \geq L(\boldsymbol{v} - \boldsymbol{u}) \tag{5.2}$$

and the functional

$$J(\boldsymbol{v}) \equiv \frac{1}{n+1}\mu_\ell a(\boldsymbol{v}, \boldsymbol{v}) + j(\boldsymbol{v}) - L(\boldsymbol{v}). \tag{5.3}$$

Similarly, to characterize a change in liquid density we use the dimensionless parameter $\rho_\ell = \frac{\hat{\rho_\ell}}{\hat{\rho}_\ell^*}$, where $\hat{\rho}_\ell^*$ is a typical liquid density, and the variational inequality

$$a(\boldsymbol{u}, \boldsymbol{v} - \boldsymbol{u}) + j(\boldsymbol{v}) - j(\boldsymbol{u}) \geq -\rho_\ell \int_\Omega (v_3 - u_3)\, d\Omega - \int_{\partial\Omega_b} \beta \left(\frac{1}{R_1} + \frac{1}{R_2}\right)(v_i - u_i) n_{b,i}\, ds. \tag{5.4}$$

Generally if the bubble velocity increases so will the dissipation rate terms. Hence from this parameter dependence we are also able to get an idea of how the physical parameters affect the bubble velocity.

5.1 Consistency

Consider two consistencies $\mu_\ell^{(1)} > \mu_\ell^{(2)}$. Let $\boldsymbol{u}^{(1)}$ be the solution corresponding to $\mu_\ell^{(1)}$, and let $\boldsymbol{u}^{(2)}$ be the solution corresponding to $\mu_\ell^{(2)}$. Now the true solution minimizes the functional (5.3). Also for the true solution

$$J(\boldsymbol{u}) = -\frac{n}{n+1}\mu_\ell a(\boldsymbol{u}, \boldsymbol{u}). \tag{5.5}$$

So for the case for $\mu_\ell^{(1)}$, we have

$$-\frac{n}{n+1}\mu_\ell^{(1)} a(\boldsymbol{u}^{(1)}, \boldsymbol{u}^{(1)}) = \frac{1}{n+1}\mu_\ell^{(1)} a(\boldsymbol{u}^{(1)}, \boldsymbol{u}^{(1)}) + j(\boldsymbol{u}^{(1)}) - L(\boldsymbol{u}^{(1)}). \tag{5.6}$$

Similarly, for the case of $\mu_\ell^{(2)}$ we can write

$$\begin{aligned} -\frac{n}{n+1}\mu_\ell^{(2)} a(\boldsymbol{u}^{(2)}, \boldsymbol{u}^{(2)}) &= \frac{1}{n+1}\mu_\ell^{(2)} a(\boldsymbol{u}^{(2)}, \boldsymbol{u}^{(2)}) + j(\boldsymbol{u}^{(2)}) - L(\boldsymbol{u}^{(2)}) \\ \Rightarrow -\frac{n}{n+1}\mu_\ell^{(2)} a(\boldsymbol{u}^{(2)}, \boldsymbol{u}^{(2)}) &\leq \frac{1}{n+1}\mu_\ell^{(2)} a(\boldsymbol{u}^{(1)}, \boldsymbol{u}^{(1)}) + j(\boldsymbol{u}^{(1)}) - L(\boldsymbol{u}^{(1)}). \end{aligned} \tag{5.7}$$

Subtracting (5.6) from (5.7)

$$\frac{n}{n+1}\mu_\ell^{(1)} a(\boldsymbol{u}^{(1)}, \boldsymbol{u}^{(1)}) - \frac{n}{n+1}\mu_\ell^{(2)} a(\boldsymbol{u}^{(2)}, \boldsymbol{u}^{(2)}) \leq \frac{1}{n+1}(\mu_\ell^{(2)} - \mu_\ell^{(1)}) a(\boldsymbol{u}^{(1)}, \boldsymbol{u}^{(1)}). \tag{5.8}$$

Since $\mu_\ell^{(1)} > \mu_\ell^{(2)}$, (5.8) implies

$$\begin{aligned}
\frac{n}{n+1}\mu_\ell^{(1)} a(\boldsymbol{u}^{(1)}, \boldsymbol{u}^{(1)}) - \frac{n}{n+1}\mu_\ell^{(2)} a(\boldsymbol{u}^{(2)}, \boldsymbol{u}^{(2)}) &\leq 0 \\
\frac{n}{n+1}\mu_\ell^{(1)} a(\boldsymbol{u}^{(1)}, \boldsymbol{u}^{(1)}) &\leq \frac{n}{n+1}\mu_\ell^{(2)} a(\boldsymbol{u}^{(2)}, \boldsymbol{u}^{(2)}) \\
\Rightarrow \mu_\ell^{(1)} a(\boldsymbol{u}^{(1)}, \boldsymbol{u}^{(1)}) &\leq \mu_\ell^{(2)} a(\boldsymbol{u}^{(2)}, \boldsymbol{u}^{(2)})
\end{aligned}$$

Thus

$$\mu_\ell^{(1)} > \mu_\ell^{(2)} \quad \Rightarrow \quad \mu_\ell^{(1)} a(\boldsymbol{u}^{(1)}, \boldsymbol{u}^{(1)}) \leq \mu_\ell^{(2)} a(\boldsymbol{u}^{(2)}, \boldsymbol{u}^{(2)}); \tag{5.9}$$

$\mu_\ell a(\boldsymbol{u}, \boldsymbol{u})$ is a decreasing function of μ_ℓ.

5.2 Yield Stress (Bingham Number)

Consider two values of the Bingham Number, $B^{(1)} < B^{(2)}$. Let $\boldsymbol{u}^{(1)}$ be the solution corresponding to $B^{(1)}$, and let $\boldsymbol{u}^{(2)}$ be the solution corresponding to $B^{(2)}$. Using the variational inequality (3.44) for $(B^{(1)}, \boldsymbol{u}^{(1)})$, with $\boldsymbol{v} = \boldsymbol{u}^{(2)}$ we get

$$a(\boldsymbol{u}^{(1)}, \boldsymbol{u}^{(2)} - \boldsymbol{u}^{(1)}) + B^{(1)} \left(\int_\Omega \dot{\boldsymbol{\gamma}}(\boldsymbol{u}^{(2)})\, d\Omega - \int_\Omega \dot{\boldsymbol{\gamma}}(\boldsymbol{u}^{(1)})\, d\Omega \right) \geq L(\boldsymbol{u}^{(2)} - \boldsymbol{u}^{(1)}) \tag{5.10}$$

Using (3.44) for $(B^{(2)}, \boldsymbol{u}^{(2)})$, now with $\boldsymbol{v} = \boldsymbol{u}^{(1)}$ we get

$$a(\boldsymbol{u}^{(2)}, \boldsymbol{u}^{(1)} - \boldsymbol{u}^{(2)}) + B^{(2)} \left(\int_\Omega \dot{\boldsymbol{\gamma}}(\boldsymbol{u}^{(1)})\, d\Omega - \int_\Omega \dot{\boldsymbol{\gamma}}(\boldsymbol{u}^{(2)})\, d\Omega \right) \geq L(\boldsymbol{u}^{(1)} - \boldsymbol{u}^{(2)}) \tag{5.11}$$

Adding (5.10) and (5.11), and recalling that $a(\cdot, \cdot)$ is linear in its second argument and that $L(\cdot)$ is linear

$$a(\boldsymbol{u}^{(1)}, \boldsymbol{u}^{(2)} - \boldsymbol{u}^{(1)}) - a(\boldsymbol{u}^{(2)}, \boldsymbol{u}^{(2)} - \boldsymbol{u}^{(1)}) + (B^{(1)} - B^{(2)}) \left(\int_\Omega \dot{\boldsymbol{\gamma}}(\boldsymbol{u}^{(2)})\, d\Omega - \int_\Omega \dot{\boldsymbol{\gamma}}(\boldsymbol{u}^{(1)})\, d\Omega \right) \geq 0. \tag{5.12}$$

Using the result from convexity and Gâteaux differentiability, (3.51), we can write

$$\frac{1}{n+1} a(\boldsymbol{u}^{(2)}, \boldsymbol{u}^{(2)}) - \frac{1}{n+1} a(\boldsymbol{u}^{(1)}, \boldsymbol{u}^{(1)}) \geq a(\boldsymbol{u}^{(1)}, \boldsymbol{u}^{(2)} - \boldsymbol{u}^{(1)}) \tag{5.13}$$

$$\frac{1}{n+1} a(\boldsymbol{u}^{(1)}, \boldsymbol{u}^{(1)}) - \frac{1}{n+1} a(\boldsymbol{u}^{(2)}, \boldsymbol{u}^{(2)}) \geq a(\boldsymbol{u}^{(2)}, \boldsymbol{u}^{(1)} - \boldsymbol{u}^{(2)}) \tag{5.14}$$

Adding (5.13) and (5.14) we see that

$$0 \geq a(\boldsymbol{u}^{(1)}, \boldsymbol{u}^{(2)} - \boldsymbol{u}^{(1)}) - a(\boldsymbol{u}^{(2)}, \boldsymbol{u}^{(2)} - \boldsymbol{u}^{(1)}). \tag{5.15}$$

It should be noted that the result in (5.15) is a general result. Combining (5.15) with (5.12),

$$(B^{(1)} - B^{(2)}) \left(\int_\Omega \dot{\boldsymbol{\gamma}}(\boldsymbol{u}^{(2)})\, d\Omega - \int_\Omega \dot{\boldsymbol{\gamma}}(\boldsymbol{u}^{(1)})\, d\Omega \right) \geq 0. \tag{5.16}$$

Thus $B^{(1)} < B^{(2)}$ implies

$$\int_\Omega \dot{\boldsymbol{\gamma}}(\boldsymbol{u}^{(2)})\, d\Omega \leq \int_\Omega \dot{\boldsymbol{\gamma}}(\boldsymbol{u}^{(1)})\, d\Omega. \tag{5.17}$$

The yield stress dissipation is a decreasing function of the Bingham number.

5.3 Density

Consider two liquid densities $\rho_\ell^{(1)} < \rho_\ell^{(2)}$. Let $\boldsymbol{u}^{(1)}$ be the solution corresponding to $\rho_\ell^{(1)}$, and let $\boldsymbol{u}^{(2)}$ be the solution corresponding to $\rho_\ell^{(2)}$. Using (5.4) for $(\rho_\ell^{(1)}, \boldsymbol{u}^{(1)})$, with $\boldsymbol{v} = \boldsymbol{u}^{(2)}$ we get

$$\begin{aligned} a(\boldsymbol{u}^{(1)}, \boldsymbol{u}^{(2)} - \boldsymbol{u}^{(1)}) + j(\boldsymbol{u}^{(2)}) - j(\boldsymbol{u}^{(1)}) \geq -\rho_\ell^{(1)} \int_\Omega (u_3^{(2)} - u_3^{(1)})\, d\Omega \\ - \int_{\partial\Omega_b} \beta \left(\frac{1}{R_1} + \frac{1}{R_2} \right) (u_i^{(2)} - u_i^{(1)}) n_{b,i}\, ds. \end{aligned} \tag{5.18}$$

Using (5.4) for $(\rho_\ell^{(2)}, \boldsymbol{u}^{(2)})$, now with $\boldsymbol{v} = \boldsymbol{u}^{(1)}$ we get

$$\begin{aligned} a(\boldsymbol{u}^{(2)}, \boldsymbol{u}^{(1)} - \boldsymbol{u}^{(2)}) + j(\boldsymbol{u}^{(1)}) - j(\boldsymbol{u}^{(2)}) \geq -\rho_\ell^{(2)} \int_\Omega (u_3^{(1)} - u_3^{(2)})\, d\Omega \\ - \int_{\partial\Omega_b} \beta \left(\frac{1}{R_1} + \frac{1}{R_2} \right) (u_i^{(1)} - u_i^{(2)}) n_{b,i}\, ds. \end{aligned} \tag{5.19}$$

Adding (5.18) and (5.19), and recalling that $a(\cdot, \cdot)$ is linear in its second argument

$$a(\boldsymbol{u}^{(1)}, \boldsymbol{u}^{(2)} - \boldsymbol{u}^{(1)}) - a(\boldsymbol{u}^{(2)}, \boldsymbol{u}^{(2)} - \boldsymbol{u}^{(1)}) \geq (\rho_\ell^{(2)} - \rho_\ell^{(1)}) \int_\Omega (u_3^{(2)} - u_3^{(1)})\, d\Omega. \tag{5.20}$$

Combining (5.15) with (5.20) we obtain

$$(\rho_\ell^{(2)} - \rho_\ell^{(1)}) \int_\Omega (u_3^{(2)} - u_3^{(1)})\, d\Omega \leq 0. \tag{5.21}$$

Thus with $\rho_\ell^{(1)} < \rho_\ell^{(2)}$,

$$\int_\Omega u_3^{(2)}\, d\Omega \leq \int_\Omega u_3^{(1)}\, d\Omega. \tag{5.22}$$

This result can be related to the bubble velocity, U_b, through $\int_\Omega u_3\, d\Omega = -V_b U_b$, where V_b is the bubble volume. Thus we conclude that the bubble velocity is an increasing function of the liquid density:

$$\rho^{(1)} < \rho^{(2)} \;\Rightarrow\; U_b^{(1)} \leq U_b^{(2)}. \tag{5.23}$$

5.4 Surface Tension

Consider two values of surface tension $\beta^{(1)} < \beta^{(2)}$. Let $\boldsymbol{u}^{(1)}$ be the solution corresponding to $\beta^{(1)}$, and let $\boldsymbol{u}^{(2)}$ be the solution corresponding to $\beta^{(2)}$. Using the variational inequality (3.44) for $(\beta^{(1)}, \boldsymbol{u}^{(1)})$, with $\boldsymbol{v} = \boldsymbol{u}^{(2)}$ we get

$$\begin{aligned} a(\boldsymbol{u}^{(1)}, \boldsymbol{u}^{(2)} - \boldsymbol{u}^{(1)}) + j(\boldsymbol{u}^{(2)}) - j(\boldsymbol{u}^{(1)}) \geq & -\int_\Omega (u_3^{(2)} - u_3^{(1)})\, d\Omega \\ & - \beta^{(1)} \int_{\partial\Omega_b} \left(\frac{1}{R_1} + \frac{1}{R_2}\right) (u_i^{(2)} - u_i^{(1)}) n_{b,i}\, ds. \end{aligned} \tag{5.24}$$

Using (3.44) for $(\beta^{(2)}, \boldsymbol{u}^{(2)})$, now with $\boldsymbol{v} = \boldsymbol{u}^{(1)}$ we get

$$\begin{aligned} a(\boldsymbol{u}^{(2)}, \boldsymbol{u}^{(1)} - \boldsymbol{u}^{(2)}) + j(\boldsymbol{u}^{(1)}) - j(\boldsymbol{u}^{(2)}) \geq & -\int_\Omega (u_3^{(1)} - u_3^{(2)})\, d\Omega \\ & - \beta^{(2)} \int_{\partial\Omega_b} \left(\frac{1}{R_1} + \frac{1}{R_2}\right) (u_i^{(1)} - u_i^{(2)}) n_{b,i}\, ds. \end{aligned} \tag{5.25}$$

Adding (5.24) and (5.25), and recalling that $a(\cdot,\cdot)$ is linear in its second argument

$$a(\boldsymbol{u}^{(1)}, \boldsymbol{u}^{(2)} - \boldsymbol{u}^{(1)}) - a(\boldsymbol{u}^{(2)}, \boldsymbol{u}^{(2)} - \boldsymbol{u}^{(1)}) \geq (\beta^{(2)} - \beta^{(1)}) \int_{\partial\Omega_b} \left(\frac{1}{R_1} + \frac{1}{R_2}\right) (u_i^{(2)} - u_i^{(1)}) n_{b,i}\, ds. \tag{5.26}$$

Combining (5.15) with (5.26) we obtain

$$(\beta^{(2)} - \beta^{(1)}) \int_{\partial\Omega_b} \left(\frac{1}{R_1} + \frac{1}{R_2}\right) (u_i^{(2)} - u_i^{(1)}) n_{b,i}\, ds \leq 0. \tag{5.27}$$

From our earlier results with the surface tension; see (4.14), and the fact that $\int_\Omega u_3\, d\Omega = -V_b U_b$, we have that

$$\int_{\partial\Omega_b} \left(\frac{1}{R_1} + \frac{1}{R_2}\right) u_i n_{b,i}\, ds = 2\pi U_b \int_{z_-}^{z_+} \frac{f'(f''f - (f')^2 - 1)}{\left((f')^2 + 1\right)^{\frac{3}{2}}}\, dz \tag{5.28}$$

Combining (5.28) with (5.27) we get

$$2\pi(\beta^{(2)}-\beta^{(1)})(U_b^{(2)}-U_b^{(1)})\int_{z_-}^{z_+}\frac{f'(f''f-(f')^2-1)}{\left((f')^2+1\right)^{\frac{3}{2}}}\,dz\le 0. \tag{5.29}$$

It turns out that for "typical" bubble shapes $\int_{z_-}^{z_+}\frac{f'(f''f-(f')^2-1)}{\left((f')^2+1\right)^{\frac{3}{2}}}\,dz<0$. Thus

$$\beta^{(1)}<\beta^{(2)}\ \Rightarrow\ U_b^{(1)}\le U_b^{(2)}; \tag{5.30}$$

the bubble velocity is an increasing function of the surface tension.

Chapter 6
Experiments

6.1 Experimental Setup

6.1.1 Experimental Apparatus

All the experimental work cited in the introduction has essentially been done using apparatus of similar construction. Our apparatus is designed along similar lines.

Our apparatus consists of a 6' long clear acrylic column that has an inner diameter of 1.5" and an outer diameter of 2". The column is attached to a clear acrylic base. Our viscoplastic fluid is pumped in through the sides of the base of the column using a progressive cavity positive displacement pump. This type of pump was chosen at it does not cause high shear rates in the fluid and it does not result in pulsatile flow. These two features are important in order to avoid damaging the long polymer chains in the viscoplastic fluid. It is the cross-linking of these polymer chains that give the fluid its yield stress. The air bubbles are injected from the centre of the base of the column by a pneumatic cylinder. The cylinder is controlled by a linear actuator which in turn is controlled through a computer. By controlling the linear displacement of the cylinder we can control the volume of air being injected into the column. Lastly, a reference grid is located directly behind the column.

Each experiment, consisting of the injection of one bubble into the column and observation of its progress after reaching a steady state, is filmed using digital video. Assuming an axisymmetric profile for the bubble, we can extract all the necessary data from the video afterwards (see Appendix C). A schematic of the experimental setup is shown in figure 6.1.

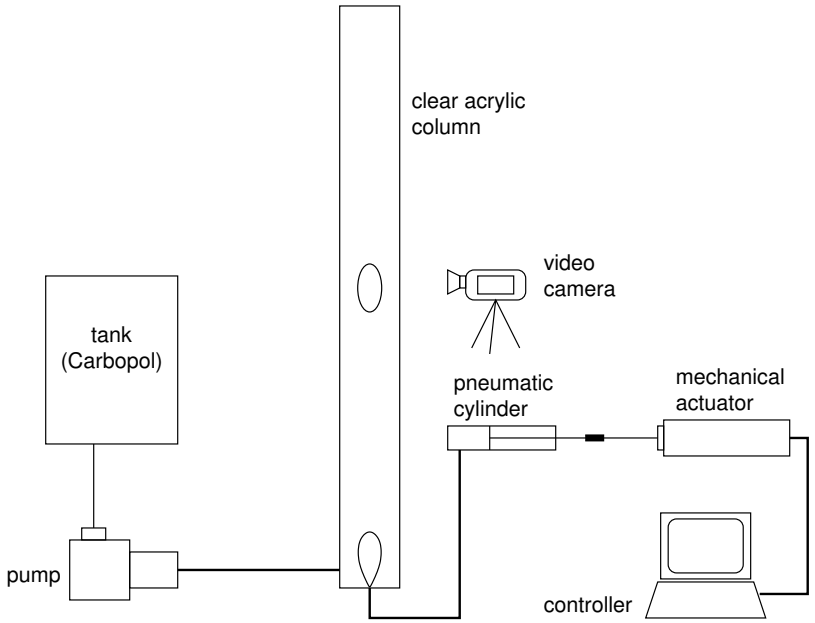

Figure 6.1: Schematic diagram of the experimental setup.

6.1.2 Viscoplastic Fluid – Carbopol

The viscoplastic fluid used in our experiments is Carbopol. It is a rheology modifying polyacrylic based polymer made by Noveon Inc. (formerly B.F. Goodrich Co.) Carbopol is an ideal experimental fluid in that it is clear and comes very close to performing as an ideal viscoplastic fluid, without any elastic behaviour at low shear rates [34]. Two Carbopol polymers (940 and EZ2) are used in order to obtain a wider range of fluid parameters. In general, the Carbopol EZ2 has a lower yield stress than Carbopol 940 for a given concentration. And for both Carbopols the yield stress increases with concentration.

Carbopol can be appropriately modelled as a Herschel-Bulkley fluid. The rheological parameters of the Carbopol solutions (yield stress, $\hat{\tau}_Y$; consistency, $\hat{\mu}_\ell$; and power law index, n) are measured using a cone and plate rheometer (Bohlin Instruments). The yield stress is directly measured by successive creep/recovery tests. This is the method suggested by Coussot [35]. A constant stress is applied to the fluid and the strain response after a fixed time is measured. When the strain response is plotted versus the applied stress there is a stress value above which the strain

response begins to increase significantly as a function of the applied stress. The stress value at which this occurs is defined to be the yield stress. The consistency, $\hat{\mu}_\ell$, and power law index, n, are determined from a controlled stress viscometry test, where the rate of strain is measured at various stresses. The parameters $\hat{\mu}_\ell$ and n are fitted to the data in a least-squares sense. For a more detailed description of the parameter measurements and an example calculation refer to Appendix D.

The density of the fluid is measured using standard specific gravity bottles and a mass balance.

6.1.3 Preparation of Carbopol Solutions

Carbopol comes as a fine polymer powder. The powder must first be dispersed in an aqueous solution and then an alkaline neutralizer must be added to thicken the solution and to produce a yield stress.

We begin with $10\,L$ of distilled water and, while mixing at a constant rate of 300–500 rpm with a Heidolph medium-duty laboratory mixer, we slowly add the desired amount of Carbopol. Once all the Carbopol has been added, the solution is mixed for an additional 4–8 hours. This is to allow for the complete hydration and mixing of the powder. The solution is then left to stand for another 4–6 hours to allow all air to escape and to allow any foam to break up. It is important to allow all bubbles to disappear before the solution is neutralized. Once the fluid has a yield stress it becomes exceedingly difficult to eliminate bubbles from the fluid.

The fluid is neutralized with a sodium hydroxide solution. While mixing at a lower rate (~ 100 rpm), the sodium hydroxide solution is added about a millilitre at a time. In between the solution is left to mix for several minutes. It is important that the rate of mixing is low enough that air is not entrained into the Carbopol. As the sodium hydroxide is added the consistency of the Carbopol increases and a yield stress develops. Thus the rate of mixing can slowly be increased with the addition of the sodium hydroxide. Sodium hydroxide is added until the Carbopol reaches a pH of 7.0. This requires roughly a 2:1 ratio (by mass) of sodium hydroxide (20% solution) to Carbopol powder.

To obtain a higher density solution sugar is first added to the distilled water.

6.1.4 Experimental Method

Prior to each experiment the column is drained, the fluid cycled through the pump, and then the column is refilled. This is to ensure that the fluid is adequately mixed between experiments. Gheissary and van den Brule [15] conducted experiments to examine the time effects and wake effects on spherical particle settling in a Carbopol solution. They observed the following: For very short time intervals between spheres begin released in the Carbopol (approximately 2 seconds) there was no noticeable change in the settling velocities. For time intervals on the order of ten minutes the settling velocity increased for following spheres to some higher limiting value. For longer time intervals the limiting settling velocity increased and the number of successive drops required to reach that value decreased. Furthermore, after waiting two hours, in an attempt to let the fluid "recover", the settling velocity of the sphere increased even further. It required approximately 72 hours for the fluid to restore itself to the initial state. Alternatively, mixing the fluid also seemed to restore it to its initial state. This strongly time dependent fluid behaviour requires one to take great care to ensure the fluid is well mixed before the column is filled. Furthermore, we also allow the bubble to travel $\sim 50\ cm$ before any measurements are taken. This is to allow the bubble to reach steady state. In the worst case this distance is approximately equal to 10–12 times the effective bubble radius, $\hat{R}$, which is still more than adequate for the bubble to reach steady state.

There is also another interesting complication that arises because of the yield stress of Carbopol. In the unyielded regions all that we are able to know about the stress is that it is below the yield stress. In reality the stress in the unyielded region is non-unique (the velocities will be unique though); for a given velocity field in Ω, we can have different stresses in the unyielded region. For this reason we cannot accurately control the volume of the injected bubble, despite being able to accurately control the cylinder actuation. Since the unyielded fluid can support a range of stresses, the injection pressure can vary over a small range. Thus the volume of the actual bubble will vary in a small range around the injected volume. For small bubbles this

could result in as much as 35% variation in volume. To prevent this from causing complications we instead calculate the volume of the bubble from the video, again making the assumption of an axisymmetric bubble profile. This leads to an accurate estimate of the true volume (see Appendix C).

6.2 Experimental Results

For our experiments we use six different mixtures of Carbopol. The mixtures and their fluid parameters are listed in Table 6.1. In each fluid we observe a series of bubbles of various volumes

Carbopol Solution	Density, $\hat{\rho}_\ell$ $(kg \cdot m^{-3})$	Power Law Index, n	Consistency, $\hat{\mu}_\ell$ $(Pa \cdot s^n)$	Yield Stress, $\hat{\tau}_Y$ (Pa)
1	1068	0.37	4.3	2.3
2	1067	0.35	6.8	4.0
3	1066	0.36	7.5	5.5
4	1158	0.39	5.8	2.5
5	1189	0.46	2.5	5.2
6	1072	0.42	3.2	2.2

Table 6.1: Fluid properties of the Carbopol mixtures.

ranging from approximately $0.5\,mL$ to $50\,mL$, and measure their velocities. The general trend for a given fluid is that as the volume increases the velocity increases rapidly; then with a further increase in volume the bubbles begin to fill the cross-section of the column, and the velocity levels off at some constant value (see figure 6.2, solution 6). In some cases the velocity will increase to some maximum value and then decrease before it levels off to a constant value (see figure 6.2, solution 2). The constant velocities at which sufficiently large bubbles $\left(\frac{\hat{R}}{\hat{R}_c} > 0.5\right)$ travel in each of the solutions is given is Table 6.2.

The possible variables upon which the bubble velocity could depend are bubble size, yield stress, fluid density, gravity, consistency, column radius, and possibly surface tension and the power

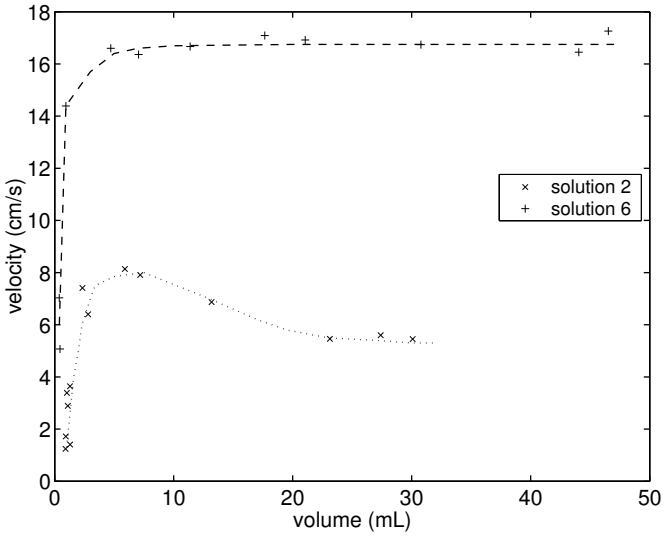

Figure 6.2: Curves of velocity versus volume for two Carbopol solutions.

law index ($\hat{R}$, $\hat{\tau}_Y$, $\hat{\rho}_\ell$, $\hat{g}$, $\hat{\mu}_\ell$, $\hat{R}_c$, $\hat{\xi}$, and n respectively). Including the bubble velocity, $\hat{U}_b$, (our dependent variable), and applying dimensional analysis we obtain six dimensionless quantities:

$$\frac{\hat{U}_b}{\sqrt{\hat{g}\hat{R}}} = Fr, \qquad \text{Froude number,}$$

$$\frac{\hat{\tau}_Y}{\hat{\rho}_\ell \hat{g} \hat{R}} = B, \qquad \text{Bingham number,}$$

$$\frac{\hat{\rho}_\ell \hat{g}^{1-\frac{n}{2}} \hat{R}^{1+\frac{n}{2}}}{\hat{\mu}_\ell} = Re^*, \qquad \text{modified Reynolds number,}$$

$$\frac{\hat{R}}{\hat{R}_c},$$

$$\frac{\hat{\xi}}{\hat{\rho}_\ell \hat{g} \hat{R}^2} = \beta, \qquad \text{and}$$

$$n.$$

It is reasonable to assume that the surface tension is constant for all experiments; therefore, from the Buckingham Pi theorem we have that for our results

$$\frac{\hat{U}_b}{\sqrt{\hat{g}\hat{R}}} = f\left(B, Re^*, \frac{\hat{R}}{\hat{R}_c}, n\right), \tag{6.1}$$

where f is some unknown function.

Carbopol Solution	Velocity of Bubbles with $\left(\frac{\hat{R}}{\hat{R}_c} > 0.5\right)$ (cm/s)
1	11.1
2	5.5
3	5.6
4	13.0
5	10.5
6	16.8

Table 6.2: Velocities of bubbles for which $\frac{\hat{R}}{\hat{R}_c} > 0.5$ in the different Carbopol solutions.

The complete data set of all bubbles in all solutions is given in figure 6.3. Again we can see the characteristic increase of velocity with bubble size until the bubbles begin to fill the column $\left(\frac{\hat{R}}{\hat{R}_c} \gtrsim 0.5\right)$, at which point the velocity levels off to a constant. In figure 6.3 a curve of constant velocity is given by $y = \frac{1}{\sqrt{\hat{R}}}$ since $Fr \propto \frac{1}{\sqrt{\hat{R}}}$.

Furthermore, for $\frac{\hat{R}}{\hat{R}_c} \gtrsim 0.5$, since we have a constant velocity, our system can be considered to have two regimes; one being $\frac{\hat{R}}{\hat{R}_c} \leq 0.5$ where f in (6.1) is dependent on $\frac{\hat{R}}{\hat{R}_c}$, and the other being $\frac{\hat{R}}{\hat{R}_c} > 0.5$ where f is independent of $\frac{\hat{R}}{\hat{R}_c}$.

When comparing the six solutions it may appear that the values of n are relatively close; however, even these differences appear to be significant. To see the effect of changing n on the bubble velocities we first note that for solution 1 and solution 6 the Bingham numbers and the modified Reynolds numbers all lie along the same curve; see figure 6.4. However, from Table 6.2 we can see that the velocities for the bubbles with $\frac{\hat{R}}{\hat{R}_c} > 0.5$ are 11.1 cm/s and 16.8 cm/s for solutions 1 and 6 respectively. This difference in velocity must be the result of the different values of n for the two solutions (0.37 and 0.42 respectively).

To examine the dependence of the velocity on the Bingham number and the modified Reynolds number we consider the data from the first four solutions only. Since the values of n for these

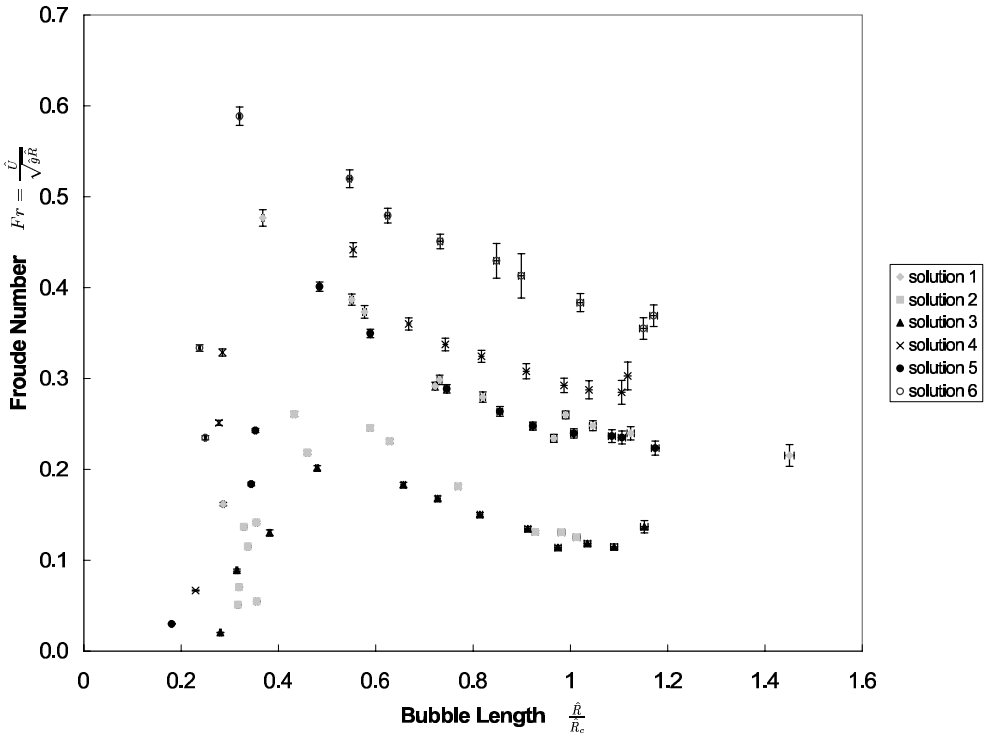

Figure 6.3: The complete data set. Froude number (non-dimensional velocity) plotted versus non-dimensional bubble length.

solutions differ by only about 10%, we hypothesize that the variation due to the differences in n should be small compared to the variation due to differences in the Bingham number and the modified Reynolds number. From the data for the first four solutions we fit, in a least-squares sense, a two-dimensional surface to the data:

$$\frac{\hat{U}_b}{\sqrt{\hat{g}\hat{R}}} = f^*\left(B, Re^*\right). \tag{6.2}$$

Contours of this surface are shown in figure 6.5. Using this surface we are able to plot cross-sections of the surface to examine the dependence of the velocity on the Bingham number and on the modified Reynolds number separately. Some cross-sections with the modified Reynolds number held fixed are given in figure 6.6. And cross-sections with the Bingham number held fixed are given in figure 6.7.

From figure 6.6 we see that for fixed Re^* as we increase the Bingham number the velocity

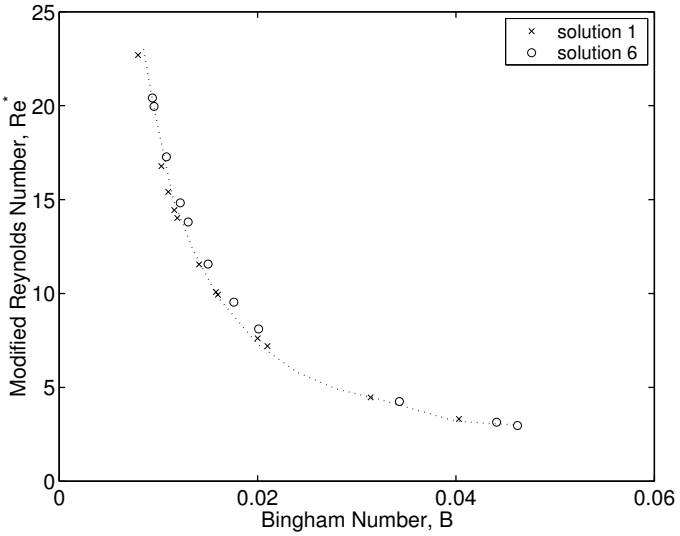

Figure 6.4: Modified Reynolds number plotted versus Bingham number. For the two solutions the data lie along the same curve (dotted line).

decreases. This makes sense physically in that if all other variables are held fixed and we increase the yield stress (increasing the Bingham number) then the bubble velocity should decrease. The results from figure 6.7 are more surprising. We see that as the Re^* decreases from a large value the velocity begins to decrease; however, as Re^* continues to decrease the velocity reaches a minimum and then begins to increase rapidly. Normally we would expect that if all other variables were held fixed and we increased the consistency of the fluid (decreasing Re^*) the drag on the bubble would increase causing the velocity to decrease. For the larger modified Reynolds numbers this appears to hold true, however at lower values this is no longer the case. It is not clear what physical phenomena produce this result.

6.3 Comparison with Analytic Results

6.3.1 Parameter Dependence

With regards to the parameter dependence, the experiments verify that an increase in the yield stress (or Bingham number) results in a decrease of velocity (result (5.17) from section 5.2). Our result for the consistency (5.9), however, only appears to be valid over certain regions of values for $\hat{\mu}_\ell$. Also for an increase in density, which results in B decreasing and Re^* increasing,

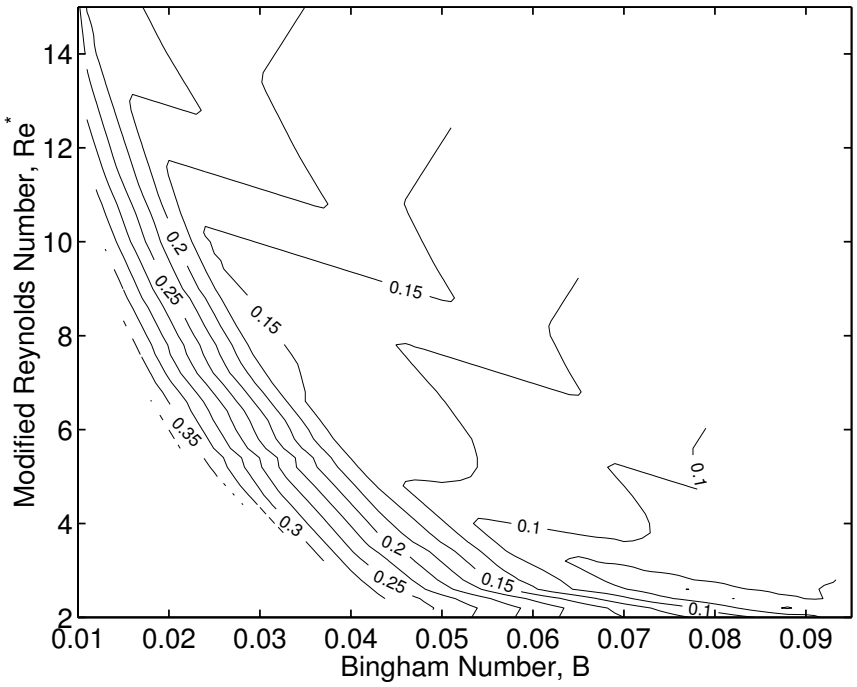

Figure 6.5: Contours of the Froude number, $\frac{\hat{U}_b}{\sqrt{\hat{g}\hat{R}}}$, plotted as a function of the Bingham number and the modified Reynolds number. The contour spacing is 0.025.

over the range of modified Reynolds numbers where the velocity is an increasing function of Re^*, we have an increase in velocity (result (5.23)). Finally since we did not specifically alter the surface tension of the solutions we are unable to verify the result concerning changes in the surface tension (5.30).

6.3.2 Stopping Conditions

While it would have been ideal to have data on bubbles that moved as well as bubbles that were stopped, with the current experimental setup it was not possible to examine stopped bubbles. Firstly, it is extremely difficult to inject a stopped bubble into the column that is not still attached to the injection nozzle. And secondly, a stopped bubble is, in general, not axisymmetric and thus it is impossible to calculate the volume from the video data. We must then suffice with only having data on moving bubbles with which to compare our stopping condition results.

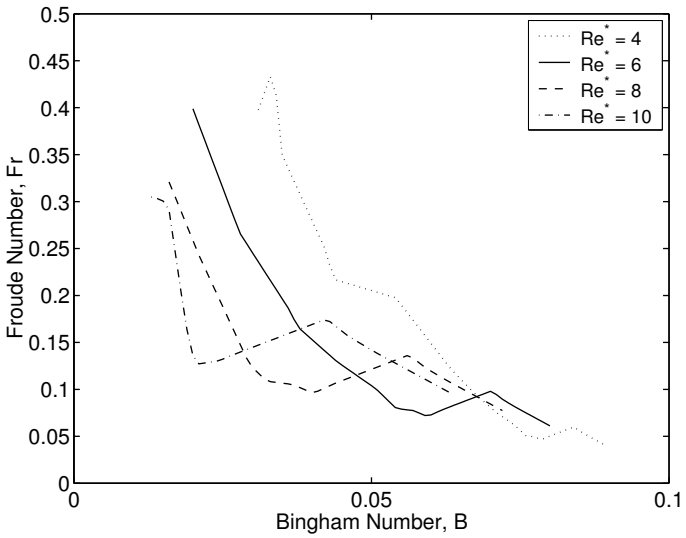

Figure 6.6: Froude number as a function of Bingham number for fixed Re^*.

It should also be noted that the stopping conditions are independent of the consistency and power law index, Re^* and n. While they influence the flow for moving bubbles, if a bubble is stopped in a given fluid, changing the consistency or power law index will not suddenly cause the bubble to start moving. The stopping conditions are only functions of the geometry of the problem (bubble shape and column radius). (Though, indirectly through the non-dimensionalization, they depend on the density and gravity.)

Our first stopping condition (4.26) is

$$B \geq \frac{1}{2\sqrt{2}}(z_+ - z_-)\left(1 - \frac{2\pi\beta}{V_b}\int_{z_-}^{z_+} \frac{f'(f''f - (f')^2 - 1)}{\left((f')^2+1\right)^{\frac{3}{2}}}\,dz\right). \tag{6.3}$$

To evaluate this it is necessary to know the value for the surface tension between Carbopol and air. Unfortunately for a yield stress fluid it is not easy to measure the surface tension without effects of the yield stress interfering. Conventional methods using capillary tubes or the Du Nouy ring method will not be able to separate surface tension effects from yield stress effects. (It should be noted that Kim et al. have devised a method of measuring the surface tension of a yield stress fluid [36].) Fortunately for our analysis, a precise value of the surface tension, $\hat{\xi}$, is not necessary. Using an approximate value of $\hat{\xi} = 0.0725\ N/m$ (the value of the surface tension between water and air), the value of the surface integral term in (6.3) turns out to be

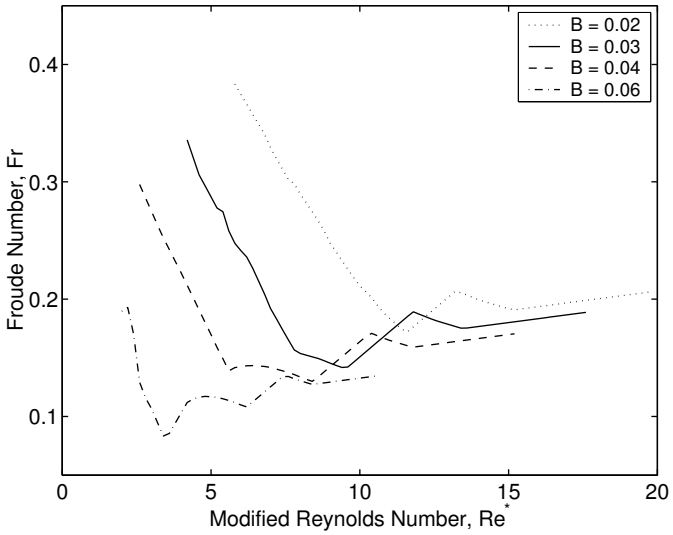

Figure 6.7: Froude number as a function of modified Reynolds number for fixed B.

several orders of magnitude smaller than the other term, i.e.,

$$\frac{2\pi\beta}{V_b}\int_{z_-}^{z_+}\frac{f'(f''f-(f')^2-1)}{\left((f')^2+1\right)^{\frac{3}{2}}}\,dz \ll 1. \tag{6.4}$$

In fact for our data

$$-0.0008 \leq \frac{2\pi\beta}{V_b}\int_{z_-}^{z_+}\frac{f'(f''f-(f')^2-1)}{\left((f')^2+1\right)^{\frac{3}{2}}}\,dz \leq 0.001. \tag{6.5}$$

Assuming the true value of $\hat{\xi}$ to be of the same order as that for water and air, we simplify (6.3) for our following analysis:

$$B \geq \frac{1}{2\sqrt{2}}(z_+ - z_-). \tag{6.6}$$

In figure 6.8 we plot our data with non-dimensional bubble length, $z_+ - z_-$, versus Bingham number. The solid line represents the curve $B = \frac{1}{2\sqrt{2}}(z_+ - z_-)$. We can see that all the bubbles (none of which were stopped) respect condition (6.6).

While none of the bubbles were spherical, the smaller bubbles could, as a very rough first approximation, be considered to be spheres. We can then use our second stopping condition (4.35) to see whether it is still a valid stopping condition. The dotted line in figure 6.8 represents the curve $B = \frac{1}{\sqrt{3}}$. Again we can see that all the bubbles respect condition (4.35):

$$B \geq \frac{1}{\sqrt{3}}. \tag{6.7}$$

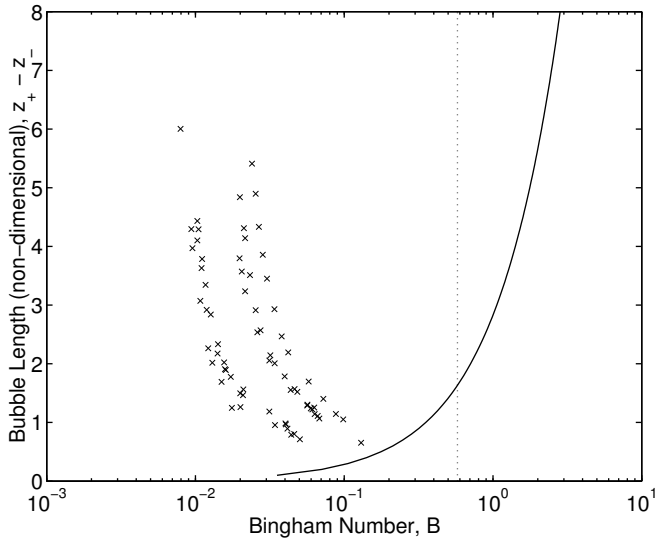

Figure 6.8: Experimental results plotted with non-dimensional bubble length versus the Bingham number. The solid line represents the curve $B = \frac{1}{2\sqrt{2}}(z_+ - z_-)$ and the dotted line represents the curve $B = \frac{1}{\sqrt{3}}$

While the bubbles with $(z_+ - z_-)$ small are closer to spheres in shape it appears that condition (6.7) is applicable to all the bubbles. Though condition (6.7) might not hold in general, one reason it may appear this way is that as $(z_+ - z_-)$ becomes larger the bubbles tend to move with a higher velocity than the smaller bubbles. Thus these bubbles are "farther away" from stopping and hence condition (6.7) could appear only to be valid. Also, if we plot the data with the Froude number versus the Bingham number, and compare this to condition (6.7) (see figure 6.9), we see that for increasing Froude numbers the bubbles are farther away from the line $B = \frac{1}{\sqrt{3}}$, i.e., are "farther away" from stopping.

Finally we have our third stopping condition for long cylindrical bubbles, (4.47):

$$B \gtrsim \frac{1}{2}\frac{{R_c}^2 - {r_b}^2}{R_c}. \tag{6.8}$$

Since none of our bubbles are actually cylindrical they do not have a constant value of r_b. Nevertheless we would like to be able to roughly compare this condition with our other conditions and with our data. So with that interest in mind we make the approximation ${r_b}^2 = \frac{4}{3(z_+ - z_-)}$; see

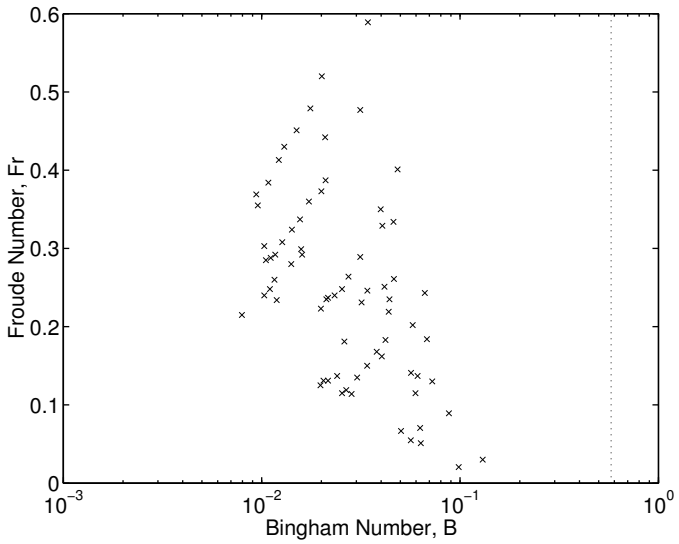

Figure 6.9: Experimental results plotted with Froude number versus the Bingham number. The dotted line represents $B = \frac{1}{\sqrt{3}}$. Note that B decreases with increasing Fr, and thus faster bubbles are further from the $B = \frac{1}{\sqrt{3}}$ line.

(4.44). This represents a sort of average effective radius of the bubble, and thus (6.8) becomes

$$B \gtrsim \frac{1}{2} \frac{{R_c}^2 - \frac{4}{3(z_+ - z_-)}}{R_c}. \tag{6.9}$$

Since the data is scaled according to the length scale $\hat{R}$, which is different for each bubble, it is difficult to plot condition (6.9) as a function of $(z_+ - z_-)$. Instead we separately calculate the critical Bingham number for each bubble and plot this along with the data (see figure 6.10). The dashed line in figure 6.10 is a best-fit line through the critical Bingham number data. Again all the data appears to respect condition (6.9). Unlike our other two conditions, as the bubble length increases the critical Bingham number decreases. This represents the idea that if a bubble is very large it can more easily fill the column entirely such that there is no layer of fluid between the bubble wall and the column walls. In this case the bubble will no longer be able to move; it has essentially separated the fluid region into two disjoint regions where fluid cannot pass from one region to the other.

Using this best-fit line we can compare all our stopping conditions to the data. Figure 6.11 shows all the data plotted with the non-dimensional bubble length versus the Bingham number

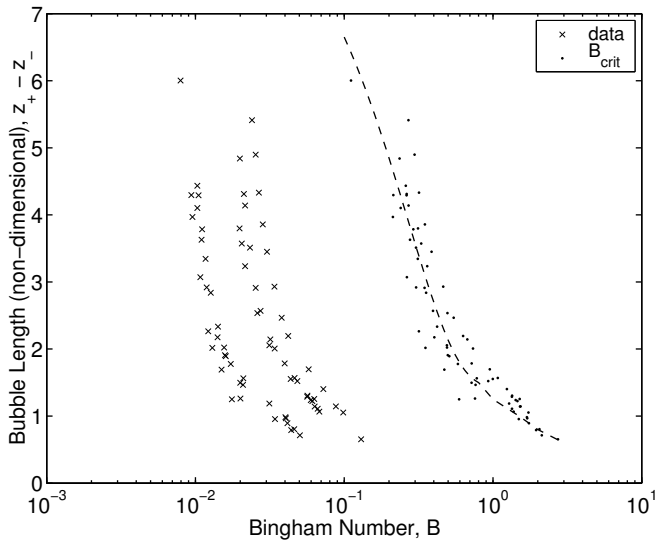

Figure 6.10: Experimental results plotted with non-dimensional bubble length versus the Bingham number. The critical Bingham numbers for the data are also plotted (dots). The dashed line is a best fit line through the critical Bingham numbers.

with all three stopping conditions included.

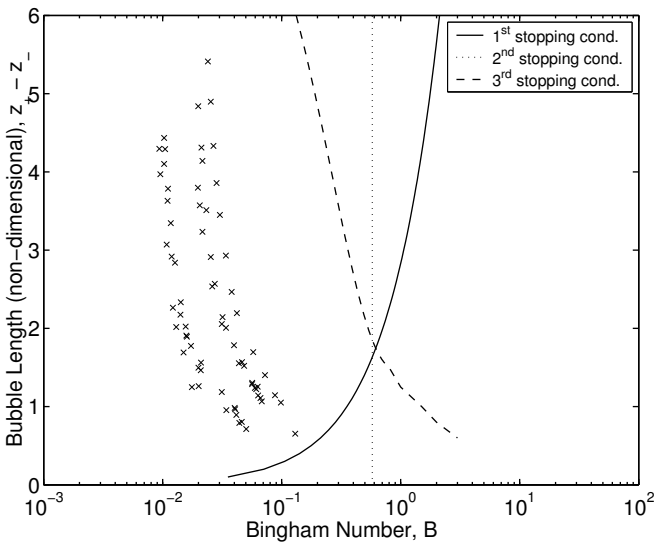

Figure 6.11: Experimental data combined with all three stopping conditions.

Bibliography

[1] J.G. Oldroyd. A rational formulation of the equations of motion of a plastic flow for a Bingham solid. *Proceedings of the Cambridge Philosophical Society*, 43:100–105, 1947.

[2] O.L.A. Santos and J.J. Azar. A study of gas migration in stagnant non-newtonian fluids. Technical report, Society of Petroleum Engineers, 1997. SPE 39019.

[3] A. Johnson, I. Rezmer-Cooper, T. Bailey, and D. McCann. Gas migration: Fast, slow or stopped. Technical report, Society of Petroleum Engineers, 1995. SPE/IADC 29342.

[4] A.B. Johnson and D.B. White. Gas rise velocities during kicks. Technical report, Society of Petroleum Engineers, 1990. SPE 20431.

[5] S.M. Bhavaraju, R.A. Mashelkar, and H.W. Blanch. Bubble motion and mass transfer in non-Newtonian fluids: Part 1. single bubble in power law and Bingham fluids. *AIChE Journal*, 24(6):1063–1070, 1978.

[6] S. Stein and H. Buggisch. Rise of pulsating bubbles in fluids with a yield stress. *Z. Angrew. Math. Mech.*, 80(11–12):827–834, 2000.

[7] A.N. Beris, J.A. Tsamopoulos, R.C. Armstrong, and R.A. Brown. Creeping motion of a sphere through a Bingham plastic. *J. Fluid Mech.*, 158:219–244, 1985.

[8] D.D. Atapattu, R.P. Chhabra, and P.H.T. Uhlherr. Creeping sphere motion in Herschel-Bulkley fluids: flow field and drag. *J. Non-Newtonian Fluid Mech.*, 59:245–265, 1995.

[9] J. Blackery and E. Mitsoulis. Creeping motion of a sphere in tubes filled with a Bingham plastic material. *J. Non-Newtonian Fluid Mech.*, 70:59–77, 1997.

[10] V. Dolejš, P. Doleček, and B. Šiška. Drag and fall velocity of a spherical particle in generalized newtonian and viscoplastic fluids. *Chemical Engineering and Processing*, 37:189–195, 1998.

[11] G Saha, N.K. Purohit, and A.K. Mitra. Spherical particle terminal settling velocity and drag in Bingham liquids. *International Journal of Mineral Processing*, 36:273–281, 1992.

[12] B.S. Padmavathi, T. Amaranath, and S.D. Nigam. Stokes flow past a sphere with mixed slip-stick boundary conditions. *Fuild Dynamics Research*, 11:229–234, 1993.

[13] L. Jossic and A. Magnin. Drag and stability of objects in a yield stress fluid. *AIChE Journal*, 47(12):2666–2672, 2001.

[14] J. Li and Y.Y. Renardy. Shear-induced rupturing of a viscous drop in a Bingham liquid. *J. Non-Newtonian Fluid Mech.*, 95:235–251, 2000.

[15] G. Gheissary and B.H.A.A. van den Brule. Unexpected phenomena observed in particle settling in non-Newtonian media. *J. Non-Newtonian Fluid Mech.*, 67:1–18, 1996.

[16] R. Clift, M.E. Weber, and J.R. Grace. *Bubbles, drops, and particles.* Academic Press, 1978.

[17] Z. Zapryanov and S. Tabakova. *Dynamics of bubbles, drops and rigid particles.* Fluid Mechanics and its Applications. Kluwer Academic Publishers, 1999.

[18] F.P. Bretherton. The motion of long bubbles in tubes. *J. Fluid Mech.*, 10:166–188, 1961.

[19] S.V. Vasil'chenko and A.G. Potapov. Gas bubble dynamics in a vicsoelastic-plastic medium. *Heat Transfer Research*, 27(1):4–8, 1996.

[20] W. Prager. *On slow visco-plastic flow*, pages 208–216. Academic Press Inc., 1954. Presented to Richard von Mises by Friends, Colleagues, and Pupils.

[21] P.P. Mosolov and V.P. Miasnikov. Variational methods in the theory of the fluidity of a viscous-plastic medium (Variatsionnye metody v teorii techenii viazko-plasticheskoi sredy). *PPM*, 29(3):468–492, 1965.

[22] P.P. Mosolov and V.P. Miasnikov. On stagnant flow regions of a viscous-plastic medium in pipes (O zastoinykh zonakh techeniia viazko-plasticheskoi sredy v trubakh). *PPM*, 30(4):705–717, 1966.

[23] P.P. Mosolov and V.P. Miasnikov. On qualitative singularities of the flow of a viscoplastic medium in pipes. *PPM*, 31(3):581–585, 1967.

[24] R. Glowinski. On the approximation of an elliptic variational inequality of the Bingham type. *Revue Francaise d'Automatique Informatique Recherche Operationnelle*, 100:13–30, 1979.

[25] R. Glowinski. *Numerical methods for nonlinear variational problems.* Springer series in computational physics. Springer-Verlag, 1984.

[26] R.R. Huilgol. Variational principles and variational inequalities for a yield stress fluid in the presence of slip. *J. Non-Newtonian Fluid Mech.*, 75:231–251, 1998.

[27] R.R. Huilgol and Q.D. Nguyen. Variational principles and variational inequalities for the unsteady flows of a yield stress fluid. *International Journal of Non-Linear Mechanics*, 36:49–67, 2001.

[28] R.R. Huilgol. Variational inequalities in the flow of yield stress fluids including inertia: Theory and applications. *Physics of Fluids*, 14(3):1269–1283, 2002.

[29] I.A. Frigaard, O. Scherzer, and G. Sona. Uniqeness and non-uniqueness in the steady displacement of two visco-plastic fluids. *Z. Angrew. Math. Mech.*, 81(2):99–118, 2001.

[30] I.A. Frigaard, S. Leimgruber, and O Scherzer. Variational methods and maximal residual wall layers. *J. Fluid Mech.*, 483:37–65, 2003.

[31] M.P. do Carmo. *Differential geometry of curves and surfaces.* Prentice Hall, Inc., 1976.

[32] H. Lamb. *Hydrodynamics.* Dover Publications, sixth edition, 1945.

[33] G.K. Batchelor. *An introduction to fluid dynamics.* Cambridge University Press, 1967.

[34] S.J. Curran, R.E. Hayes, A. Afacan, M.C. Williams, and P.A. Tanguy. Properties of Carbopol solutions as models for yield-stress fluids. *Journal of Food Science*, 67(1):176–180, 2002.

[35] P. Coussot. *Mudflow rheology and dynamics.* IAHR monograph series. A.A. Balkema, 1997.

[36] S. Kim, Y.I. Cho, W.N. Hogenauer, and K.R. Kensey. A method of isolating surface tension and yield stress effects in a U-shaped scanning capillary-tube viscometer using a Casson model. *J. Non-Newtonian Fluid Mech.*, 103:205–219, 2002.

Appendix A
A Result on the Effect of Walls

If we consider the flow of a bubble in an infinite domain, there will be a finite distance away from the bubble where the fluid will be unyielded. In this unyielded region far away from the bubble, we can "disturb" the fluid without it affecting the propagation of the bubble. So for example, we can introduce walls (of any shape) anywhere in this unyielded region and the flow in the region surrounding the bubble will not change. Or if there are already walls in this unyielded region we can move the the walls within this unyielded region without affecting the flow.

Physically this makes sense in that to calculate the flow around the bubble the boundary conditions (not on the bubble surface) must be applied at the yield surface. Hence if we disturb the fluid outside the yield surface without it affecting the shape of the yield surface, there is no way for that information to reach the bubble.

Mathematically this results follows from our rate of strain minimization (3.53): The true velocity field minimizes the functional

$$J_\Omega(\boldsymbol{v}) = \frac{1}{n+1} a(\boldsymbol{v},\boldsymbol{v}) + j(\boldsymbol{v}) - L(\boldsymbol{v}) \tag{A.1}$$

over the functional space $V(\Omega)$, where

$$V(\Omega) = \left\{ \boldsymbol{v} = (v_1, v_2, v_3) \middle| v_i \in C^\infty(\Omega),\ \frac{\partial v_i}{\partial x_i} = 0 \text{ in } \Omega, \text{ and } v_i = 0 \text{ on } \partial\Omega_w \right\} \tag{A.2}$$

and all the integrals in (A.1) are over Ω.

Consider two domains Ω_1 and Ω_2 with $\Omega_1 \subset \Omega_2$. In each domain we have a bubble of exactly the same shape, that is $\partial\Omega_{1,b} = \partial\Omega_{2,b}$. We know that if a velocity field minimizes (A.1) then it is the unique minimizer. So we let $\boldsymbol{u^{(1)}}$ minimize $J_{\Omega_1}(\boldsymbol{v})$ over $V(\Omega_1)$ and let $\boldsymbol{u^{(2)}}$ minimize $J_{\Omega_2}(\boldsymbol{v})$ over $V(\Omega_2)$. Furthermore we assume that in $\Omega_2 \setminus \{\Omega_1\}$ $\boldsymbol{u^{(2)}} = 0$, i.e., that the walls of both domains are in the unyielded region. This arrangement is depicted in figure A.1.

On $\partial\Omega_{1,w}$ (the walls), $\boldsymbol{u^{(2)}} = 0$ and on $\partial\Omega_{1,b}$, $\boldsymbol{u^{(2)}}$ satisfies the necessary boundary conditions, namely (3.20)–(3.22). Thus, truncated appropriately, $\boldsymbol{u^{(2)}} \in V(\Omega_1)$.

Since in $\Omega_2 \setminus \{\Omega_1\}$, $\boldsymbol{u^{(2)}} = 0 \ \Rightarrow\ \dot{\boldsymbol{\gamma}}(\boldsymbol{u^{(2)}}) = 0$ in $\Omega_2 \setminus \{\Omega_1\} \ \Rightarrow\ J_{\Omega_2}(\boldsymbol{u^{(2)}}) = 0$ in $\Omega_2 \setminus \{\Omega_1\}$. We claim now that $\boldsymbol{u^{(2)}}$ also minimizes $J_{\Omega_1}(\boldsymbol{v})$ over $V(\Omega_1)$. If it did not there would exist

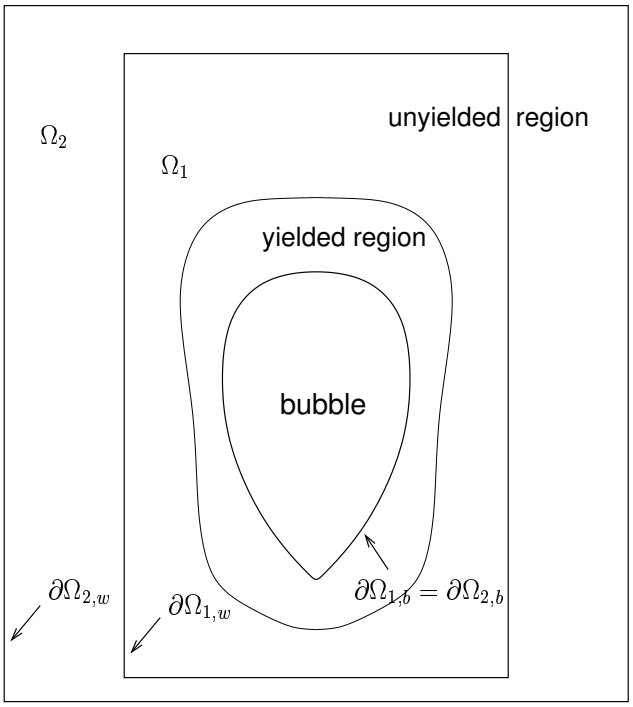

Figure A.1: A bubble propagating in two different domains.

$\boldsymbol{u^*} \in V(\Omega_1)$ such that $J_{\Omega_1}(\boldsymbol{u^*}) < J_{\Omega_1}(\boldsymbol{u^{(2)}})$ and the velocity field

$$u^*_{\Omega_2} = \begin{cases} u^* & \text{in } \Omega_1 \\ 0 & \text{in } \Omega_2 \setminus \{\Omega_1\} \end{cases}, \qquad u^*_{\Omega_2} \in V(\Omega_2)$$

would give

$$J_{\Omega_2}(\boldsymbol{u^*}) < J_{\Omega_2}(\boldsymbol{u^{(2)}})$$

which is impossible. Therefore $\boldsymbol{u^{(2)}}$ minimizes $J_{\Omega_1}(\boldsymbol{v})$ over $V(\Omega_1)$ and by uniqueness $\boldsymbol{u^{(2)}} = \boldsymbol{u^{(1)}}$ in Ω_1. The flow does not depend on the position of the walls in the unyielded region.

Appendix B

Some Differential Geometry Results for Surfaces

These results are taken from do Carmo [31]. In general, for a two dimensional surface parameterized by $\boldsymbol{x} = \boldsymbol{x}(s,t)$, where $s_i \le s \le s_f$ and $t_i \le t \le t_f$, the metric tensor, $g_{\alpha\beta}$, for the surface is given by

$$g_{\alpha\beta}(s,t) = \begin{pmatrix} \boldsymbol{x}_s \cdot \boldsymbol{x}_s & \boldsymbol{x}_s \cdot \boldsymbol{x}_t \\ \boldsymbol{x}_t \cdot \boldsymbol{x}_s & \boldsymbol{x}_t \cdot \boldsymbol{x}_t \end{pmatrix}, \tag{B.1}$$

where $\boldsymbol{x}_s = \frac{\partial \boldsymbol{x}}{\partial s}$, and $\boldsymbol{x}_t = \frac{\partial \boldsymbol{x}}{\partial t}$.

A unit normal to the surface is given by

$$\boldsymbol{N}(s,t) = \frac{\boldsymbol{x}_t \times \boldsymbol{x}_s}{|\boldsymbol{x}_t \times \boldsymbol{x}_s|}. \tag{B.2}$$

And the second fundamental form tensor is given by

$$b_{\alpha\beta}(s,t) = \begin{pmatrix} \boldsymbol{x}_{ss} \cdot \boldsymbol{N} & \boldsymbol{x}_{st} \cdot \boldsymbol{N} \\ \boldsymbol{x}_{st} \cdot \boldsymbol{N} & \boldsymbol{x}_{tt} \cdot \boldsymbol{N} \end{pmatrix}, \tag{B.3}$$

where $\boldsymbol{x}_{ss} = \frac{\partial^2 \boldsymbol{x}}{\partial s^2}$, $\boldsymbol{x}_{st} = \frac{\partial^2 \boldsymbol{x}}{\partial s \partial t}$, and $\boldsymbol{x}_{tt} = \frac{\partial^2 \boldsymbol{x}}{\partial t^2}$.

Then the mean curvature, $H(s,t)$, of the surface is given by

$$H(s,t) \equiv \frac{1}{2}\left(\frac{1}{R_1} + \frac{1}{R_2}\right) = \frac{1}{2} g^{\alpha\beta} b_{\alpha\beta}. \tag{B.4}$$

And for an integral over the surface

$$\int_{\boldsymbol{x}(s,t)} ds = \int_{s_i}^{s_f} \int_{t_i}^{t_f} \|\boldsymbol{x}_s \times \boldsymbol{x}_t\| \, dt \, ds. \tag{B.5}$$

Now for a "bubble-like" surface of revolution, revolved about the z-axis, as in figure B.1, one possible parameterization is given by

$$\boldsymbol{x}(z,\theta) \equiv (x_1, x_2, x_3) = (x, y, z) = \big(f(z)\cos\theta, f(z)\sin\theta, z\big), \tag{B.6}$$

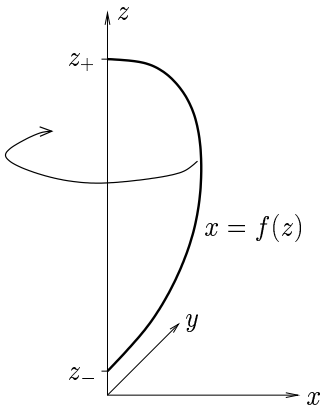

Figure B.1: Surface of revolution.

where $z_- \leq z \leq z_+$ and $0 \leq \theta < 2\pi$. So

$$\begin{aligned} \boldsymbol{x}_z &= (f' \cos\theta, f' \sin\theta, 1), \\ \boldsymbol{x}_\theta &= (-f \sin\theta, f \cos\theta, 0) \end{aligned}$$

and thus the metric tensor, (B.1), is given by

$$g_{\alpha\beta}(z,\theta) = \begin{pmatrix} (f')^2 + 1 & 0 \\ 0 & f^2 \end{pmatrix}. \tag{B.7}$$

Note that there is no θ dependence in the metric. The tensor $g^{\alpha\beta}$ is simply the inverse of $g_{\alpha\beta}$:

$$g^{\alpha\beta}(z,\theta) = \begin{pmatrix} \frac{1}{(f')^2+1} & 0 \\ 0 & \frac{1}{f^2} \end{pmatrix}. \tag{B.8}$$

From (B.2) we obtain the outward unit normal for the surface:

$$\boldsymbol{N} = \frac{1}{f\sqrt{(f')^2+1}}(f\cos\theta, f\sin\theta, -ff'). \tag{B.9}$$

From our parameterization (B.6)

$$\begin{aligned} \boldsymbol{x}_{zz} &= (f'' \cos\theta, f'' \sin\theta, 0), \\ \boldsymbol{x}_{z\theta} &= (-f' \sin\theta, f' \cos\theta, 0), \\ \boldsymbol{x}_{\theta\theta} &= (-f \cos\theta, -f \sin\theta, 0), \end{aligned}$$

and therefore the second fundamental form tensor, given by (B.3), is

$$b_{\alpha\beta}(z,\theta) = \begin{pmatrix} \frac{f''}{\sqrt{(f')^2+1}} & 0 \\ 0 & -\frac{f}{\sqrt{(f')^2+1}} \end{pmatrix}. \tag{B.10}$$

Thus the mean curvature of our surface of revolution is given by

$$H(z) = \frac{1}{2}\left(\frac{1}{R_1} + \frac{1}{R_2}\right) = \frac{1}{2}\left(\frac{f''}{\left((f')^2+1\right)^{\frac{3}{2}}} - \frac{1}{f\sqrt{(f')^2+1}}\right),$$

and we have the result

$$\left(\frac{1}{R_1} + \frac{1}{R_2}\right) = \frac{f''f - (f')^2 - 1}{f\left((f')^2+1\right)^{\frac{3}{2}}}. \tag{B.11}$$

The sign of the mean curvature depends on the choice of the normal. If we had chosen the inward normal of the bubble, there would be a negative sign in front of the right hand side of (B.11). To determine which sign we need, consider the case of a cylindrical bubble where $f(z) = C$, a positive constant. Then from (B.11) we obtain

$$\left(\frac{1}{R_1} + \frac{1}{R_2}\right) = -\frac{1}{C}.$$

However we want the curvature of the cylindrical bubble to be positive. Therefore we must add a negative sign to the right hand side of (B.11).

Thus we have the final result

$$\left(\frac{1}{R_1} + \frac{1}{R_2}\right) = -\frac{f''f - (f')^2 - 1}{f\left((f')^2+1\right)^{\frac{3}{2}}}. \tag{B.12}$$

Also, for an integral over this surface of revolution, we have

$$\int_{\boldsymbol{x}(z,\theta)} ds = \int_0^{2\pi}\int_{z_-}^{z_+} f\sqrt{(f')^2+1}\, dz\, d\theta. \tag{B.13}$$

Appendix C
Data Extraction and Error Analysis

C.1 Velocity Calculation

From the digital video of each experiment we calculate the velocity by measuring the time required for a bubble to travel a fixed distance. The video is taken at a rate of 60 frames per second. Figure C.1 shows two frames from the video of an experiment. Using the reference

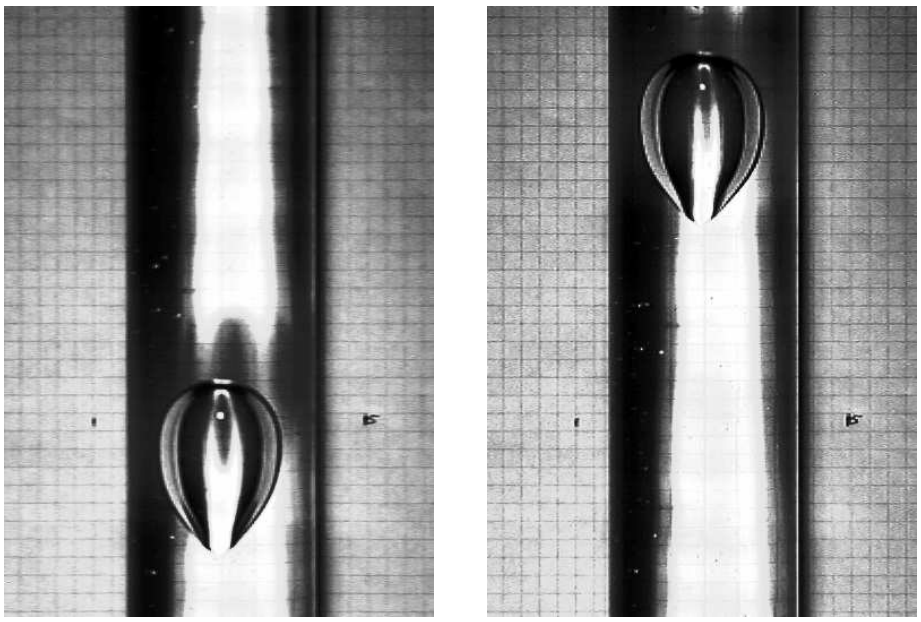

(a) (b)

Figure C.1: Video frames of an experiment. (a) $t = 0\,s$, (b) $t = 1.28\,s$

grid (spacing of 0.2") we determine that the bubble has travelled a distance of $8.79\,cm\ \pm 0.5\%$. This represents a measurement error of ± 0.1 squares. From the frame indices on the video we determine the elapsed time between the two frames to be $1.28\,s\ \pm 0.7\%$. This represents an measurement accuracy up to $\pm\frac{1}{120}\,s$. Thus, in this case, the velocity is $6.87\,cm/s\ \pm 0.9\%$. The

error calculation is done separately for each experiment, as the percentage error will vary with the distance travelled and time between the given frames. It should also be noted that the scaling effect of having the reference grid *behind* the bubble is accounted for when calculating the distance the bubble travels.

C.2 Shape Dependent Quantities

While the velocity can simply and easily be calculated by examining two frames and determining the distance the bubble has travelled in a specified amount of time, for quantities that depend on the shape of the bubble (volume, surface integrals) we need to extract the shape of the profile of the bubble from the video. In order to do this we apply an edge detection algorithm (Matlab's "edge" function with the Laplacian of Gaussian method) to an image of the bubble. With a little cleaning up of the result to eliminate false edges, we can obtain the profile of the bubble. Figure C.2 shows the actual bubble and the profile obtained from the edge detection. Again the effects of scaling and optical distortion due to the cylindrical geometry (see appendix E) are accounted for in this process.

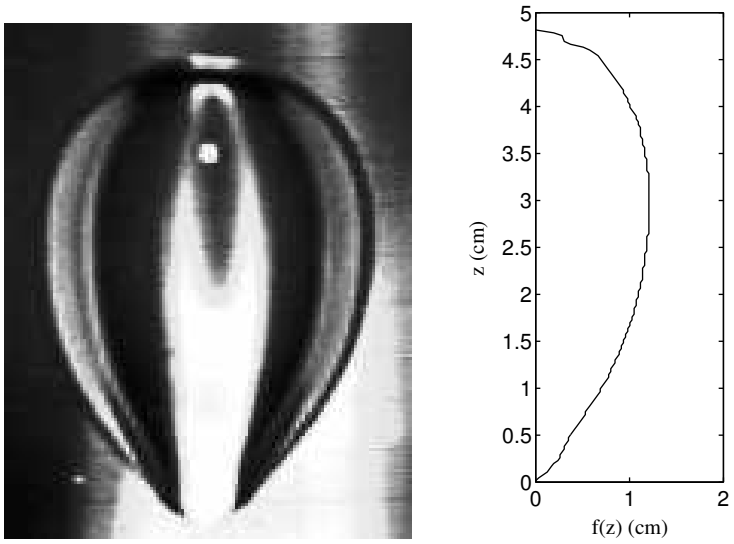

(a) (b)

Figure C.2: Profile of a bubble. (a) actual bubble (same as figure C.1a), (b) the profile obtained using our edge detection method. The apparent discrepancy in the profile when compared to the video is a result of the cylindrical geometry, for which we have corrected.

Once the bubble profile is obtained the volume can be easily calculated; however calculation of the surface integral is still a bit tricky. Due to the finite pixel size the bubble profile is not very smooth when we consider its derivatives with respect to z. Since the surface integral is dependent on the first and second derivatives of the profile with respect to z, we need to

somehow smooth the bubble profile to obtain a reasonable result. We do this by fitting a polynomial, in the least-squares sense, to the data for the profile (using Matlab's "polyfit" function). The degree of the polynomial is chosen to be between 6-9. We find that this provides a smooth approximation to the bubble profile without being so accurate as to contain the small oscillations which are the result of the pixelation.

C.2.1 Assumption of Axisymmetry

To obtain data pertaining to the shape of the bubble we have made the assumption of an axisymmetric bubble profile. To verify that this assumption is reasonable we compare the profiles obtained by looking at the left half and the right half of a bubble. The profiles are plotted in figure C.3.

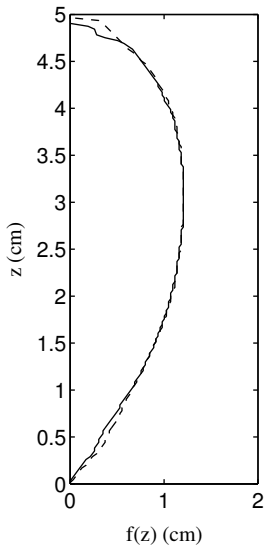

Figure C.3: Profiles of a bubble obtained by looking at the left half (dashed line) and at the right half (solid line).

The assumption is quite good except at the nose and tail of the bubble where the edge detection has difficulty resolving the edges. Nevertheless, this results in an error of only $0.07\,mL$. This represents a 0.5% error in the volume.

C.2.2 Accuracy of the Edge Detection Method

To estimate the accuracy of our edge detection method several circles of know diameter were photographed and the edge detection method was used to obtain a profile for each circle. Using these profiles we then calculated the volume of the equivalent sphere (obtained by revolving the

circles) and the value of the bubble surface integral

$$\hat{S} = \int_{\hat{z}_-}^{\hat{z}_+} \frac{\hat{f}'(\hat{f}''\hat{f} - (\hat{f}')^2 - 1)}{\left((\hat{f}')^2 + 1\right)^{\frac{3}{2}}}\, dz \tag{C.1}$$

The results of this are presented Table (C.1). For the circles the true value of the $\hat{S}$ is zero.

Circle Diameter (cm)	Equivalent Volume (mL)	Calculated Volume (mL)	Percentage Error	Actual Surface Integral Value (cm)	Calculated Surface Integral Value (cm)
2	4.19	4.27	1.9	0	-0.0023
4	32.51	33.66	3.5	0	-0.0014
8	268.08	268.78	0.3	0	-0.0141

Table C.1: Error in the calculation of shape dependent quantities for test circles.

Appendix D
Measurement of Rheological Parameters

All the measurements are taken using Bohlin Instuments' CVOR 200 rotational rheometer. The tests are done at a constant temperature of $22\,^{\circ}C$, which is approximately the temperature of the laboratory in which the experiments are conducted.

D.1 Yield Stress

To determine the yield stress, $\hat{\tau}_Y$, we conduct a series of creep tests on a sample of the viscoplastic fluid. For each creep test a constant stress is applied to the sample and after $300\,s$ the strain is measured. We normally increase the applied stress between successive tests by 0.5 or $1\,Pa$. A graph showing the strain after $300\,s$ for various applied stresses is given in figure D.1. We can clearly see two regions, one where the strain does not change significantly when the applied stress is increased, and one where the strain begin to increase significantly with the applied stress. The stress value at which the change between these two regimes occurs (in this case $5.2\,Pa$) is defined to be the yield stress of the fluid. The measurement of the yield stress can be made to an accuracy of $\pm 0.2\ Pa$.

D.2 Consistency and Power Law Index

To determine the consistency, $\hat{\mu}_\ell$, and the power law index, n, we conduct a controlled stress viscometry test. The rate of strain, $\hat{\dot{\boldsymbol{\gamma}}}$, is measured at various stresses, $\hat{\boldsymbol{\tau}}_\ell$. This results in the curve given in figure D.2.

The constitutive equation for a Herschel-Bulkley fluid can be written as

$$\begin{aligned} \hat{\dot{\boldsymbol{\gamma}}}(\hat{\boldsymbol{u}}) &= 0 && \text{if } \hat{\boldsymbol{\tau}}_\ell(\hat{\boldsymbol{u}}) \leq \hat{\tau}_Y, \\ \hat{\boldsymbol{\tau}}_\ell(\hat{\boldsymbol{u}}) &= \hat{\mu}_\ell \hat{\dot{\boldsymbol{\gamma}}}(\hat{\boldsymbol{u}})^n + \hat{\tau}_Y && \text{if } \hat{\boldsymbol{\tau}}_\ell(\hat{\boldsymbol{u}}) > \hat{\tau}_Y. \end{aligned}$$

Having already calculated $\hat{\tau}_Y$, we fit the parameters $\hat{\mu}_\ell$ and n to the data in figure D.2 in a least-squares sense. For example, for the sample shown in figure D.2 we obtain the values $\hat{\mu}_\ell = 2.48\,Pa \cdot s^n$ and $n = 0.462$. The masurement of $\hat{\mu}_\ell$ and n can be made to an accuracy of $\pm 6\%$ and $\pm 15\%$ respectively.

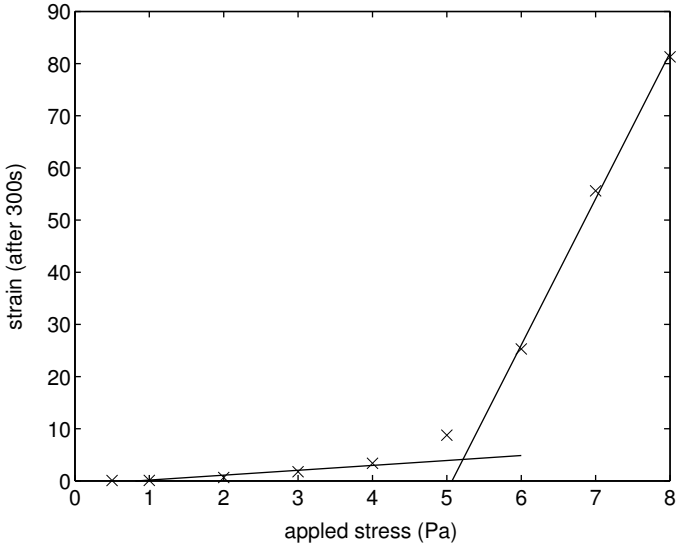

Figure D.1: Strain response after $300\,s$ for a sample of Carbopol at various stresses. The lines are to aid visualization.

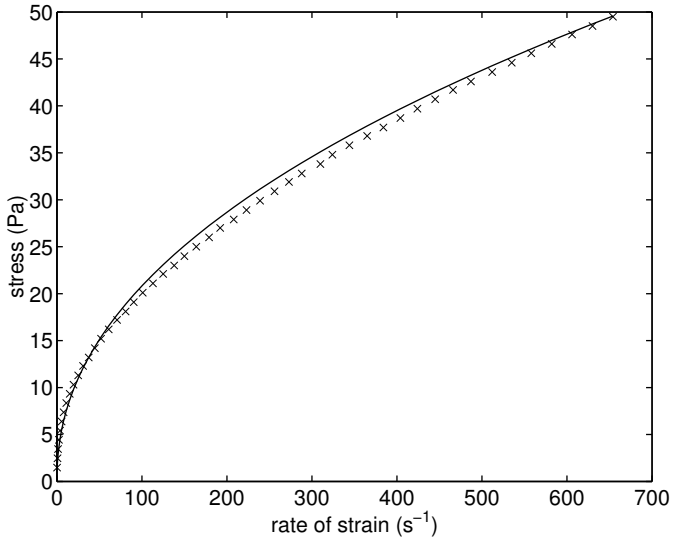

Figure D.2: Stress plotted versus rate of strain for a sample of Carbopol. The solid line represents the least-squares fit.

Appendix E

Optical Distortion Due to Cylindrical Geometry

An exaggerated top view of the cylindrical geometry of the bubble column is given in figure E.1. r, R_1, and R_2 are respectively the bubble radius (at a given height), the inner radius of the cylinder, and the outer radius of the cylinder. L is the distance from the camera to the front edge of the column and r^* is the apparent radius of the bubble. n_1, n_2, and n_3 are the indices of refraction of the air, the clear acrylic of the column, and the viscoplastic liquid respectively. Given r^*, R_1, R_2, L, n_1, n_2, and n_3, we need to calculate r. (The other angles, lengths, and

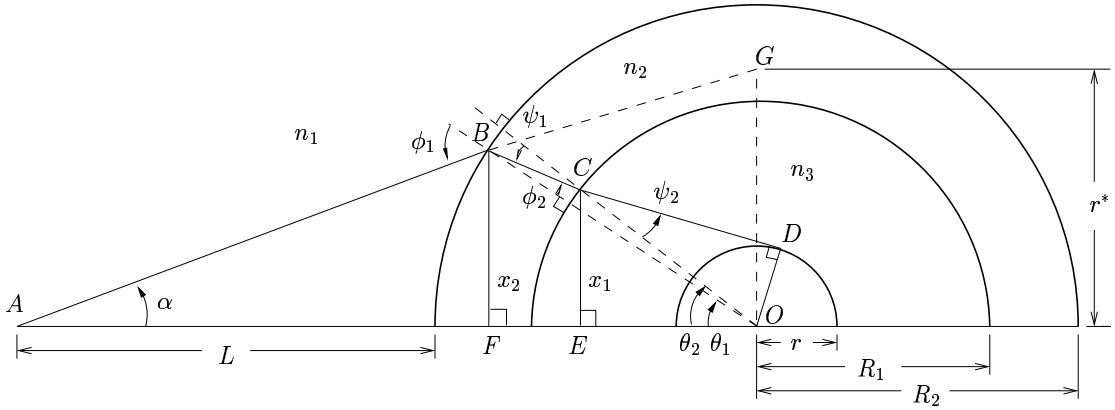

Figure E.1: Schematic of the cylindrical geometry.

points in figure E.1 are used to simplify our calculations.)

Using the notation of figure E.1, Snell's law applied to the interface between the acrylic column and the viscoplastic liquid is

$$n_3 \sin\psi_2 = n_2 \sin\psi_1. \tag{E.1}$$

Also from $\triangle CDO$ and $\triangle BCO$ respectively, we have

$$r = R_1 \sin\psi_2 \tag{E.2}$$

$$\psi_1 = (\theta_2 - \theta_1) + \phi_2. \tag{E.3}$$

Combining (E.1)–(E.3) we obtain

$$\begin{aligned} r &= \frac{R_1 n_2}{n_3} sin(\theta_2 - \theta_1 + \phi_2) \\ &= \frac{R_1 n_2}{n_3}[(\sin\theta_2 \cos\theta_1 - \sin\theta_1 \cos\theta_2)\cos\phi_2 + (\cos\theta_2 \cos\theta_1 + \sin\theta_2 \sin\theta_1)\sin\phi_2]. \end{aligned} \tag{E.4}$$

If we can calculate the values of the sine and cosine functions in (E.4), in terms of the given quantities, then we can determine r.

Applying Snell's law to the interface between the air and the clear acrylic we have

$$n_2 \sin\phi_2 = n_1 \sin\phi_1. \tag{E.5}$$

From $\triangle ABO$ we see that

$$\phi_1 = \theta_1 + \alpha. \tag{E.6}$$

Combining (E.5) and (E.6) we have

$$\begin{aligned} \sin\phi_2 &= \frac{n_1}{n_2}\sin(\theta_1 + \alpha) \\ &= \frac{n_1}{n_2}(\sin\theta_1 \cos\alpha + \sin\alpha \cos\theta_1), \qquad \text{and} \end{aligned} \tag{E.7}$$

$$\cos\phi_2 = \sqrt{1 - \sin^2\phi_2}. \tag{E.8}$$

Now from $\triangle AGO$

$$\tan\alpha = \frac{r^*}{L + R_2}$$

$$\Rightarrow \sin\alpha = \frac{r^*}{\sqrt{r^{*2} + (L + R_2)^2}}, \qquad \text{and} \qquad \cos\alpha = \frac{L + R_2}{\sqrt{r^{*2} + (L + R_2)^2}}. \tag{E.9}$$

In order to calculate $\sin\theta_1$, $\cos\theta_1$, $\sin\theta_2$, and $\cos\theta_2$ from the given quantities, we note that

$$\sin\theta_1 = \frac{x_2}{R_2} \qquad \text{and} \qquad \cos\theta_1 = \frac{\sqrt{{R_2}^2 - {x_2}^2}}{R_2}, \tag{E.10}$$

$$\sin\theta_2 = \frac{x_1}{R_1} \qquad \text{and} \qquad \cos\theta_2 = \frac{\sqrt{{R_1}^2 - {x_1}^2}}{R_1}, . \tag{E.11}$$

Now all that remains is to determine the values of x_1 and x_2.

From $\triangle AGO$ and $\triangle ABF$ we can see that

$$\tan\alpha = \frac{r^*}{L + R_2}, \qquad \text{and} \tag{E.12}$$

$$\tan\alpha = \frac{x_2}{L + R_2 - \sqrt{{R_2}^2 - {x_2}^2}}. \tag{E.13}$$

$R_2 - \sqrt{{R_2}^2 - {x_2}^2}$ is the distance from the front point of the column to point F. Equating (E.12) and (E.13) and simplifying we obtain a quadratic equation for x_2:

$$[(L + R_2)^2 + {r^*}^2]\,{x_2}^2 - 2r^*(L + R_2)^2\,x_2 + {r^*}^2(L^2 + 2LR_2) = 0,$$

which has roots

$$x_2 = \frac{2r^*(L+R_2)^2 \pm \sqrt{4r^{*2}(L+R_2)^4 - 4r^{*2}(L^2+2LR_2)[(L+R_2)^2+r^{*2}]}}{2[(L+R_2)^2+r^{*2}]}. \tag{E.14}$$

Using the requirement that $x_2 < r^*$, we take the smaller of the two roots (i.e., negative square root). Thus using (E.14) with (E.10) we can calculate the values of $\sin\theta_1$ and $\cos\theta_1$, in term of the given quantities. Furthermore using (E.9) and (E.10) in (E.7) and (E.8) we can calculate the values of $\sin\phi_2$ and $\cos\phi_2$.

By considering $\triangle FBO$ and $\triangle ECO$ we note that for x_1

$$x_1 = x_2 - \left(\sqrt{{R_2}^2 - {x_2}^2} - \sqrt{{R_1}^2 - {x_1}^2}\right)\tan(\theta_1 - \phi_2).$$

Simplifying we get a quadratic for x_1 in terms of known quantities:

$$[1+\tan^2(\theta_1-\phi_2)]\,{x_1}^2 + \left[-2x_2 + 2\sqrt{{R_2}^2-{x_2}^2}\tan(\theta_1-\phi_2)\right] x_1 + \left\{\left[x_2 - \sqrt{{R_2}^2-{x_2}^2}\tan(\theta_1-\phi_2)\right]^2 - {R_1}^2\tan^2(\theta_1-\phi_2)\right\} = 0. \tag{E.15}$$

In this case we want the larger of the two roots of (E.15). Note that x_2 is known from (E.14) and $\tan^2(\theta_1-\phi_2)$ can be calculated from the values of $\sin\theta_1$, $\cos\theta_1$, $\sin\phi_2$, and $\cos\phi_2$, which we have already calculated. Thus we can now calculate the value of r.